Unmanned Surface Vessel (USV) Systems for Bridge Inspection

Final Report

FDOT Contract Number: BDV27-977-07

August 18, 2016

Submitted by:

Karl von Ellenrieder, Ph.D.

Florida Atlantic University

Dept of Ocean & Mechanical Engineering

101 N. Beach Rd. Dania Beach, FL 33001

(954) 924-7232, Email: ellenrie@fau.edu

Submitted to:

Florida Department of Transportation, Research Center

Program Manager: Ed Hutchinson

605 Suwannee St., MS 27, Tallahassee, FL 32399

co-Project Manager: Richard Kerr

605 Suwannee St., MS 52, Tallahassee, FL 32399

Disclaimer

The opinions, findings, and conclusions expressed in this publication are those of the author and not necessarily those of the Florida Dept. of Transportation or the U. S. Dept. of Transportation.

Metric Conversion Chart

SYMBOL	WHEN YOU KNOW	MULTIPLY BY	TO FIND	SYMBOL
		LENGTH		
in	inches	25.4	millimeters	mm
ft	feet	0.305	meters	m
yd	yards	0.914	meters	m
mi	miles	1.61	kilometers	km
		VOLUME		
fl oz	fluid ounces	29.57	milliliters	mL
gal	gallons	3.785	liters	L
ft^3	cubic feet	0.028	cubic meters	m^3
yd^3	cubic yards	0.765	cubic meters	m^3
		NOTE: volumes greater than 1000 L shall be shown in m^3		
		MASS		
oz	ounces	28.35	grams	g
lb	pounds	0.454	kilograms	kg
T	short tons (2000 lb)	0.907	megagrams (or "metric	Mg (or "t")
		TEMPERATURE (exact degrees)		
°F	Fahrenheit	5 (F-32)/9 or (F-32)/1.8	Celsius	°C

Technical Report Documentation Page

1. Report No.	2. Government Accession No.	3. Recipient's Catalog No.
4. Title and Subtitle *Unmanned Surface Vessel (USV) Systems for Bridge Inspection.*		5. Report Date *August 2016*
		6. Performing Organization Code
7. Author(s) *Karl von Ellenrieder and Jared Wampler*		8. Performing Organization Report No.
9. Performing Organization Name and Address *Florida Atlantic University* *Department of Ocean & Mechanical Engineering* *101 N. Beach Rd., Dania Beach, FL 33004-3023*		10. Work Unit No. (TRAIS)
		11. Contract or Grant No. *BDV27-977-07*
12. Sponsoring Agency Name and Address *Florida Department of Transportation* *Research Center* *605 Suwannee Street, MS 30* *Tallahassee, FL 32399*		13. Type of Report and Period Covered *Final Report* *June 2015-June 2016*
		14. Sponsoring Agency Code
15. Supplementary Notes		

16. Abstract

The use of unmanned surface vehicles (USVs) for bridge inspection has been explored. The following issues were considered: (1) the requirements of and current techniques utilized in on-water bridge inspection; (2) USV design and configuration considerations for USV-based bridge inspection; (3) use of acoustic sensing techniques for imaging underwater bridge structures and channel bottom features; (4) the control and dynamic positioning of USVs for bridge inspection; (5) the use of advanced robotics techniques for improving vehicle navigation under bridges and the mapping of bridge features; and lastly, (6) recommendations for the addition of standard operating procedures to accommodate the use of USVs for bridge inspection. A proof of concept system was developed and tested using an existing USV at Florida Atlantic University (FAU) outfitted with a real-time imagining sonar. Field experiments were conducted with the system at several sites near the city of Carrabelle, Florida and in Dania Beach, Florida. Live demonstrations of the system were also conducted at the 2015 Florida Automated Vehicles Summit. The system was able to autonomously collect images of bridge structures, both underwater and at the waterline, by traversing a series of preprogrammed waypoints along a bridge and station-keeping at locations of interest. The results of the field tests and background literature survey are presented, and a set of recommendations for use of USV-based bridge inspection systems is given. It is suggested that the application of advanced robotics techniques for Human-Robot-Interaction and autonomous mapping/imaging can improve the preliminary inspection approach implemented during this study.

17. Key Word *Unmanned Surface Vehicles, Bridge Inspection, Autonomous Control, Real-Time Imaging Sonar, Underwater Inspection*	18. Distribution Statement *No restrictions.*		
19. Security Classif. (of this report) *Unclassified*	20. Security Classif. (of this page) *Unclassified*	21. No. of Pages *168*	22. Price

Form DOT F 1700.7 (8-72) Reproduction of completed page authorized

Acknowledgements

This research effort would not have been possible without the guidance and funding support provided by the Florida Department of Transportation (FDOT). In particular, special thanks to the Project Managers, Mr. Ed Hutchinson and Mr. Richard Kerr, and to the support provided by Mr. Tanner Martin and Mr. David Sherman.

In addition, the following people at Florida Atlantic University assisted by kindly providing technical advice and support: Prof. Pierre Beaujean, Mr. Ed Henderson, Mr. John Kielbasa, and Mr. Anthony Levine. Thank you for your support.

Also, special thanks to Mr. Bruce McCormack and his team at the Gulf Unmanned Systems Center for their assistance with conducting some of the field experiments and for freely providing their substantial field experience and knowledge of the environment during our operations near Carrabelle, FL.

The contributions from the following students at Florida Atlantic University were essential to this research project:

• Dr. Huajin "Ariel" Qu – Ph.D. Student in Mechanical Engineering (graduated Spring 2016)

• Dr. Edoardo Sarda – Ph.D. Student in Ocean Engineering (graduated Spring 2016)

• Mr. Travis Moscicki – B.S. Student in Ocean Engineering

• Mr. William Wiard – B.S. Student in Ocean Engineering

Executive Summary

The purpose of this report is to present the research conducted under Florida Department of Transportation (FDOT) Contract BDV27-977-07, “Unmanned Surface Vessel (USV) Systems for Bridge Inspection”. During this effort, the following issues were identified and explored: (1) the requirements of and current techniques utilized in on-water bridge inspection; (2) USV design and configuration considerations for USV-based bridge inspection; (3) use of acoustic sensing techniques for imaging underwater bridge structures and channel bottom features; (4) the control and dynamic positioning of USVs for bridge inspection; (5) the use of advanced robotics techniques for improving vehicle navigation under bridges and the mapping of bridge features; and lastly, (6) recommendations for the addition of standard operating procedures to accommodate the use of USVs for bridge inspection. To obtain first-hand experience on the use of USV-based bridge inspection systems, a proof of concept system was configured and tested using an existing USV at Florida Atlantic University (FAU). Field experiments were conducted with the system at several sites in Northern Florida, near the city of Carrabelle, as well as, in Southern Florida in the vicinity of the FAU SeaTech Campus in Dania Beach. Additionally, live demonstrations of the system were conducted at the Florida Automated Vehicles Symposium in the Port of Jacksonville, FL. The results of the field tests and background literature survey are presented, and a set of recommendations for use of USV-based bridge inspection systems is given.

Table of Contents

List of Figures

List of Tables

List of Abbreviations and Acronyms

2D	2 Dimensional
3D	3 Dimensional
AGM	Absorbent Glass Mat Battery
Ah	Amp-hour
AUV	Autonomous Underwater Vehicle
AWG	American Wire Gauge
AWP	Area of the Waterplane
CA	California
CAD	Computer-Aided Design
CAT 5	Category 5 Ethernet Cable
CCD	Charge Coupled Device
COLREGs	International Regulations for Preventing Collisions at Sea (1972)
DC	Direct Currrent
DOF	Degree of Freedom
DVL	Doppler Velocimetry Logger
FAU	Florida Atlantic University
FDOT	Florida Department of Transportation
FHWA	Federal HighWay Administration
FL	Florida
GNC	Guidance Navigation and Control
GPS	Global Positioning System
GUI	Graphical User Interface
GUSC	Gulf Unmanned Systems Center
HRI	Human-Robot Interaction
Hwy	Highway
IMU	Inertial Measurement Unit
kHz	KiloHertz
LCG	Longitudinal Center of Gravity
LED	Light Emitting Diode
LiDAR	Light Detection And Ranging
LiNiMnCo	Lithium Nickel Manganese Cobalt Oxide Battery
LiPO	Lithium Ion Polymer Battery
LOA	Length Overall
LWL	Length on the Waterline
MHz	MegaHertz
MIMO	Multi Input Multi Output
NDE	Non Destructive Evaluation

NDT	Non Destructive Testing
NED	North East Down
PD	Porportional Derivative
PI	Principle Investigator
PID	Porportional Integral Derivative
RADAR	RAdio Detection AndRanging
RC	Remote Control
RF	Radio Frequency
ROV	Remotely Operated Vehicle
RTK-GPS	Real Time Kinematic GPS
SAR	Synthetic Aperture RADAR
SLAM	System Localization and Mapping
SNAME	Society of Naval Architects and Marine Engineers
SWATH	Small Waterplane Area Twin Hull
UMV	Unmanned Marine Vehicle
UUV	Unmanned Underwater Vehicle
WAAS	Wide Area Augmentation System
WAM-V	Wave Adaptive Modular Vehicle

1 Introduction/Objectives

1.1 Background and Need

In the US, there are approximately 575,000 highway bridges, and about 85% of them span waterways [1]. Nearly 25% of all bridges in the U.S. are considered deficient or obsolete and are in need of replacement. In comparison, the State of Florida is doing better than the national average and ranks among the lowest nationwide for the percentage of bridges that are considered structurally deficient. However, the task of inspecting and maintaining the state's extensive network of approximately 11,450 bridges is arduous. The FDOT inspects each bridge at least once every two years, and more often when necessitated by age or structural concern. Thus, technological solutions that can make help make the bridge inspection process less costly, more efficient, and safer for personnel are paramount.

Figure 1: An example of corrosion damage caused by the diffusion of saltwater chlorides into concrete.

Bridges that span warm seawater are especially susceptible to corrosion. The "splash zone" is the section of a bridge piling or support structure at the water's surface where seawater repeatedly splashes and then evaporates in the wind and sun, leaving behind a thin residue of concentrated salt. The salt from this residue diffuses into bridge pilings and can very quickly cause steel portions of the structure (such as the rebar inside of concrete pilings) to corrode (see Figure 1) [2].

Thus, the regular examination of such bridge supports is important. However, the inspection of bridge pilings at the waterline and underwater can be difficult. Fast flowing tidal

currents, waves, strong coastal winds, and the presence of wildlife are common environmental factors that can make water-based bridge inspection difficult and sometimes dangerous for personnel. Visual and tactile examination by divers is the primary method used for underwater bridge inspection. Tactile exams become necessary when the water is turbid and human inspectors must touch or feel bridge structures to detect flaws, damage or deterioration – it can be very difficult to quantify the results of this technique [1, 3].

Given that so many bridges span rivers, canals, and saltwater areas, unmanned marine vehicles are an attractive technology for bridge inspection. There are several classes of unmanned marine vehicles, including: 1) remotely operated vehicles (ROVs), which are continuously teleoperated from a support vessel or shore base, 2) autonomous/unmanned underwater vehicles (AUVs/UUVs), which are preprogrammed to perform specific trajectories and then released to perform them without human intervention, and 3) unmanned surface vehicles (USVs), which are effectively robotic boats that can either be teleoperated or operated autonomously without human input. Trade studies of unmanned marine vehicles suggest that USVs are the most suitable for performing the entire scope of tasks required for robotic bridge inspection [4, 5]. USVs have been increasingly used in a variety of marine applications including ocean sampling, maritime search and rescue, hydrologic surveys, harbor surveillance and defense [6-11].

Manned bridge inspection is a mature field that utilizes techniques developed over generations. Human-USV teams may one day be capable of performing semi-autonomous bridge inspection with initial surveys conducted by a USV to identify possible areas of concern, with more careful, targeted surveys handled by either follow-on USV-based measurements, diver-conducted inspections or, more likely, a combination of both.

1.2 Main Research Objectives

The objectives of this effort have been to:

1. Identify which FDOT on-water bridge inspection needs and requirements might be satisfied through use of USV-based systems.
2. Assess the current capabilities of USVs to determine how they may be most effectively used for bridge inspection.
3. Perform preliminary, proof of concept, USV-based bridge inspection demonstration experiments using an existing USV.
4. Provide recommendations to the FDOT Transportation Statistics Office and the FDOT Maintenance Office for how USVs can be best used to conduct, or assist, bridge inspections.

1.3 Organization of the Report

Previous work on unmanned bridge inspection, focused on the use of marine vehicles, is reviewed in Chapter 2; current inspection practices, including tools/instrumentation and procedures, are outlined in Chapter 3; Chapter 4 presents an overview of the current state of the art in unmanned surface vehicles and acoustic sensing technologies for underwater inspection; the proof of concept USV-based bridge inspection system developed under this effort is presented in Chapter 5; the results of preliminary field tests using the proof of concept system are given in Chapter 6; and lastly a set of recommendations for the integration of USV-based bridge inspection systems into FDOT operating procedures and suggestions for future research are presented in Chapter 7.

2 Previous Research/Literature Review

The focus this literature survey is on water-based systems for inspection at the waterline and underwater, and does not consider the use of aerial [12-15] or ground-based [16- 20] unmanned systems. A review of current bridge inspection practices and the associated technologies is provided in Chapter 3 below. Here, we focus on the use of unmanned vehicles for bridge inspection.

There are several classes of unmanned marine vehicles, including: 1) remotely operated vehicles (ROVs), which are continuously teleoperated from a support vessel or shore base, 2) autonomous/unmanned underwater vehicles (AUVs/UUVs), which are preprogrammed to perform specific trajectories and then released to perform them without human intervention, and 3) unmanned surface vehicles (USVs), which are effectively robotic boats that can either be teleoperated or operated autonomously without human input. Trade studies of unmanned marine vehicles suggest that USVs are the most suitable for performing the entire scope of tasks required for robotic bridge inspection [5, 21]. USVs have been increasingly used in a variety of marine applications including ocean sampling, maritime search and rescue, hydrologic surveys, harbor surveillance and defense [7-11,22-28]. USVs have also been used to assist AUVs for studying various types of marine species, coral reefs and searching for natural resources [29].

Manned bridge inspection is a mature field that utilizes techniques developed over generations. Human-USV teams may one day be capable of performing semi-autonomous bridge inspection with initial surveys conducted by a USV to identify possible areas of concern, with more careful, targeted surveys handled by either follow-on USV-based measurements, diver-conducted inspections or, more likely, a combination of both.

Murphy et al. [5] performed a preliminary study of bridge inspection using USVs, AUVs and ROVs, in the context of hurricane recovery operations (**Figure 2**).

Figure 2: The USV (left), ROV (center) and AUV (right) tested by Murphy et al. [5].

The USV was able to transit to the inspection site autonomously, but the survey itself was conducted using teleoperation with one person responsible for controlling a DIDSON imaging sonar and a second person responsible for positioning the vehicle. The team noted several challenges with bridge inspection, most importantly having to do with localization, station-keeping and determining the relative alignment between the imaging sonar and vehicle (the sensor was knocked out of alignment during the survey). This work identified several milestones for the improvement of post-disaster bridge inspections, which are also applicable for routine bridge inspections:

1. *Standardize mission payloads.* UMVs should have an acoustic camera and a video camera to cover both high and low levels of turbidity. Given that inspection may involve slow movements close to structures, side scan sonars which rely on motion do not appear appropriate.

2. *Health monitoring.* A UMV should have sufficient sensors or encoders to correctly determine the position of its components and the overall health.
3. *Improved teleoperation through better human-robot interaction*. HRI is a significant weakness in UMVs. Studies are needed to resolve competing displays (see [11] versus [39]), while payloads such as two-way audio and extra displays can facilitate team coordination.
4. *3D obstacle avoidance.* UMVs need to avoid obstacles above and below the waterline but also consider the tides and depths. Above the waterline range sensors must be hardened to work when splashed with water. Obstacle avoidance is expected to speed navigation and improve the overall safety of operations.
5. *Station-keeping.* Significant advances in vehicle control must be made to enable station-keeping. This is expected to reduce the load on the mission specialist and engineers because they have a steady image to look at and eventually reduce the number of people involved in the robot team.
6. *Handle large data sets.* As UMVs become more successful at inspection, a huge amount of imagery and data will be generated and must be handled.
7. *Cooperative sensing.* Current systems put the responsibility for surveying the entire structure and identifying damage or scour on the human. Advances in control and in image processing should be able to ensure coverage of the structure and assist the image interpretation by cueing areas of interest. These advances in control theory and artificial intelligence would likely increase performance and the reliability of the inspections.

Some of these topics lie within the realm of advanced robotics techniques and are still in the early stages of research and development. Along these lines, some additional, related literature is

surveyed below in Section 7.2 within the context of avenues for future research for the development of USV-based bridge inspection systems.

3 Inspection Practices

3.1 FHWA

The FHWA Underwater Inspection of Bridges [30] defines three levels of underwater inspection. The minimum level for an underwater inspection is 100% Level I and 10% Level II.

Level I Underwater Inspection is a swim-by inspection at arms-length of all underwater elements of the structure. When visibility is limited the Level I inspection would consist of feeling all surfaces of the underwater portion of the structure. A Level I underwater inspection would also include looking for evidence of scour, the undermining of foundations and the exposure of normally buried portions of the structure.

Level II Underwater Inspection involves cleaning and close inspection of a limited portion of bridge structures.

A Level III inspection is a highly detailed inspection of a critical structure or structural element, or a member where extensive repair or possible replacement is contemplated. This level of inspection includes extensive cleaning, detailed measurements, and selected non-destructive and partially destructive testing techniques.

3.2 FDOT

3.2.1 Manned Bridge Inspection

Bridge inspection techniques are generally categorized along three broad lines:

1. Visual Inspection.
2. Non-Destructive Testing (NDT).
3. Material Sampling (Coring, removal and testing).

Typically, visual inspections are conducted first. Dirt and debris are removed to permit visual observation and measurement. Photography and video are used to record significant details. NDT is usually reserved for the augmentation of visual inspections in situations where additional, targeted measurements are required because an item of concern is discovered. NDT is generally not practical for large scale use on a bridge. Lastly, in cases where it is necessary to evaluate a structure before a major restoration, to search for hidden defects or to perform an analysis of the material properties of a structure, destructive testing is performed. As destructive testing typically requires that structural materials from various bridge components are sampled through coring or cutting, it is only done when necessary.

Both above- and under-water inspections must normally be conducted at least once every 24 months, but may be required more often after an unusual event (e.g., hurricanes, floods, earthquakes, fires, explosions and accidents), or when bridge components receive poor ratings in prior inspections. Moveable mechanical, hydraulic and electrical bridge components (including submarine cables) must be inspected at least once every 12 months. Note that when the depth of water is less than 3 feet, underwater inspections are not required.

Underwater bridge deficiencies and deterioration may be caused by any one or a combination of the following factors:

- Age of bridge.
- Environmental attack on bridge.
- Excessive loading of the bridge.
- Collision damage to the bridge.
- Deficiencies in the original construction of the bridge.
- Inadequate design.

- Changes in bottom elevation in and around the substructure units of the bridge due to scour or other causes.

3.2.2 Bridge Components Surveyed during Underwater Inspections

The following bridge features, at a minimum, are examined during an underwater inspection:

Pile Bents – Piles are examined for signs of deterioration or damage.

- Steel piles: Steel piles are susceptible to corrosion in the splash zone and tidal zone, and have been found to be severely deteriorated at deeper water depths. Piles that are concrete jacketed in the tidal zone must be checked for signs of corrosion from the area just below the concrete jacket all the way down to the mud line.
- Timber Piles: Timber piles are surveyed from the water line to the mud line for marine borer attacks.
- Pre-stressed Piles: Pre-stressed piles are checked for longitudinal cracking, especially hollow pre-stressed piles.
- Piles under Piers: The above also applies to piles under piers, where footing is set above a river or sea bottom.

Dolphins and Fenders – Dolphins and fenders are examined below the waterline for deterioration and borer attack, and for any damage caused by vessels or large floating objects.

Pier and Abutments – Where portions of these substructures are exposed below water, they are examined for any deterioration and any evidence of movement.

Scour – The bottom around the piers of abutments are checked for local scour. The stream bed and channel are inspected for general scour and stream shifting. All scour countermeasures are inspected.

Submarine Cables – Cables are inspected for the following:

- Damage to the cable from vessels or floating debris
- Kinks
- Exposure of the cable, when it should be buried
- The age and condition of the cable and any need for replacement
- If a cable's location is uncharted, inspectors must plot its current location.

Culvert – The stream channels of culverts are checked for erosion, scour, and alignment shifting. Culvert ends are inspected for undermining, scour and evidence of piping.

3.2.3 Advanced Bridge Inspection Techniques

Advanced bridge inspection techniques are usually utilized when inspectors want to further investigate a suspected deficiency found during a visual inspection, usually on internal bridge features that are not easily accessible. Advanced inspection methods are typically separated into two broad categories: (1) non-destructive testing (NDT or sometimes also referred to as NDE) refers to techniques that do not affect the usefulness of the bridge component being tested, and (2) other (destructive) test methods that can affect structural integrity during testing.

3.2.3.1 *Nondestructive Testing*

Nondestructive testing techniques for concrete (and steel) structures include (1) acoustic wave sonic/ultrasonic velocity measurements and laser ultrasonic testing, (2) electrical methods, (3) ground-penetrating radar, (4) electromagnetic methods, (5) mechanical impact techniques, such as delamination detection machinery, impact-echo testing and pulse velocity methods, (6)

infrared thermography, and (7) radiographic/nuclear techniques, such as neutron probes, neutron absorption, x-ray and gamma ray radiographic methods.

The large size and power requirements of ground-penetrating radar and electromagnetic methods, such as the Hermes Bridge Inspection system, may make them impractical for USV-based bridge inspection. Small sized electromagnetic sensors, such as pachometers and eddy current sensors exist and may be implemented on USVs, but they typically cover very small measurement areas (up to about 3 inches) and so may not be practical, as complete coverage of a structure would take a significant amount of time (additionally, they may difficult to use underwater when any biological growth is present). Some electromagnetic methods, such as magnetic flux leakage, work by detecting anomalies in normal flux patterns created by discontinuities in a ferrous material saturated by a magnetic field. The strong magnetic fields used in these approaches can affect navigational instrumentation (e.g., flux gate compasses) and is not recommended for use on unmanned vehicles. Since water is a conducting electrolyte and would make the outside of underwater bridge supports equipotential surfaces, electrical methods that utilize half-cell potentials (e.g., copper sulfate electrodes) to detect corrosion would have to be altered by employing reference electrodes. However, because of this the measurement system would require a hard-wired electrical connection to the bridge, which could severely limit vehicle motion. Infrared thermography works by measuring the radiant heat flux from a surface, which is a function of both its temperature and its emissivity. Above the waterline this technique might be adequate, but below the water's surface algal growth and surface discoloration of the structure due to stains from tannins and other biological agents in the water and will make the infrared data difficult to process. Radiographic techniques involve exposing a structure to penetrating radiation so that the radiation passes through the structure and is recorded on a medium (e.g., film, or a CCD

array) placed against the opposite side of structure. For thinner or less dense materials, electrically generated X-rays are commonly used, and for thicker or denser materials, gamma radiation is generally used. Use of these techniques on bridge structures in the field would require a vehicle (or multiple vehicles) large enough to mount the emitter and recording media. At this point in time, use of radiographic techniques on unmanned surface vehicles appears to be impractical, especially below the waterline.

Thus, the advanced techniques that may be most appropriate for use on unmanned systems include:

1. Acoustic Wave Sonic/Ultrasonic Velocity Measurements: Bridge abutments and concrete supports are often tested with portable, hand-held sensors (Figure 3). Existing sensors consist of an automated data acquisition system with a sound source and multiple sensors (accelerometers) to measure the propagation time of sound across the surface of a structure. The technique can be used to identify areas of internal cracking (including delamination) and deteriorated concrete. It can also be used to provide an estimate of the strength and elastic modulus of the concrete. The method can be used for detailed evaluations of large areas. It may be possible to modify existing systems so that they can be mounted on unmanned vehicles and held against bridge structures during an autonomous bridge survey

Figure 3: Acoustic sensing system [31].

2. Mechanical Impact Techniques, such as Delamination Detection Machinery, Impact-Echo Testing and Pulse Velocity Methods: These approaches generally use some sort of mechanical impact device, such as firing small metal balls at a concrete surface or tapping it with a metal sphere and measuring the structures vibrational response. Delamination Echo Machinery may be too large for an unmanned platform, but the other two techniques could be appropriate. Pulse velocity methods measure the transit time of impact-generated sound waves through a structure. They can be used to evaluate concrete quality and to estimate its compressive strength. Impact-Echo Testing techniques (Figure 4) measure the propagation rate of impact-generated low-frequency stress waves within a structure. This technique can provide more diagnostic information than Pulse Velocity methods, such as the size and location of cracks, delamination, voids, honeycombing, and debonding in plain, reinforced and post-tensioned concrete structures.

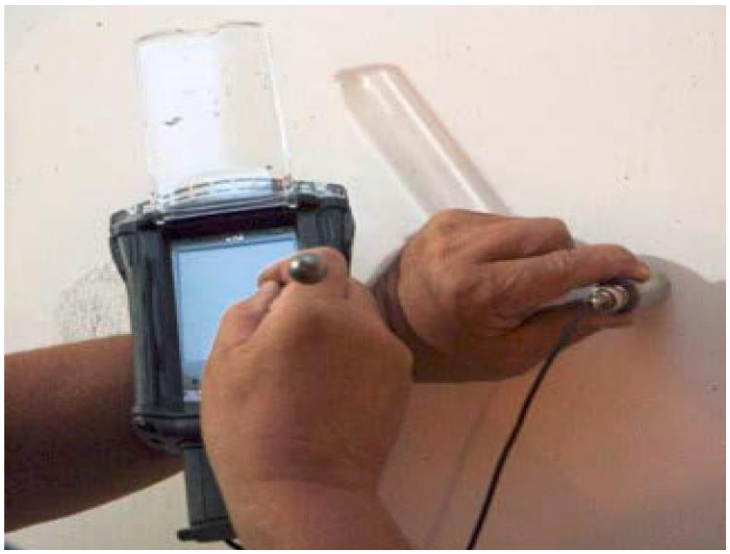

Figure 4: Impact-Echo Testing Equipment [31].

Note that, while these techniques might be most feasible for use on unmanned systems from a size, power and implementation standpoint, each of them would likely need to be modified or calibrated for use on bridges supports near or below the waterline, especially on concrete structures. Concrete is porous and water and chlorides have a tendency to diffuse into the material, changing its acoustic properties. Additionally, biological surface growth, such as oysters and mussels may need to be removed using some sort of tooling before the techniques can be applied. Additional information about these approaches can be found in [31-32].

3.2.3.2 *Other Testing Methods (Destructive)*

Other testing methods exist for measuring concrete/steel strength, steel hardness, concrete permeability, moisture content, and concrete chloride penetration, but these methods generally require the collection of sample materials from bridge structures for later analysis in the lab [31]. Sample collection techniques generally involve drilling, coring or gouging material from strategically selected sites on a bridge structure. These techniques would likely require some sort

of device that would permit an unmanned vehicle to be temporarily fixed to a structure. It is also anticipated that the tooling needed would require substantial power and that it will be preferable for a human operator to monitor, or teleoperate, the sample collection instrumentation in real time to ensure that no unnecessary or undesirable damage to bridge structures occurs. Similar operations are regularly conducted in the offshore oil industry and owing to both powering and teleoperational needs, they typically employ tethered remotely operated vehicles (ROVs), rather than autonomous systems. Thus, it is expected that the focus, at least initially, for unmanned autonomous bridge inspection systems will be on NDT and imaging (both acoustic and optical).

3.3 Tools

The underwater inspection process can be painstaking, as hand tools are used for either cleaning or measuring. For measuring, an underwater inspector may use a ruler, tape, calipers or levels. As with above portions of a bridge, visual inspection of underwater structures requires that dirt, debris and organic growth (e.g., algae, oysters and mussels) are removed. The extent of the cleaning required depends on the amount of growth encountered and the type of inspection performed. For cleaning, underwater inspectors often use a chipping hammer, a scraper, a wire brush or a small pry bar. To speed up the inspection process, power tools may be used for cleaning, drilling and cutting, and include:

- Whirl-away rotary cleaning tools. Toothed rollers are placed against the surface to be cleaned and, as their circular housing rotates, abrade the surface, cleaning back to the original material.
- Water blaster (similar to a pressure washer) is also a power tool designed for the speedy cleaning of the bridge structure to enable detailed inspection.

- Power hammers (jack hammers) are often used for cleaning or clearing debris or encrustation from substructure elements.
- Underwater power drills are commonly used to drill attachment points for protection or reinforcement of structure elements.
- Underwater saws (a submersible version of a circular saw).
- Underwater cutting torches (for cutting steel, concrete or wood).

The results of underwater inspections are documented using:

- Underwater paper and pens may be used by the underwater inspector to document the inspections findings.
- Voice communication between the diver and a topside note taker. The diver may communicate the inspection findings during the inspections. The note taker should repeat the findings to the diver to verify the findings.
- Voice recording may be made and transcribed later.
- Underwater cameras or video cameras may be used.

3.4 Procedures

3.4.1 General

At each bridge inspection site, a Lead Underwater Inspector oversees each underwater inspection team. An example of inspection divers can be seen in Figure 5. The teams consist of the Lead Underwater Inspector (who must be a Florida certified DOT diver), one or more additional certified DOT divers, a tender (who is responsible for ensuring that the dive profile is followed and that the dive station is maintained), and a boat operator, who is competent at small boat handling. The Lead Underwater Inspector is responsible for coordination with other known

activities in the inspection area, briefing the team members and planning the dive operation. The size of an underwater inspection team varies, depending on the visibility of the water, the depth and whether or not air is supplied from the surface. In all cases at least one or two standby divers are required in case of emergency. When diving in enclosed or confined inspection areas, which are not large enough to accommodate two underwater inspectors, at least one inspector must be stationed at the underwater point of entry and an orientation dive line used. The use of surface supplied air is preferred for these situations.

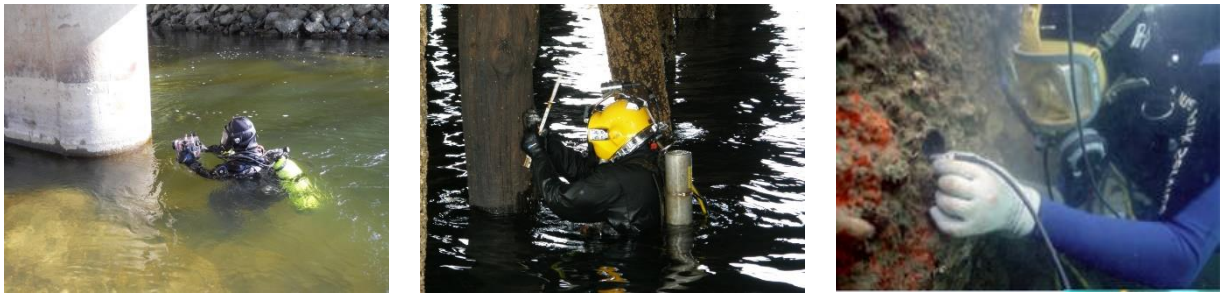

Figure 5: Water-based bridge inspection by dive teams.

The three levels of underwater inspection explained in Section 3.1 above would normally be conducted.

3.4.2 Underwater Bridge Inspection Equipment

The underwater inspection process can be painstaking, as hand tools are used for either cleaning or measuring. For measuring, an underwater inspector may use a ruler, tape, calipers or levels. As with above portions of a bridge, visual inspection of underwater structures require that dirt, debris and organic growth (e.g., algae, oysters and mussels) are removed. The extent of the cleaning required depends on the amount of growth encountered and the type of inspection performed. For cleaning, underwater inspectors often use a chipping hammer, a scraper, a wire brush or a small

pry bar. To speed up the inspection process, power tools may be used for cleaning, drilling and cutting, and include:

- Whirl-away rotary cleaning tools. Toothed rollers are placed against the surface to be cleaned and, as their circular housing rotates, abrade the surface, cleaning back to the original material.
- Water blaster (similar to a pressure washer) is also a power tool designed for the speedy cleaning of the bridge structure to enable detailed inspection.
- Power hammers (jack hammers) are often used for cleaning or clearing debris or encrustation from substructure elements.
- Underwater power drills are commonly used to drill attachment points for protection or reinforcement of structure elements.
- Underwater saws (a submersible version of a circular saw).
- Underwater cutting torches (for cutting steel, concrete or wood).

The results of underwater inspections are documented using:

- Underwater paper and pens may be used by the underwater inspector to document the inspections findings.
- Voice communication between the diver and a topside note taker. The diver may communicate the inspection findings during the inspections. The note taker should repeat the findings to the diver to verify the findings.
- Voice recording may be made and transcribed later.

Underwater cameras or video cameras may be used.

4 Status of Technologies

4.1 Unmanned Surface Vessels

As noted in [7], surface vehicles are well-suited for unmanned, autonomous bridge inspection as they have important advantages over underwater vehicles: they can be more accurately controlled and localized through GPS, they can carry a larger payload, and they can continuously broadcast imagery data to observers in real-time.

4.1.1 Concept of Operations

It is anticipated that one of the main uses of USV-based bridge inspection systems will be for performing an initial survey of the underwater structure, the surrounding river bottom or seafloor, and the structure at and slightly above the waterline. The survey will be used to help inspectors identify areas of concern that a dive team should focus on and to understand when more targeted inspection, NDT, and destructive testing techniques might need to be later applied. Current underwater bridge inspection teams consist of about 3-5 people. The USV-based bridge inspection system will be deployed at bridge sites by a team of comparable size. Possibly, dive teams that currently perform underwater survey could be trained to also use a USV-based bridge inspection system or supplemented with one or two more people, who specialize in the use of the USV-based system. The system will be deployed at remote or difficult-to-access sites from a light truck (e.g., pickup or van) and tended on the water by a small vessel, such as a john boat. It will be possible to launch the system from a small boat ramp, when available, or to be disassembled and carried to the water on foot. As part of its normal pre-inspection routine, the inspection team would use its knowledge of the bridge site and the results of prior inspections to select specific positions

(waypoints) and corresponding bridge features that the USV-based system will be preprogrammed to survey. During the survey, the system will autonomously transit to the inspection site and then travel through the desired waypoints while performing its measurements. It is likely that some measurements may require the vehicle to maintain a fixed position and orientation, thus the vehicle will have the capability of 'station-keeping' for several minutes at a time. For both safety and efficiency reasons, the system will have sufficient automatic obstacle avoidance and reactive trajectory planning capabilities so that it does not need to be continuously monitored by the inspection team. At the same time, the system maintains constant communications with the inspection team and relevant data are displayed in an easy to interpret user interface, so that its progress can be monitored and it can be temporarily teleoperated or redirected to an area of interest by the inspectors, whenever necessary. Telemetered data are recorded at the inspector's base station. Additionally, the sensor measurements, photos and video are recorded on board the USV to be downloaded later for more detailed post-processing and reporting. When a survey is complete or terminated by the inspection team, the USV can autonomously return to the launch point at shore. It would then be retrieved from either a boat ramp or on foot (after disassembly) and reloaded onto its light truck for transport.

4.1.2 Functional Considerations for System Design

The design of any system is driven by a combination of (often competing) requirements that ultimately determine its final configuration [33]. The design requirements for unmanned vehicle based bridge inspection systems can be formulated taking into account the following basic considerations, among others:

1. Environmental Conditions:
    a. USV-based bridge inspection systems will be deployed in tidal waters and rivers where currents can be strong. For example, it is common for tidal currents to approach 4-5 knots under bridges in the U.S. Intracoastal Waterway near Port Everglades in Dania Beach, FL. Unmanned inspection vehicles will need sufficient thrust to maneuver, and possibly hold position, in strong currents for the duration of an inspection mission.
    b. The river waters flowing from inland to offshore often carry an abundance of vegetation, which can produce tannins that can reduce underwater visibility by giving the water a dark brown/tea color. Fast flowing waters can also transport a significant amount of silt, debris, and other organic matter, which reduces visibility. Thus, unmanned inspection systems will need the capability to operate in waters where visibility may only be a few inches (as low as 2-3 inches).
    c. Marine growth often vigorously attaches itself to underwater structures. Technologies that permit the visualization of bridge structures through at least some common forms of marine growth, such as algae, are beneficial.
    d. Unmanned marine systems performing underwater inspection may also be affected by waves when operating in coastal waters, or by the wakes of fast moving vessels when used in areas with substantial boat traffic.
    e. Bridges located in coastal or open areas often experience a ‘wind-tunnel’ effect where air speeds up as it passes underneath and around the bridge structure. Strong winds can affect an unmanned vehicle’s ability to accurately maneuver along a desired trajectory or to station keep.

f. Debris can sometimes collect at the base of bridge supports, especially after flooding. The USV should have a design (low draft, ducted propellers, etc.) and automatic control system that reduces the likelihood of snagging on underwater obstacles.

g. The system should be capable of operating in water depths of 3’-25’.

2. Sensing Considerations:

   a. It is expected that acoustic imaging technologies would be the most appropriate for visualization. The size, weight and powering requirements of these systems must be accommodated.

   b. Additionally, an unmanned vehicle used for bridge inspection must have the capability of accurately knowing its position and orientation, so it is precisely understood to which parts of a bridge’s structure a measurement corresponds. The large amount of metal in bridge structures can adversely affect sensors, such as flux gate compasses, so that heading information is not accurately known. One other possible issue is that positioning sensors, such as GPS systems, can require line of sight with overhead satellites. When passing under or near large bridges, the reception of GPS signals can be adversely affected [34]. Use of an acoustic imaging sensor across a long distance (6-30 feet) may require measurements to be motion compensated or the platform to be dynamically positioned (station keeping). This may involve the mounting of additional instrumentation, such as a precise inertial measurement unit (IMU), very close to the sensor itself.

c. As described above in Section 3.2.1.2, the use of NDT technologies can place additional placement requirements on an unmanned vehicle, such as the ability to temporarily affix itself to a structure during a measurement.

3. Deployment Considerations:
    a. Current underwater inspection teams consist of only 3-5 people. It would be desirable if the same team could operate an unmanned system during the course of their work, or if the system were deployable by a separate team of comparable size.
    b. Given that some bridges are remotely located or difficult to access (owing to vegetation, traffic, etc.), it would be desirable for the system to be small enough and light enough to be deployed from a small truck and tended on the water by a small vessel, such as a john boat.
    c. As mentioned in Section 4.1.1, the system should be sufficiently autonomous so that it does not need to be continuously monitored by the inspection team. It should also permit teleoperation or user redirection to areas of interest. After any interruption, the system should be capable of autonomously resuming its normal operation.
    d. The system should have the capability of constant communications with the inspection team. When communications drop out, the system should automatically reconnect as soon as conditions permit.
    e. The system should have a user interface that allows an operator to view measurements in near real time, in bright sunlight and in normal outdoor working conditions. The user interface should be capable of providing sufficient information

and a balanced operator workload, so that bridge inspectors can make clear, well-informed decisions about the results of a survey as they come in.

f. During on water travel to a bridge inspection site the vehicle may need to operate in the vicinity of other boat traffic. In such a circumstance, the ability of the system to autonomously interact with other vessels according to COLREGs rules could be very useful. In addition, it may be necessary for the unmanned system to be capable of obstacle avoidance, to avoid collisions with stationary obstacles, such as bridge supports, dolphins or underwater debris.

4.1.3 Hullform Design Considerations

From a design standpoint, one of the main advantages USVs have over manned vessels is that their configuration does not need to accommodate the space and safety requirements of human operators. Because of this, USV design can be more highly optimized according to sensing, maneuvering or deployment requirements. Thus, USVs come in a wide variety of hull forms [7], [35-36], from Small-Waterplane Area Twin Hull (SWATH) vessels [11], [37] to wide-bodied tug-shaped boats [38].

USV design is sometimes mainly driven by sensing or automation considerations. Unfortunately, a very important, but often overlooked, component of USV design is hullform selection. The shape of the USV's hull has a tremendous impact on how much power is required to drive it through the water, which, in turn, affects the amount of time the system can be operated. The hullform also has an impact on the USV's seakeeping ability (response to waves), maneuverability (turning and straight line tracking motion) and overall suitability as a sensor platform. Often hulls are selected based solely on cost or availability, when substantial performance improvements can be obtained through a more careful consideration of the hullform.

A non-dimensional parameter called the Froude number is typically used to determine the most appropriate hullform for a vessel and is defined as

$$F = \frac{U}{\sqrt{gL}},$$

Where U is the desired operating speed, g is gravity and L is the length of the hull. Thus, a combination of vessel speed and hull length determine the operating Froude number of a USV. Hullforms are categorized along three broad lines according to Froude number [39]:

1. $F < 0.4$ Displacement hulls: These tend to be very rounded. During operation, most of the weight of a displacement vessel is supported by the amount of water displaced. When operated at $F \geq 0.4$ the water resistance becomes very large and a substantial amount of power is required for propulsion.
2. $0.4 < F < 1.0$ Semidisplacement Hulls: This type of hullform tends to be long and slender with a fine (sharp) bow, long straight midsection and blunt stern.
3. $F \geq 1.0$ Planing Hulls: This type of hull tends to be short and blunt with a series of sharp corners called chines that run longitudinally along its length. Because of their sharp corners, planing hulls tend to be very inefficient at low speeds.

If it is assumed that a bridge inspection system may need to be operated in currents as high as 4-5 knots, then in order for the vehicle to make way against the current, it is desirable that it be capable of moving with a speed as high as 8 knots relative to the water. If the USV must be small enough that it can be transported by light truck and handled by a small team, then hulls no longer than about 14 feet would be desired. Based on this combination of vessel speed and length, the maximum operational Froude number of the USV will be about $F_{max} \approx 0.7$. Given that the vessel may be operated at values this large, it would be undesirable to use a displacement hull. Also, since

planing hullforms would have more drag at low Froude numbers, a planing hull is not appropriate. The hullform most compatible with use in USV based bridge inspection is the semidisplacement hull. The most common types of displacement hullforms include monohull (single hulled) vessels, catamarans (double hulled), trimarans (triple hulls) and SWATH vessels. Given that a USV-based bridge inspection system will need to be based on a fairly stable platform, with minimal wave- or current-induced motion, catamaran, trimaran and SWATH hullforms are preferable to monohulls. Trimarans tend to be stable, but are heavier, susceptible to wetdeck slamming in waves, and can be difficult to maneuver [40]. Thus, SWATH vessels and catamarans appear to be the best choices for USV-based bridge inspection systems.

4.1.3.1 *SWATH Vessels*

As shown in previous studies [11], [37], SWATH vessels have good seakeeping properties and can provide nice stable platforms for bathymetric survey and sensing. One added benefit is that their large underwater hullforms tend to have a long straight keel, which can be convenient for mounting wheels or treads on so that the vehicle can be operated amphibiously on both land and water [37] (**Figure 6**). This feature can make deployment easier in hard to reach locations. A disadvantage of SWATH vessels is that they tend to have a large draft, which can increase drag and make passage in areas with underwater debris difficult.

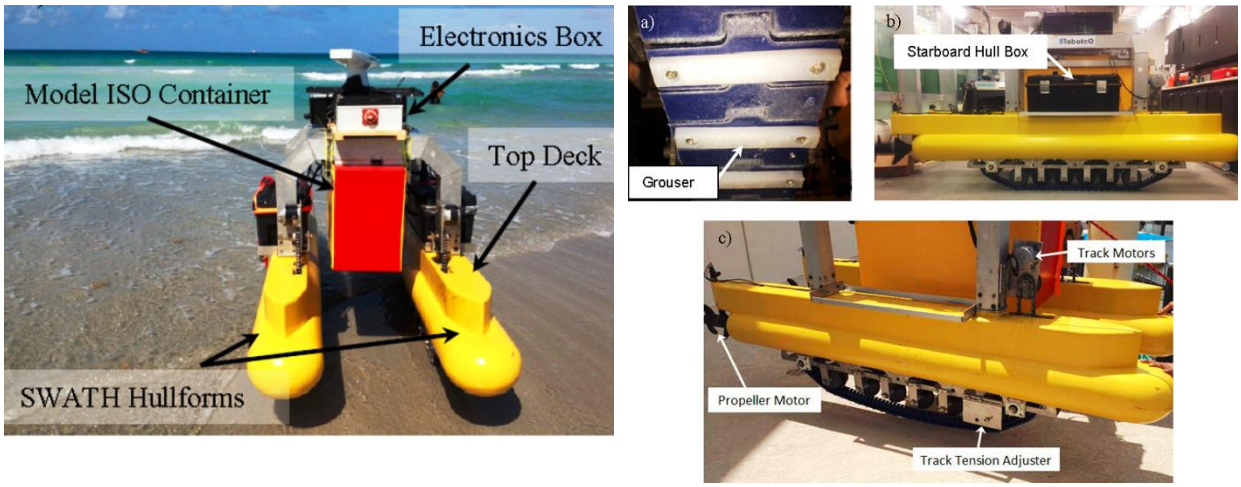

Figure 6: The DUKW-Ling Amphibious USV [37].

4.1.3.2 *Catamaran Hullforms*

Catamarans may be the best all-around choice of hullform to use for the range of conditions expected during USV-based bridge inspection. They have: low drag characteristics over the range of operational Froude numbers expected; can provide a stable sensor platform, which can further augmented through the use of advanced suspension techniques (**Figure 7**) to provide good seakeeping characteristics [41-43]; can be easily configured with dual propellers at each transom stern to use differential thrust for maneuvering, which simplifies control and improves maneuverability.

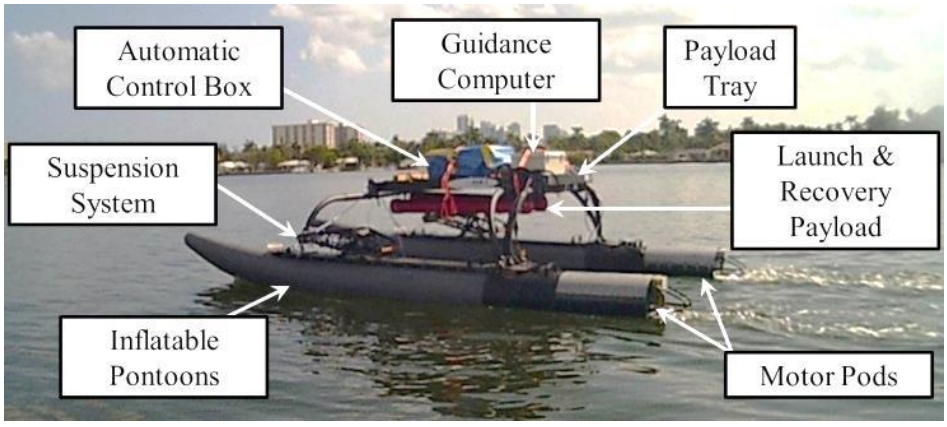

Figure 7: The USV14 configured for a simulated AUV launch and recovery experiment [44].

4.1.4 Propulsion System Design Considerations

In principle, both waterjet and propeller based propulsion are well-suited for bridge inspection USVs. An advantage of using waterjets is that they can be configured to be operated near the maximum efficiency of a DC motor without the need for gearing [44-45]. Waterjet systems also have a lower draft than propellers as their inlets can be configured to be flush with the bottom of the hull, whereas propellers must be submerged at least one propeller diameter beneath the waterline to prevent ventilation [46]. However, small, low speed waterjets are not common place, so that waterjet propelled USV designs tend to utilize RC hobby systems, which suffer from low mechanical reliability and can be easily damaged by the intrusion of waterborne debris, such as mangrove seeds and twigs. Waterjets designed for jetskis are more robust, but are intended for higher operational speeds (~55 knots max.) and so are not well-suited to the much lower speeds (~8 knots max.) expected to be appropriate for bridge inspections.

Some propeller systems, such as electric trolling motors [37,47-48], are a good choice as they are mass produced for the recreational fishing industry, relatively inexpensive ($200-$300), widely available, and are designed to be operated over the range of speeds required for USV-based bridge inspection. One drawback of trolling motors is that they should be augmented with an add-on duct or fairing as they are generally produced without one and can be a danger when operated near divers. An additional option would be to purchase ducted propellers designed for underwater ROVs. While these are usually fairly rugged and provide a substantial amount of thrust, they tend to be expensive.

4.1.5 Powering Considerations

A power-related systems engineering issue of importance for transport is the type of battery storage to be used on-board the USV. LiPo batteries are lightweight and well-suited for unmanned systems

but are considered hazardous materials and can be difficult and costly to ship. Some manufacturers, such as Torqueedo are now regularly shipping large LiPO battery packs with their small boat propulsion systems. These appear to be fairly robust but are more costly (~$5,000 each) than other alternatives, such as AGM lead acid batteries. Deep cycle marine AGM lead acid batteries are inexpensive (~$300 worth of batteries would propel a 14-foot vessel for about 6 hours) and can be purchased at almost any auto parts store. However, their high weight reduces the amount of instrumentation/payload that can be carried aboard the USV and makes deployment more cumbersome. Possible powering configurations to consider for the future development include the use of hybrid fossil-fuel/electric power [49] and the use of hydrogen fuel cells [50-51].

4.1.6 USV Imaging, Autonomy, and Control Considerations

Today, unmanned surface vehicles (USVs) are not truly capable of ``persistent autonomy´´ due to the wide variety of tasks they must perform and the complexity of their operating environments. It is likely that early versions of a USV-based bridge inspection system will rely on relatively simple autonomous systems that use scripted operations and waypoint tracking to perform surveys. However, in the long run there are several developing technologies that should be brought to bear to make the operation of such systems robust, reliable and easy to use for bridge inspectors to use.

4.2 Remote Sensing/Imagery

Underwater imaging techniques include both optical and non-optical technologies [52]. Optical approaches include underwater photography and underwater videography. Non-optical techniques include sonar (acoustic), laser and radar systems.

The image quality of optical systems is strongly affected by turbidity. Additionally, the camera range and lighting of photographic and videographic systems often prohibit a panoramic

view, so that only two dimensional perspectives are possible. Thus, non-optical technologies perform better for underwater bridge inspection [53].

Laser techniques, such as scanning LiDAR, can produce accurate underwater images, but possess limited range in turbid water [54-55]. It is more widely used in the inspection of offshore structures were water clarity is less of an issue. Current research has focused on combining LiDAR with photographic and acoustic techniques to produce high quality images.

Radar technologies can produce underwater images of internal defects, such as cracks in concrete structures or subsurface channel-bottom geotechnical strata layers, and Synthetic Aperture Radar (SAR) can be used to image large areas of seafloor topography [53].

Of all of the approaches, acoustic imaging techniques appear to have the most promise for underwater bridge inspection, as they can be used in very turbid waters. Sonar imaging techniques can be broadly classified as either 3D or 2D techniques. 2D systems tend to have the best definition when the angle of incidence is very high and 3D systems work better when the angle of incidence is low [53]. Sonar imaging techniques appear to be most promising for: the rapid assessment of a bridge's underwater structure; scour detection and documentation; underwater construction inspection; and enhancing diver safety and efficiency at challenging dive sites.

4.2.1 3D Acoustic Imaging Systems

1. Fathometers/Echosounders are single beam sonar systems that can be used to measure depth. When combined with GPS, they can be configured to collect three dimensional depth maps of a channel. Operating frequencies typically range from 24 kHz to 340 kHz. Frequencies near 200 kHz are most typically used as sub-bottom penetration is not normally desired. The three dimensional depth maps can be used to quantitatively identify

scour depressions, areas of aggradation, and channel-bottom objects, such as exposed pier footings or debris accumulation. Through the use of multi-mission mapping, profiles from successive underwater bridge inspections can be overlayed and compared to detect possible channel-related problems. Drawbacks to the use of fathometers are that: they cannot be used to collect data outside the path of the vessel transporting the transducer; when used in deep water the sonar operator must be careful not to confuse an exposed bridge footing or other submerged obstruction with the channel bottom.

2. Multi-beam swath sonar systems produce detailed mapping in a beam which is very thin in the longitudinal direction, but very wide in the transverse direction (swath width). Most systems are boat-mounted and require forward motion of the vessel to cover a large area of the seafloor. The operating frequencies of multi-beam systems is generally in the rage of 0.7 MHz to 1.8 MHz. The swath width of the beam is generally about 7 times the water depth. Since the direction of the beam can change with the attitude of the vessel, swath sonar data must be motion compensated. The main advantage of swath sonar is that it can quickly produce large quantities of three dimensional data, which can be used to document spalling, scaling and foundation undermining (**Figure 8**). Drawbacks are that the large amount of data can be time consuming to post process, the associated motion compensation techniques require more complex instrumentation, and it is difficult to smoothly transition from acquiring channel bottom data to data along the face of a vertical structure when a swath system is mounted in a downward looking configuration.

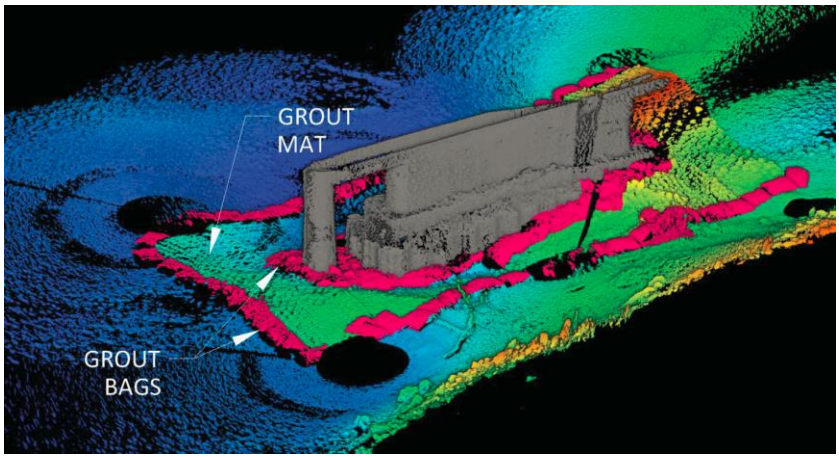

Figure 8: Multibeam sonar image of bridge undermining repaired with grout bags [53].

3. Real-time multi-beam Sonar systems are modified versions of multi-beam swath sonars that use many rows and columns of narrow beams (**Figure 9**) to produce three-dimensional images that are updated in real time. Images are produced with a high frame rate, similar to watching a video. The systems are designed to be mounted from a small boat and can be easily adapted to unmanned systems, such as ROVs and USVs. One advantage of these systems is that multipath imaging errors are reduced because scanned objects are continuously esonified from different angles, resulting in datasets with lower acoustic noise and fewer acoustic shadows. As with swath sonar systems, measurements must be motion compensated.

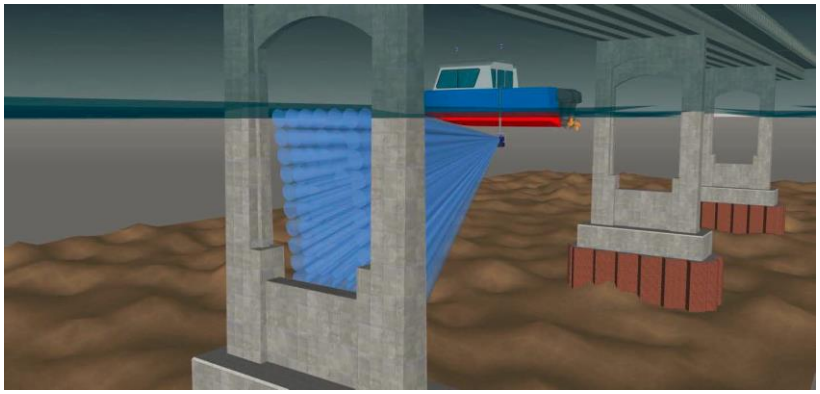

Figure 9: Real-time multi-beam sonar beam pattern [53].

4.2.2 2D Acoustic Imaging Systems

2D imaging sonars use fan-blade-shaped acoustic beams coupled with forward motion of the system to produce an image. When the images are stitched together along the direction of travel, they form a continuous image of the bottom and any objects located there or in the water column. The beam is typically narrow in one dimension (about 1^{o}) and wide in the other (about 35^{o}-60^{o}).

1. Side-Scan Sonar systems typically operate at frequencies between 83 kHz and 800 kHz. Side scan sonar can be used to quickly and efficiently obtain images of large areas of a channel bottom and is the tool of choice for large scale search operations. Imagery can be used for delineating exposed sediment, the detection of underwater debris and determining the location and configuration of submerged structures, pipelines and cables. Limitations to the use of side scan sonar include difficulty in mapping vertical structures and that image quality is partially dependent on how well a constant speed can be maintained in a direction transverse to the beam and on motion compensation for environmentally-induced roll or pitch oscillations of the scanning vehicle.
2. Sector-Scanning Sonar works similarly to side scan sonar, however, the system is typically mounted from a fixed location and the sensor is rotated to produce images. Scanning sonars typically operate at frequencies in the range of 330 kHz to 2.25 MHz. The frequency most commonly used for bottom channel mapping and structural imaging is about 675 kHz. The primary advantage of scanning sonar is its ability to obtain detailed images that extend from the channel bottom to waterline. The disadvantages of this technique are that it requires a stable mounting position and that image quality can strongly depend on sonar positioning and stability.

4.2.3 Environmental Considerations:

1. Turbidity can affect results at certain sonar frequencies.
2. Current can affect the positioning and deployment of sonar heads.
3. Marine growth, such as mussels, can obstruct the detailed imaging of structures. However, it is usually still possible to obtain images of sufficient quality that the overall condition of bridge structures can be assessed.
4. Air bubbles suspended in the water column, trapped by turbulence or eddies in fast-flowing water near a bridge, can limit the ability to collect sonar data.
5. Very deep water can result in low resolution images, and very shallow water can produce multipath errors in the sonar images. Knowledge of the inspection site and equipment is important for assessing the feasibility of using sonar at each bridge site.

5 Proof of Concept

5.1 Hardware

5.1.1 The WAM-V USV16 Platform

The USV used here is a 4.9-m (16-foot) Wave Adaptive Modular-Vessel (WAM-V), the USV16 (Figure 10). It is a twin hull, pontoon style vessel designed and built by Marine Advanced Research, Inc. of Berkeley, CA USA. The vessel structure consists of two inflatable pontoons, a payload tray connected to the pontoons by two supporting arches and a suspension system. The USV16 is designed to mitigate the heave, pitch and roll response of the payload tray when the vehicle operates in waves. The vehicle's physical characteristics are shown in Table 1.

.

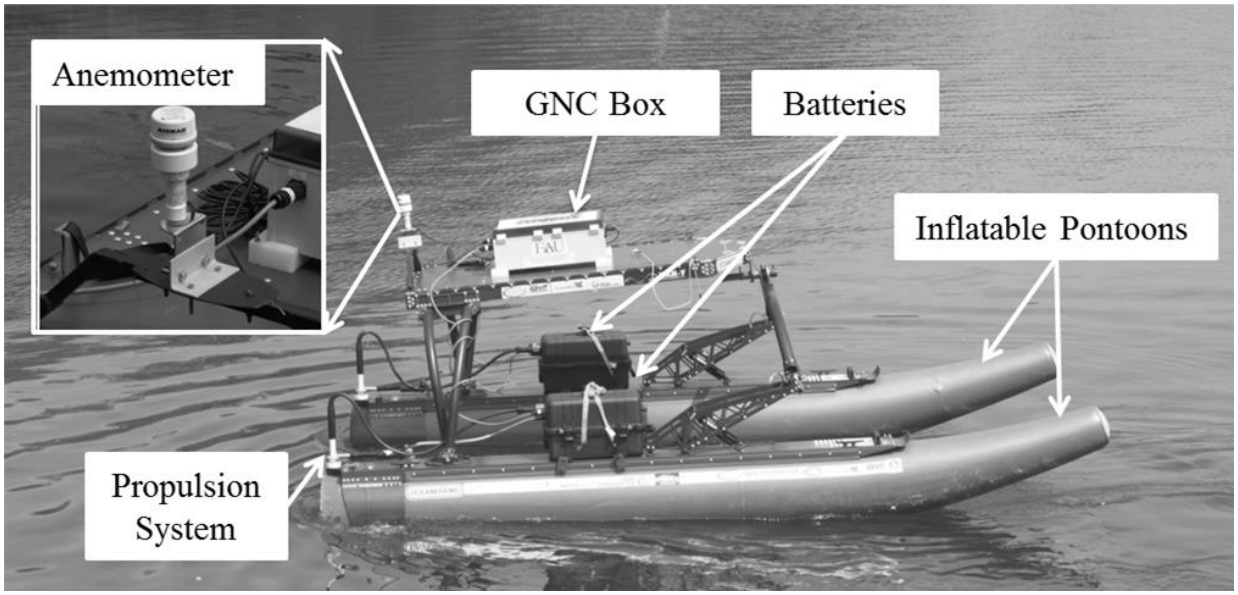

Figure 10: The WAM-V USV16 during on-water station-keeping tests in the Intracoastal Waterway.

Table 1: Principle characteristics of the WAM-V USV16. the location of the "keel" is taken as the bottom of the pontoons. w.r.t. is an acronym for the phrase "with respect to".

Parameter	Value
Length overall (L)	4.05 [m]
Length on the waterline (LWL)	3.20 [m]
Draft (aft and mid-length)	0.30 and 0.23 [m]
Beam overall (BOA)	2.44 [m]
Beam on the waterline (BWL)	2.39 [m]
Depth (keel to pontoon skid top)	0.43 [m]
Area of the waterplane (AWP)	1.6 [m^2]
Centerline-to-centerline side hull separation (B)	1.83 [m]
Length-to-beam ratio (L/B)	2.0
Volumetric displacement (∇)	0.5 [m^3]
Mass	180 [kg]
Mass moment of inertia about z axis (estimated with CAD)	250 [kg-m^2]
Longitudinal center of gravity (LCG) w.r.t. aft plane of engine pods	1.30 [m]

5.1.1.1 *Propulsion System*

A fully-actuated azimuthing propulsion system was already available on the USV16. However, the existing system had to be modified to accommodate the higher voltage of the batteries needed for the new thrusters. The original design included two 30 pound electric thrusters, each powered by a separate 12 volt lead acid battery, and two 35 pound, 6 inch stroke, linear actuators capable

of rotating the thrusters through an azimuthal angle of $\pm 45^{o}$ with respect to the vehicle's longitudinal direction (Figure 11).

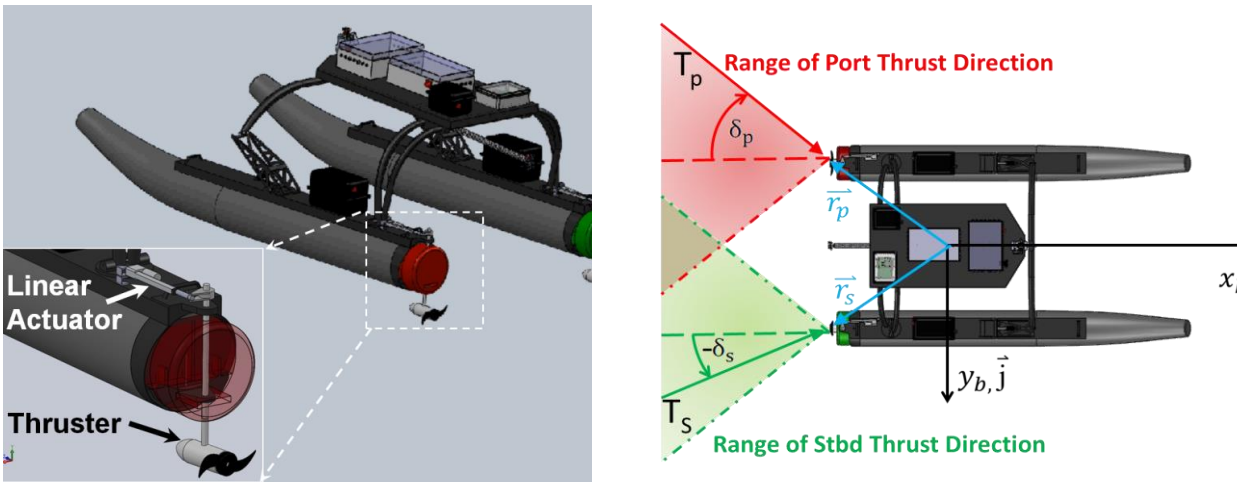

Figure 11: Left: Linear actuator and azimuthing thruster configuration for the WAM-V USV16. Right: Range of thrust distribution on the WAM-V USV16; the direction of thrust can also be reversed, when needed.

With this configuration the thrust on each hull (T_p and T_s) can be directed in various directions based on the azimuth angle on each side (δ_p and δ_s), enabling the vehicle to output multiple combinations of forces and moments. The moment is calculated based on the moment arms ($\vec{r}_p$ and $\vec{r}_s$), shown in Figure 11.

The thrusters on the pre-existing system were upgraded to a set of two 55-pound, 24 volt Minn Kota thrusters. These changes necessitated increasing the size of the motor power cables from 12 AWG to 8 AWG, changing the power supply batteries from 12 volt lead acid to a pair of 36 volt LiNiMnCo batteries, changing the motor controllers and installing a step down voltage converter from 36 volts to 12 volts to provide power for the existing linear actuator motor controllers. All electronic modifications were performed in the FAU SeaTech electronics shop. When the thrusters were converted from a 12 volt to 24 volt system, we first explored the continued use of lead acid batteries, as they are cheaper and more readily available, but it was felt that adding

an additional 12 volt lead acid battery to each hull would increase the weight of the system too much. The PI had a pair of 36 volt 30 Ah (Amp-hour) LiNiMnCo batteries available from a previous USV project, so these were utilized to save development time (Figure 12). Each thruster is driven by a separate thruster. When the motor voltage was increased, the motor controller used to drive each thruster also had to be changed. The original system used a pair of Roboteq LDC1430 motor controllers. These were changed to a pair of Roboteq MDC 1460s. These particular models were selected, as the lab has had a significant amount of experience using similar systems, they are compatible with our existing system and they required only slight configuration changes in firmware settings for implementation on our vehicle. In order to save costs on the development of the hydraulically actuated sonar boom (described in the task2B deliverable), we repurposed one of the existing Roboteq LDC1430 motor controllers for use on the sonar deployment system.

Figure 12: The LiNiMnCo 36 V, 30 Ah batteries.

A pair of 12-volt Firgelli FA-PO-35-12-06 linear actuators capable of producing 35 pounds of force with a 6-inch travel are used to rotate the thrusters to provide maneuvering forces along different desired directions (see Figure 11 and Figure 13). As the linear actuator controllers use a 12-volt power input (the linear actuator motors themselves are 12-volt units), a step-down voltage converter from 36 volts to 12 volts was also installed in the propulsion control box. We initially had installed a step-down voltage converter manufactured by Power Sources Unlimited, but found that the system had an excessive amount of noise with the device so that when the thrusters were commanded to produce large thrust, the linear actuators would start to chatter. We replaced the units from Power Sources Unlimited with a pair of Murata UWE-12/10-Q48NB-c step down voltage converters (one for each battery) and found that the chattering issue with the linear actuators was resolved.

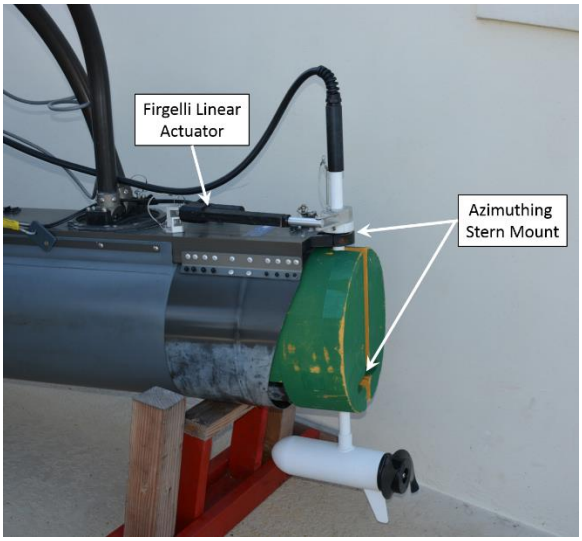

Figure 13: Final configuration of azimuthing thruster.

All of the components described above are housed in the same propulsion unit control boxes, previously used on the USV16 with the 30-pound thruster system Figure 14. The cases used are Pelican 1460 IP67-rated watertight boxes, modified with the addition of bulkhead connectors and foam padding to accommodate the batteries and electronics needed for each propulsion system. Also incorporated into each propulsion control box is a large push button-activated kill switch that permits users to cut power to the propulsion system without also shutting off power to the vehicle's guidance, navigation, and control (GNC) system. This permits us to quickly stop the propellers (and the boat) should there be an electronic or software malfunction, without damaging

the much more sensitive computer systems and instrumentation responsible for GNC of the vehicle. The system is configured such that actuation of either kill switch will shut off both propellers. When pressed, the each kill switch activates a pair of solid state relays (Crydom D06100) that creates an open circuit in the battery supply to the thruster Roboteq motor drivers. Back emf produced by the motor when power is cut, is dissipated in a diode-resistor circuit at the battery input, as well as within the Roboteq (the system is designed by the manufacturer to accommodate rapid shutoff). Additionally, a 60 Amp circuit breaker is installed to help prevent any damage to the Roboteq motor controller, solid state relay and Firgelli linear actuator controllers from unintended power surges.

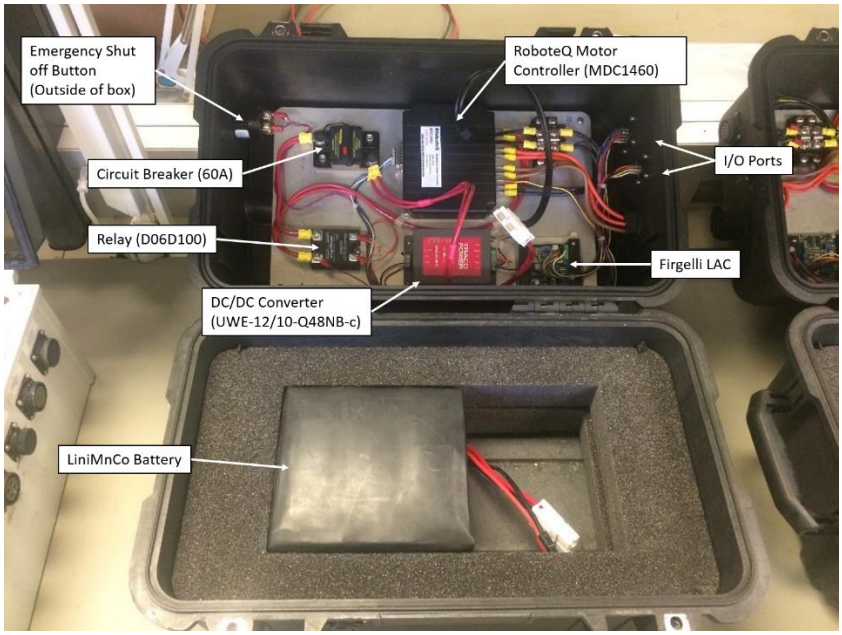

Figure 14: One of two modified propulsion system control boxes (one for port side and another for starboard side).

Mechanical modifications to the existing vehicle were minimal. It was possible to mount the new 55-pound thrusters using the same stern transom mounts used for the original 30 pound thrusters. In addition to the thrusters themselves, the only new mechanical hardware required was a pair of 42 inch long by 1 inch diameter fiberglass tubes that served as propeller shafts (Figure 15) and a pair of Weedless Wedge II propellers (Part number IND 2091160 WDLS WDG II). In the FAU SeaTech machine shop the propeller shafts were cut down to 32 inches and glued into the fitting at the top of each thruster. The leads for the thruster motors are routed through the propeller shaft and connected to the propulsion unit boxes through a large cable connector (Bulgin 900 Series Buccaneer PX0911-PXA911 Flex Cable Connector).

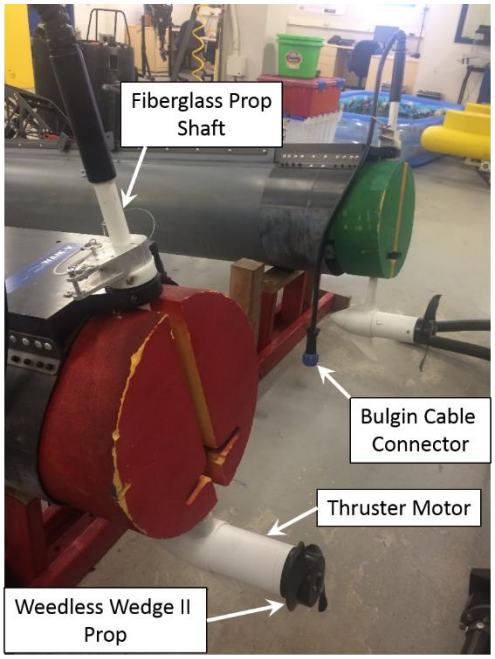

Figure 15: 55-pound thrusters mounted on USV16.

In order to validate the performance of the revised propulsion system, a series of Bollard Pull Tests were performed in the FAU SeaTech Marina. In brief, a "Bollard Pull" is a frequently used experiment to measure of the thrust-producing capability of a watercraft propulsion system. The USV16 was moored to a pier piling using an in-line force transducer to measure the amount of thrust produced by the vehicle under different commanded motor power. The vehicle was situated with sufficient clearance along the sides and bottom of the vehicle to ensure that there would be a continuous flow through of water around the propellers. A computer was used to set the commanded thrust from 10% of full power through to full motor power. For each motor command the force generated in the mooring line was continuously measured over a period of 30

seconds. The tests show that the thrust provided by the revised propulsion system gives about a 60% increase in available thrust (97 pounds versus 60 pounds); see Table 2, Figure 16 and **Figure 17**. The recorded values were used to determine the magnitude of the desired motor commands in the control system software.

Table 2: Forward and reverse thrust generated in a series of Bollard Pull tests for a range of commanded motor values.

Forward Thrust		Reverse Thrust	
% Motor Command	Thrust (lbs)	% Thrust	% Motor Command
10	0	-10	0
20	0	-20	0
30	5	-30	-2
40	15.5	-40	-8.5
50	25	-50	-17
60	37	-60	-26
70	53	-70	-35.5
80	66	-80	-48
90	84	-90	-57.5
100	97	-100	-70.5

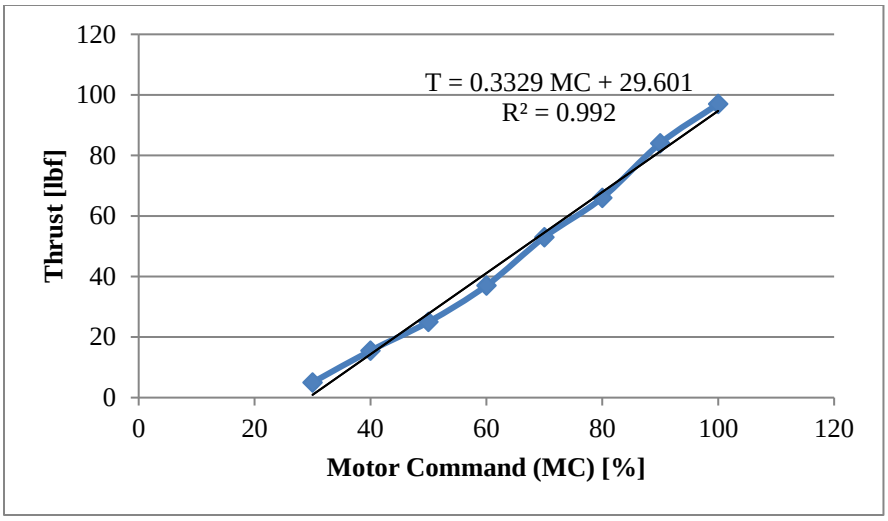

Figure 16: Measured thrust vs. motor command for forward Bollard Pull test.

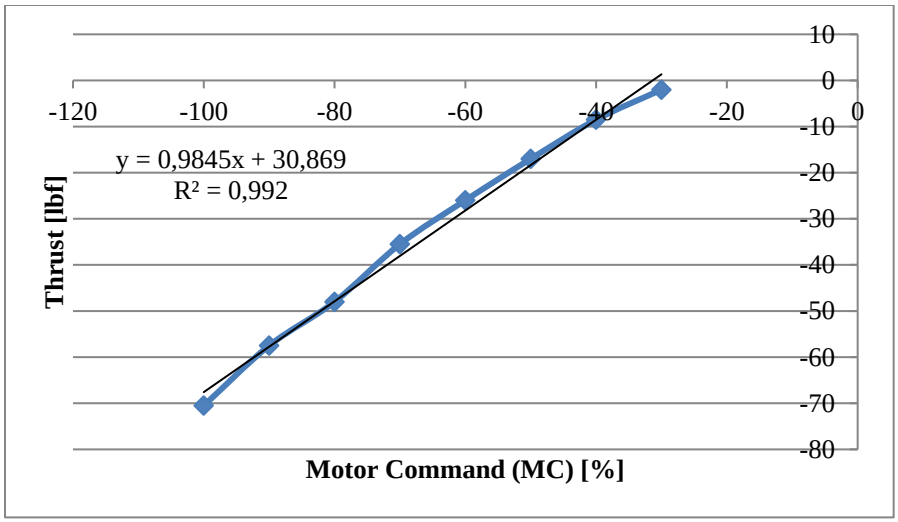

Figure 17: Measured thrust vs. motor command for reverse Bollard Pull test.

As mentioned above, a fully-actuated azimuthing propulsion system was already available on the USV16. However, the control allocation system had to be retuned to accommodate the higher power thrusters. Here the specifics of the control allocation system are provided. The configuration of the propulsion system makes it possible to generate motion in a desired direction using more than one combination of thrust values and thruster angles (see Figure 11). In order to ensure that undue battery power is not expended so that the vehicle can operate for as long as possible, it is

necessary to implement a control allocation system. The control allocation system receives its input from the feedback and feedforward controllers on the vehicle in the form of commanded forces and moments (Figure 18). The control allocation system then outputs the propeller speeds and azimuth angles that will achieve the desired forces and moments in a way that minimizes the power expended.

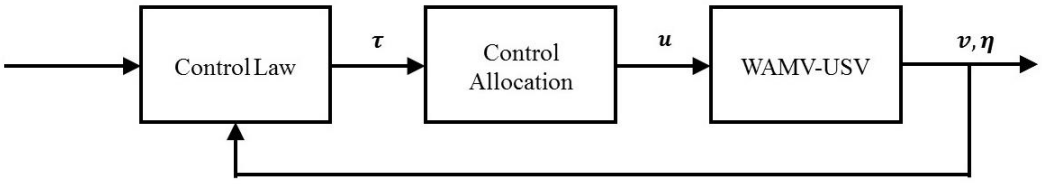

Figure 18: Block diagram of USV16 control allocation system.

Since the amplitude and rate of the thrusters and azimuthing actuators are limited, control allocation is a constrained optimization problem. A detailed explanation of this approach can be found in [56], it is partially repeated here for completeness.

5.1.1.1.1 Extended Force Representation

For the m outputs of the controller, $\boldsymbol{\tau} \in \mathbb{R}^m$, let $\mathbf{f} \in \mathbb{R}^{2k}$ be the actuator forces in the surge and sway directions at each of the k actuators,

$$\mathbf{f} = \left[F_{x_1}\ F_{y_1} \ldots F_{x_i}\ F_{y_i} \ldots F_{x_k}\ F_{y_k}\right]^T$$

A transformation matrix $\boldsymbol{T} \in \mathbb{R}^{2k \times m}$ from the controller output force $\boldsymbol{\tau}$ (or $\boldsymbol{\tau_1}$) to the actuator frame force vector $\mathbf{f}$ can be defined as:

$$\boldsymbol{\tau} = \boldsymbol{T}\mathbf{f}$$

where $\boldsymbol{T}$ is generically defined as:

$$\mathbf{T} = \begin{bmatrix} 1 & 0 & \dots & 1 & 0 \\ 0 & 1 & \dots & 0 & 1 \\ -l_{y_1} & l_{x_1} & \dots & -l_{y_k} & l_{x_k} \end{bmatrix}$$

The constants l_{x_i} and l_{y_i} represent the longitudinal and lateral distances to the ith actuator measured with respect to the vehicle center of gravity. The propulsion system mounted on the USV16 consists of two linear actuators and two thrusters (Figure 11), therefore $k = 4$. Thus, the generic equations are rewritten to define $\mathbf{f}$ and $\boldsymbol{T}$ for the system used:

$$\mathbf{f} = \begin{bmatrix} F_{x_p} & F_{y_p} & F_{x_s} & F_{y_s} \end{bmatrix}^T$$

$$\mathbf{T} = \begin{bmatrix} 1 & 0 & 1 & 0 \\ 0 & 1 & 0 & 1 \\ -l_{y_\mathrm{p}} & l_{x_\mathrm{p}} & -l_{y_s} & l_{x_s} \end{bmatrix}$$

The subscripts s and p stand for the starboard and port sides, respectively. The solution to the allocation problem now rests in finding an inverse to the rectangular transformation matrix $\mathbf{T}$.

5.1.1.1.2 Lagrangian Multiplier Solution

A cost function C is set up to minimize the force output from each actuator subject to a positive definite weight matrix $\mathbf{W} \in \mathbb{R}^{2k \times 2k}$,

$$\min_{\mathbf{f}} \{C = \mathbf{f}^{\mathbf{T}}\mathbf{W}\mathbf{f}\}$$

The optimization problem is subject to the constraint $\boldsymbol{\tau} - \mathbf{T}\mathbf{f} = \mathbf{0}$, i.e., the error between the desired control forces and the attainable control forces is minimized. The weight matrix $\mathbf{W}$ is set to skew the control forces towards the most efficient actuators. This is especially important for systems with rudders or control fins, as these actuators provide greater control authority with less power consumption.

A Lagrangrian is then set up as in,

$$L(\mathbf{f}, \boldsymbol{\lambda}) = \mathbf{f}^{\mathrm{T}}\mathbf{W}\mathbf{f} + \boldsymbol{\lambda}^{\mathrm{T}}(\boldsymbol{\tau} - \mathbf{T}\mathbf{f})$$

Differentiating $L(\mathbf{f}, \boldsymbol{\lambda})$ with respect to **f,** one can show that the solution for **f** reduces to $\mathbf{f} = \mathbf{T}_{\mathbf{w}}^{\dagger}\boldsymbol{\tau}$, where the inverse of the weighted transformation matrix is,

$$\mathbf{T}_{\mathbf{w}}^{\dagger} = \mathbf{W}^{-1}\mathbf{T}^{\mathrm{T}}(\mathbf{T}\mathbf{W}^{-1}\mathbf{T}^{\mathrm{T}})^{-1}$$

If a vehicle has port/starboard symmetry with identical actuators, the weight matrix **W** can be taken as the identity matrix, $\mathbf{W} = \mathbf{I} \in \mathbb{R}^{2k \times 2k}$, and the inverse of the transformation matrix becomes the Moore-Penrose pseudoinverse of the transformation matrix, $\mathbf{T}_{\mathbf{w}}^{\dagger} = \mathbf{T}^{\mathrm{T}}(\mathbf{T}\mathbf{T}^{\mathrm{T}})^{-1}$.

Once the component force vector **f** is found, a four-quadrant *arctan* function can be applied to find the desired azimuth angles $\delta_p = \tan^{-1}(F_{y_p}/F_{x_p})$ and $\delta_s = \tan^{-1}(F_{y_s}/F_{x_s})$, and to calculate the magnitude of the thrust at each propeller $T_p = \sqrt{F_{x_p}^2 + F_{y_p}^2}$ and $T_s = \sqrt{F_{x_s}^2 + F_{y_s}^2}$. The block for the control allocation described is provided in Figure 19.

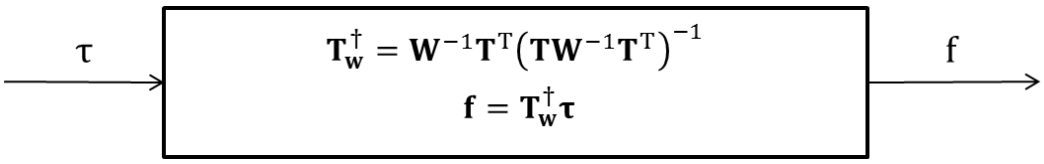

Figure 19: Control allocation using the extended thrust representation to convert from desired forces τ to an extended thrust representation f.

Owing to physical limitations on the travel of the linear actuators, the azimuth range of each propeller is from -45° to +45°. However, a 180° offset from a value in this range is also attainable by reversing the propeller. A logic scheme is implemented on top of the control allocation that sets the thrust to zero if the allocation scheme requests an unachievable angle, and reverses it if an

angle from -135º to 135º is required. This scheme is illustrated in Figure 20. reverses thrust $T_p = -T_p$ when $135 < |\delta_p| < 180$ and $T_s = -T_s$ when $135 < |\delta_s| < 180$. Thrust is set to zero, $T_p = 0$ when $45 < |\delta_p| < 135$ and $T_s = 0$ when $45 < |\delta_s| < 135$. Careful tuning of controller parameters is necessary to ensure that these constraints are not violated. The approach produces a computationally efficient answer to the control allocation optimization problem, which is possible to implement on the USV16's embedded processor.

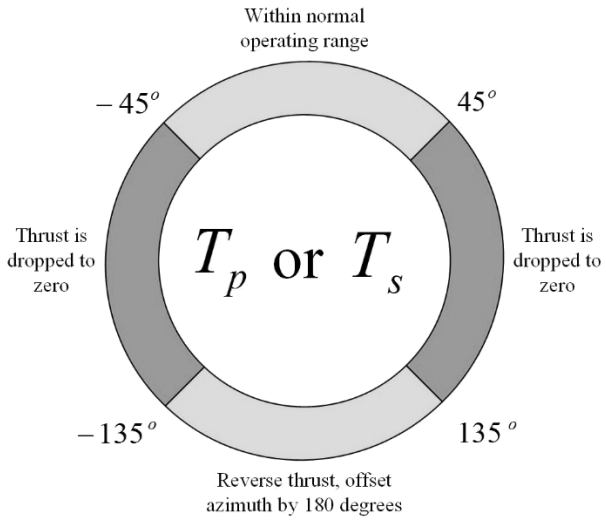

Figure 20: Control allocation logic.

Due to the fact that the time responses of the thrusters and linear actuators aren't precisely modeled within the allocation scheme, the resultant forces and angles commanded are low-pass filtered with a user-set cutoff frequency to maintain a feasible response from the propulsion system. The low-pass filters used here are simple first order, infinite impulse response filters with a single time constant that is used to set the cut-off frequency. The time constant is set to conservatively match the actuator dynamics. Two separate low-pass filters were used to filter the control allocation output for the azimuth as well as thrust for each motor. The time constant for the thrust filter was found to be about an order of magnitude greater than that of the azimuth filter.

5.1.1.2 *Nonlinear Low-Level Controller*

In addition to adapting the control allocation system, the low-level controller responsible for station keeping and trajectory tracking of the USV16 was also updated for this effort. Firstly, system identification experiments were conducted to determine the maneuvering properties of the vehicle after modifications to the propulsion system. In addition to the bollard pull tests described above, these tests included acceleration tests, circle tests and zig-zag tests. All system characterization sea trials were conducted near the FAU SeaTech Campus in North Lake, Hollywood, FL. The location was chosen such that it would provide a benign environment with minimum wind, current and wave disturbances. Vehicle state, as well as wind speed and direction, were recorded throughout the experiments.

5.1.1.2.1 System Identification

The acceleration tests were conducted to estimate the linear and nonlinear drag terms in the surge direction. The USV16 was started from rest and accelerated with a throttle range of 70-100% on both motors for 60 seconds. When the vehicle achieved steady-state speed, the drag forces in the surge direction were equal to propulsion forces. Linear and nonlinear drag coefficients in the surge direction, X_u and $X_{u|u|}$, were determined by quadratic curve fitting of surge speeds and drag forces, as shown in Figure 21.

The equations and linearized numerical values of the hydrodynamic coefficients used in the model are listed in Table 3.

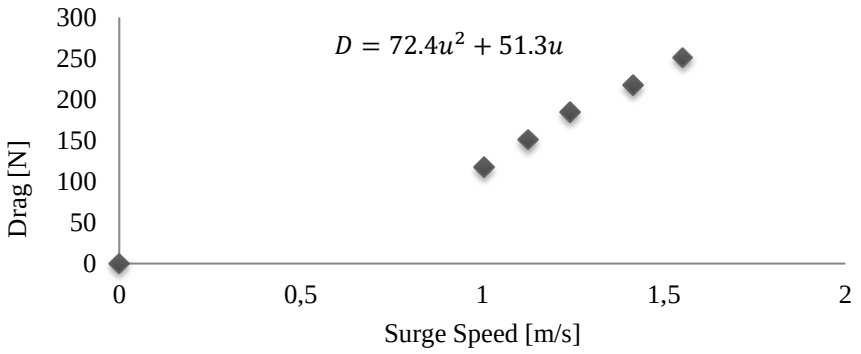

Figure 21: Quadratic fit of surge speed and drag in surge direction for USV16 model.

Table 3: Hydrodynamic coefficients for the WAM-V USV16 [48]. All hydrodynamics terms not listed in this table are assumed to be zero.

Coefficient Name	Non-Dimensional Factor	Dimensional Term
$X_{\dot{u}}$	-0.05	m
$Y_{\dot{v}}$	0.9	$\pi\rho T^2 L$
$N_{\dot{r}}$	1.2	$\frac{4.75}{2}\pi\rho\frac{B}{2}T^4 + \pi\rho T^2\frac{[(L-LCG)^3 + LCG^3]}{3}$
$Y_{\dot{r}}$	0.5	$\pi\rho T^2\frac{[(L-LCG)^2 + LCG^2]}{2}$
$N_{\dot{v}}$	0.5	$\pi\rho T^2\frac{[(L-LCG)^2 + LCG^2]}{2}$
X_u	(See Figure 21)	
Y_v	-0.5	$\rho\lvert v\rvert\left[1.1 + 0.0045\frac{L}{T} - 0.1\frac{B_{hull}}{T} + 0.016\left(\frac{B_{hull}}{T}\right)^2\right]\left(\frac{\pi TL}{2}\right)$
N_r	-0.65	$\pi\rho\sqrt{(u^2+v^2)}T^2L^2$
Y_r	-0.4	$\pi\rho\sqrt{(u^2+v^2)}T^2L)$
$X_{u\lvert u\rvert}$	(See Figure 21)	

The hydrodynamic coefficients were estimated with the equations shown in Table 3 to provide a starting point for development of the dynamic model of the USV. The values obtained were then entered in the three-degrees-of-freedom equations of motion and manually tuned so that applying the same input conditions in simulation and during sea trials would result in the same state output. The objective was to refine the estimated hydrodynamic coefficients and to produce a dynamic model of the USV that could be considered representative of the vehicle itself. For this purpose, the vehicle state was recorded through sea trials, and the same open-loop scenario was recreated in simulation. After the acceleration test, circle tests and zig-zag tests were performed. During the circle test, the vehicle was first accelerated with 100% throttle on both sides for 20 seconds, then port and starboard were set to -100% and 100% throttle, respectively, for 30 seconds. Following this procedure, the vehicle was able to spin in a circle around its center of gravity with minimal surge and sway velocity; N_r, the drag moment coefficient from yaw rate, could therefore be isolated. The circle test was also performed in a different manner by setting port and starboard to 0% and 100% throttle. Following this procedure, the vehicle was able to steer around a turning radius; the drag coefficient in the sway directions from sway velocity Y_v could therefore be estimated. During the zig-zag tests, the vehicle was first accelerated with 100% throttle on both sides for 20 seconds, then port and starboard were set to 100% and 0% throttle alternately four times on each side. The zig-zag test was utilized solely to evaluate the model by comparing field data with simulations. Comparison of simulation and experimental results for the acceleration test, circle test, and zig-zag test is shown in Figure 22, Figure 23, and Figure 24, respectively. In Figure 22, it can be noted that the theoretical vehicle deceleration for both 70% and 100% throttle commands was more rapid than the experimental deceleration under the same circumstances. A possible explanation is that the water accelerated by the USV was still moving forward when

conducting the experiments, therefore the vehicle began to decelerate, leading to a slower decay rate. In addition, unmodeled wind and current may have played a major role is affecting the deceleration of the USV during sea trials.

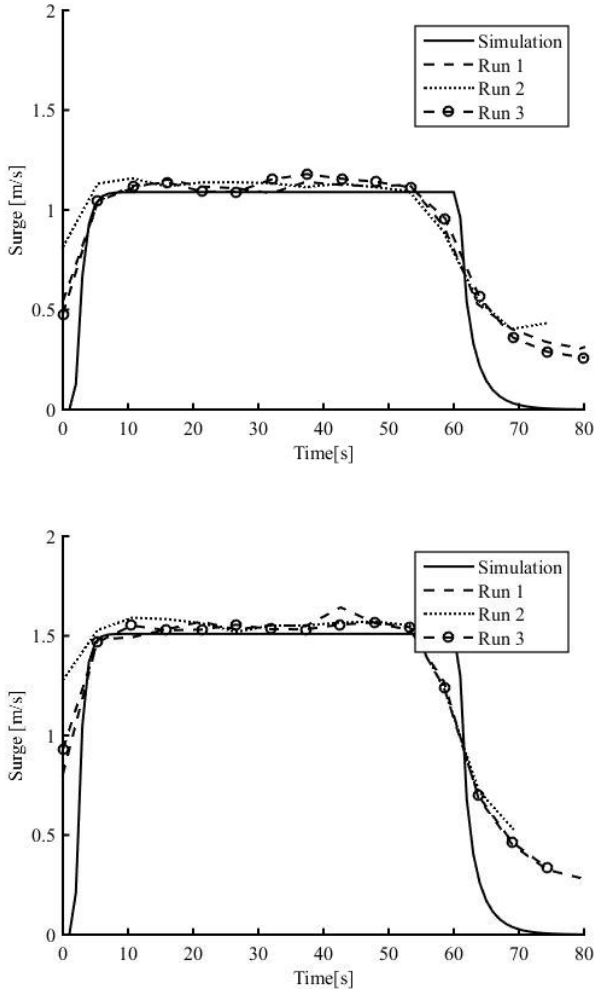

Figure 22: Surge speed of simulation and experimental results of 70% throttle command (left) and 100% throttle command (right) during acceleration tests.

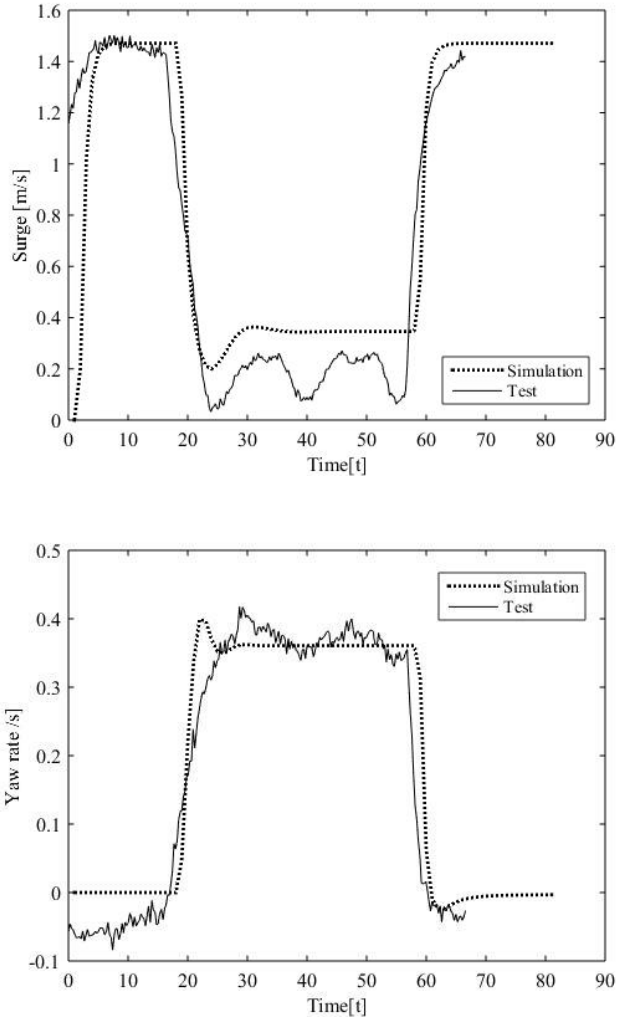

Figure 23: Surge and yaw speeds of simulation and experimental results during circle tests.

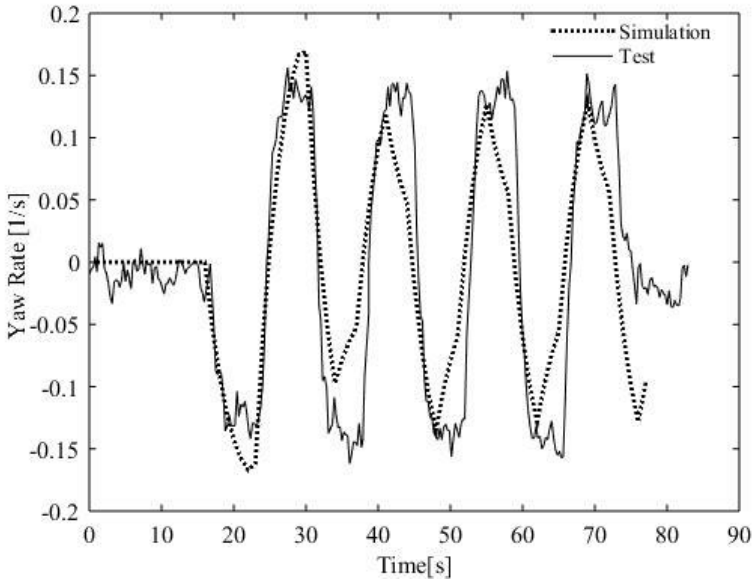

Figure 24: Yaw rates of simulation and experimental results during zigzag tests with 100% throttle command.

5.1.1.3 *Equations of Motion*

The WAM-V USV16 is configured to operate at low speeds (1-2 knots) and in mild sea states (SS 0/1). Thus, the vehicle's motion is assumed to be planar with linear motion in the x_b and y_b directions and rotation about the z_b axis (Figure 25). A three DOF (surge, sway and yaw) dynamic model is used to develop the equations of motion, the detailed development presented in [48] and [47] is partially repeated here for completeness:

$$\boldsymbol{M\dot{v} + C(v)v + D(v)v = \tau + \tau_w},$$

$$\boldsymbol{\dot{\eta}} = \left[\dot{x}\ \dot{y}\ \dot{\psi}\right]^T,$$

and

$$\boldsymbol{v} = [u\ v\ r]^T.$$

Where $\boldsymbol{M}$ is the mass matrix, $\boldsymbol{C}(\boldsymbol{v})$ is the Coriolis matrix, $\boldsymbol{D}(\boldsymbol{v})$ is the drag matrix, $\boldsymbol{\tau}$ is the vector of forces and moment generated by the propulsion system, and $\boldsymbol{\tau_w}$ is the vector of forces and moment caused by the wind. $\boldsymbol{M}$ and $\boldsymbol{C}(\boldsymbol{v})$ include both rigid body terms ($\boldsymbol{M_{RB}}$ and $\boldsymbol{C_{RB}}(\boldsymbol{v})$) and added mass terms ($\boldsymbol{M_{AM}}$ and $\boldsymbol{C_{AM}}(\boldsymbol{v})$). $\boldsymbol{D}(\boldsymbol{v})$ includes both the linear drag term ($\boldsymbol{D_l}$) and nonlinear drag term ($\boldsymbol{D_{nl}}(\boldsymbol{v})$). The vector $\dot{\boldsymbol{\eta}}$ describes the vehicle's North ($\dot{x}$), East ($\dot{y}$) velocities and the angular velocity ($\dot{\psi}$) around the z axis in an inertial reference frame, $\boldsymbol{\eta} = [x, y, \psi]^T$, and the vector $\boldsymbol{v}$ contains the vehicle surge velocity (u), sway velocity (v) and yaw rate (r) in the body-fixed frame. These two coordinate systems are illustrated in Figure 25.

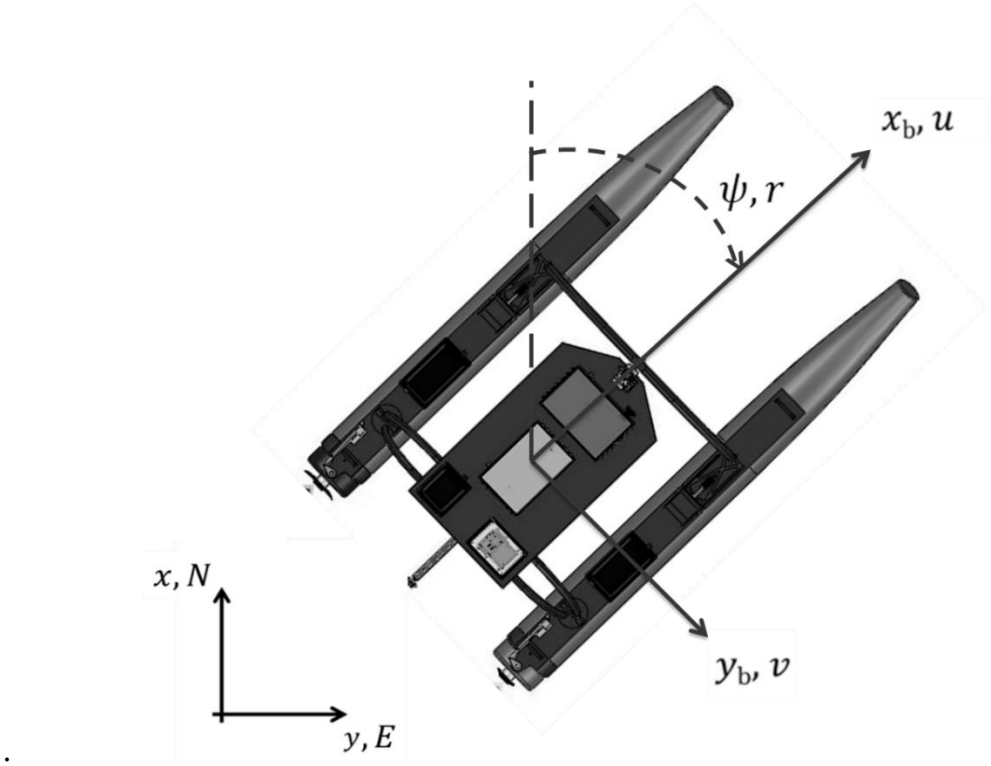

Figure 25: Top view of WAM-V USV16 with body-fixed coordinate system overlaid. x_b and y_b denote vessel surge and sway axes, respectively.

The transformation matrix for converting from body-fixed to earth-fixed frames is given by the rotation matrix:

$$\boldsymbol{J}(\boldsymbol{\eta}) = \begin{bmatrix} \cos\psi & -\sin\psi & 0 \\ \sin\psi & \cos\psi & 0 \\ 0 & 0 & 1 \end{bmatrix}.$$

$\boldsymbol{M}$ is an inertia tensor that is the sum of a rigid body mass matrix, $\boldsymbol{M_{RB}}$, and an added mass matrix, $\boldsymbol{M}_{AM}$:

$$\boldsymbol{M} = \boldsymbol{M_{RB}} + \boldsymbol{M}_{AM} = \begin{bmatrix} m - X_{\dot{u}} & 0 & -my_G \\ 0 & m - Y_{\dot{v}} & mx_G - Y_{\dot{r}} \\ -my_G & mx_G - N_{\dot{v}} & I_z - N_{\dot{r}} \end{bmatrix},$$

where, m denotes the mass of the USV16, x_G and y_G are the coordinates of the vessel center of mass in the body-fixed frame, and I_z denotes moment of inertia about the z_b-axis. All the terms representing the hydrodynamic coefficients in the mass matrix utilize SNAME (1950) nomenclature for representing a force or moment created by motion in a specific degree of freedom. The subscript on each coefficient denotes the cause of the force/moment (e.g., $Y_{\dot{r}}$ prodcues a force in the y_b direction from a change in the yaw rate $\dot{r}$).

$\boldsymbol{C}(\boldsymbol{v})$ is a Coriolis matrix, which includes the sum of a rigid body term, $\boldsymbol{C}_{RB}(\boldsymbol{v})$, and added mass term, $\boldsymbol{C}_{AM}(\boldsymbol{v})$:

$$\boldsymbol{C}(\boldsymbol{v}) = \boldsymbol{C}_{RB} + \boldsymbol{C}_{AM} = \begin{bmatrix} 0 & 0 & -m(x_G r + v) \\ 0 & 0 & -m(y_G r - u) \\ m(x_G r + v) & m(y_G r - u) & 0 \end{bmatrix} + \begin{bmatrix} 0 & 0 & Y_{\dot{v}} v + \left(\frac{Y_{\dot{r}} + N_{\dot{v}}}{2}\right) r \\ 0 & 0 & -X_{\dot{u}} u \\ -Y_{\dot{v}} v - \left(\frac{Y_{\dot{r}} + N_{\dot{v}}}{2}\right) r & +X_{\dot{u}} u & 0 \end{bmatrix}$$

The model designates the body-fixed origin at the center of gravity and assumes port/starboard symmetry, making $x_G = 0$ and $y_G = 0$. $\boldsymbol{D}(\boldsymbol{v})$ is the summation of linear and nonlinear drag matrices:

$$\boldsymbol{D}(\boldsymbol{v}) = \boldsymbol{D_l} + \boldsymbol{D}_{nl}(\boldsymbol{v})$$

where,

$$\boldsymbol{D_l} = \begin{bmatrix} X_u & 0 & 0 \\ 0 & Y_v & Y_r \\ 0 & N_v & N_r \end{bmatrix}$$

and,

$$\boldsymbol{D_{nl}} = \begin{bmatrix} X_{u|u|}|u| & 0 & 0 \\ 0 & Y_{v|v|}|v| + Y_{v|r|}|r| & Y_{r|v|}|v| + Y_{r|r|}|r| \\ 0 & N_{v|v|}|v| + N_{v|r|}|r| & N_{r|v|}|v| + N_{r|r|}|r| \end{bmatrix}.$$

The surge direction port drag and starboard drag terms, D_p and D_s, respectively, are modeled using the polynomial curve fit derived from experimental testing (Figure 21). A coordinate transformation is carried out to obtain the velocities of each individual pontoon hull because they are offset from the CG. These transformed velocities are used in the drag model below as u_p and u_s:

$$D_p = \left({}^{X_{u|u|}}/_{2}\right)|u_p|u_p + \left({}^{X_u}/_{2}\right)u_p$$

$$D_s = \left({}^{X_{u|u|}}/_{2}\right)|u_s|u_s + \left({}^{X_u}/_{2}\right)u_s$$

Incorporating the moment created by the two drag forces D_p and D_s, the term

$$\left(D_s - D_p\right)B/2$$

is added to the yaw moment (not modeled in $\boldsymbol{D}(\boldsymbol{v})$).

$\boldsymbol{\tau}$ is a vector of the forces and moment generated by the propulsion system:

$$\boldsymbol{\tau} = \begin{bmatrix} T_x \\ T_y \\ M_z \end{bmatrix}.$$

T_x , T_y and M_z are the thrust in x_b and y_b direction, and resulting moment around the z_b axis. The USV16 generates the propulsion forces and turning moment with two azimuth thrusters, providing respectively n_p and n_s Revolutions Per Minute (RPM) on the port and starboard side respectively, and thruster turning angles $\delta = [\delta_{p,}\delta_s]^T$ (Figure 11). We assume that thrust has a linear relationship with RPM, so that $T_p = \frac{n_p}{n_{max}} \times T_{max}$ and $T_s = \frac{n_s}{n_{max}} \times T_{max}$, where n_{max} and $T_{max} = 120N$ are the maximum RPM and maximum thrust each thruster can output. T_x , T_y and M_z can be calculated, respectively as:

$T_x = (\boldsymbol{T_p} + \boldsymbol{T_s}) \cdot \boldsymbol{i}$,

$T_y = (\boldsymbol{T_p} + \boldsymbol{T_s}) \cdot \boldsymbol{j}$,

$M_z = \boldsymbol{r_p} \times \boldsymbol{T_p} + \boldsymbol{r_s} \times \boldsymbol{T_s}$.

Here $\boldsymbol{i}$ and $\boldsymbol{j}$ are unit vectors in the x_b and y_b directions, respectively; $\boldsymbol{r_p} = -L_{GT}\boldsymbol{i} - \frac{B}{2}\boldsymbol{j}$, $\boldsymbol{r_s} = -L_{GT}\boldsymbol{i} + \frac{B}{2}\boldsymbol{j}$ are the port and starboard moment arms, respectively; L_{GT} is the longitudinal distance between the center of gravity and the thruster; and B is the centerline to centerline hull separation shown in Figure 25.

5.1.1.4 *Low-level Sliding Mode Controller Development*

In general, robust control strategies can be implemented to improve the response of a system when its dynamic model or the nature of the environmental disturbances that act upon it are uncertain. A robust sliding mode station-keeping controller was designed and implemented on the USV16 to mitigate slowly varying environmental disturbances, such as tidal currents, that the system cannot

directly measure through its sensors. A discussion of the development of this controller was presented in [48] and is partially repeated here for completeness. The advantage of this approach is that the control signal is not required to be highly precise, since the sliding mode controller is invariant to small disturbances entering the system through the control channel. Sliding mode control theory is therefore considered highly suitable for the purpose of controlling a USV, tasked to maintain position and heading over an extended period of time, operating in an environment disturbed by slowly varying water currents.

A reference trajectory is first defined as:

$$\dot{\boldsymbol{\eta}}_{\boldsymbol{r}} = \dot{\boldsymbol{\eta}}_d - \boldsymbol{\Lambda}\boldsymbol{\eta}_t.$$

Here $\dot{\boldsymbol{\eta}}_d = [\dot{x}_d \quad \dot{y}_d \quad r_d]^T$ is the derivative of the desired state of the vehicle, $\boldsymbol{\Lambda}$ is a diagonal design matrix based on Lyapunov exponents, and $\boldsymbol{\eta}_t$ is the earth-fixed tracking error vector. For the station-keeping of marine vehicles, the desired state $\boldsymbol{\eta}_d = [x_d \quad y_d \quad \psi_d]^T$ contains the desired position in the North-East-Down coordinate frame (x_d and y_d) and desired heading ψ_d, while its derivative is $\dot{\boldsymbol{\eta}}_d = [0 \quad 0 \quad 0]$ since $\dot{x}_d, \dot{y}_d, r_d \to 0$ as the system approaches steady-state. With these terms a sliding surface function is can be defined as:

$$\boldsymbol{s} = \dot{\boldsymbol{\eta}}_t + 2\boldsymbol{\Lambda}\boldsymbol{\eta}_t + \boldsymbol{\Lambda}^2 \int_0^t \boldsymbol{\eta}_t dt.$$

The an integral term is included to contend with slowly varying sources of errors. This enables the system to be more stable over extended periods of time, at the cost of requiring a longer period of time to reach steady-state. The robustness of the controller is therefore prioritized over its performance. The same integral term is also introduced, for the purpose of minimizing unmodeled environmental disturbance, in a newly defined reference trajectory:

$$\dot{\boldsymbol{\eta}}_r = \dot{\boldsymbol{\eta}}_d - 2\boldsymbol{\Lambda}\boldsymbol{\eta}_t - \boldsymbol{\Lambda}^2 \int_0^t \boldsymbol{\eta}_t dt.$$

The control law ensures that if the system deviates from the surface $\boldsymbol{s}$, it is forced back to it. Once on the surface, the under-modeled system reduces to an exponentially stable, second-order system. The system's response therefore depends heavily on the choice of the sliding surface. As a result, the system will possess considerable robustness against slowly varying external perturbations, like currents, and incorrectly modeled dynamics. The sliding mode control law is defined as follows:

$$\boldsymbol{\tau} = \boldsymbol{M_1}\left[\boldsymbol{J}(\boldsymbol{\eta})^T\ddot{\boldsymbol{\eta}}_r + \boldsymbol{J}(\dot{\boldsymbol{\eta}})^T\dot{\boldsymbol{\eta}}_r\right] + \boldsymbol{C_1}(\boldsymbol{v})\boldsymbol{J}(\boldsymbol{\eta})^T\dot{\boldsymbol{\eta}}_r + \boldsymbol{D_1}(\boldsymbol{v})\boldsymbol{J}(\boldsymbol{\eta})^T\dot{\boldsymbol{\eta}}_r - \boldsymbol{J}(\boldsymbol{\eta})^T\boldsymbol{R} * sat(\boldsymbol{E}^{-1} * \boldsymbol{s}).$$

The last term in the control law includes the bound on the uncertainties $\boldsymbol{R}$ and the boundary layer thickness $\boldsymbol{E}$ around the sliding surface $\boldsymbol{s}$. $\boldsymbol{R}$ can be considered a positive definite diagonal gain matrix, and $\boldsymbol{E}$ is a vector defining the boundary layer within which the system will slide along the surface $\boldsymbol{s}$.

The saturation function (sat) is used instead of the traditional signum function to reduce the chattering effect. In a situation where the system is continuously disturbed by external forces that make it deviate from steady state, applying a discontinuous control signal enables it to deviate momentarily from its standard behavior. As a result, the system is forced back to its desired state. This is exactly what happens when attempting to station-keep a USV in an environment disturbed by slowly varying, unsteady, and unmodeled currents. When a disturbance forces the vehicle away from its desired state, the sliding mode controller is able to bring the system back to its desired state by exiting the sliding surface bounded by $\boldsymbol{E}$ momentarily. As the system reenters the boundary layer, it will constantly slide along the surface minimizing the error.

Once the system enters the boundary layer $\boldsymbol{E}$, the discontinuous control signal forces the system to slide along a cross-section of the state space $\boldsymbol{s}$, bounded by $\boldsymbol{R}$. In other words, as the system's errors are within specific boundaries dictated by $\boldsymbol{E}$, the control signal will vary based on

$\boldsymbol{s}$, so that $\boldsymbol{s} < |\boldsymbol{R}|$. A proper representation of such phenomena requires a three-dimensional plot to show the sliding surface bounded by $\boldsymbol{E}$ and $\boldsymbol{R}$. For simplicity, an illustration of a linear signal for each element in $\boldsymbol{R}$ and $\boldsymbol{E}$ is given in a two-dimensional plot and can be seen in Figure 26.

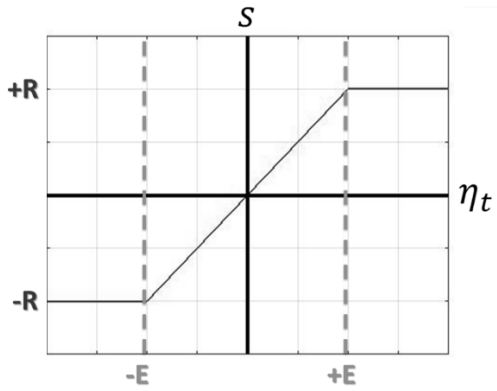

Figure 26: Illustration of Saturation Function for a single saturation argument for sliding mode controller.

Both, the bound on the uncertainties matrix $\boldsymbol{R}$ and the boundary layer thickness $\boldsymbol{E}$, were initially selected based on the results of previous experiments, then tuned during in-water testing. It is important to note that that chattering and saturation of the control signal can compromise the functionality of the sliding mode controller, when used for the purpose of station-keeping heading and position of a USV. This was evident during sea trials. Fine tuning the values of $\boldsymbol{R}$ and $\boldsymbol{E}$ was therefore crucial to enable the vehicle to perform its desired maneuver. The control block for the sliding mode station-keeping controller described is provided in Figure 27.

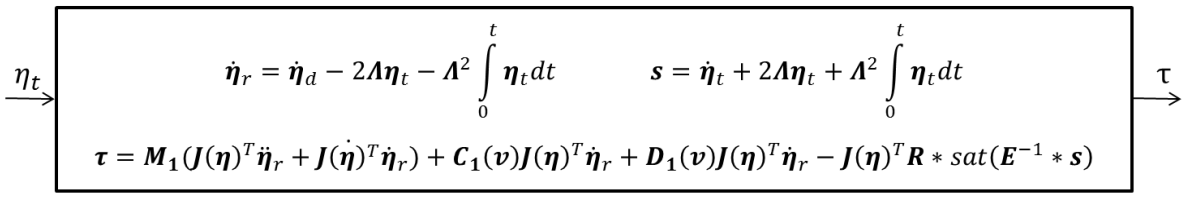

Figure 27: Sliding Mode station-keeping controller.

5.1.1.5 *Wind Feedforward Control*

As the USV16 is lightweight and has a large windage area it can be strongly affected by the presence of wind. The wind forces and moment acting on the vehicle are modeled as:

$$\boldsymbol{\tau_w} = q \begin{bmatrix} C_X(\gamma_{rw}) A_{Fw} \\ C_Y(\gamma_{rw}) A_{Lw} \\ C_N(\gamma_{rw}) A_{Lw} L_{aa} \end{bmatrix},$$

where A_{Fw} and A_{Lw} are the frontal and lateral projected windage area (Figure 28), γ_{rw} is apparent angle of attack and q is the dynamic pressure found using

$$q = \frac{1}{2} \rho_a V_{rw}^2,$$

where $\rho_a = 1.2\ kg/m^3$ is the density of the air, and V_{rw} is the apparent wind speed (Figure 31). Both apparent wind speed and direction were measured with an existing ultrasonic anemometer. Representative wind data, including apparent wind speed and direction are shown in Figure 29. The corresponding power spectral density $S(f)$ of the turbulent speed fluctuations in the wind data in Figure 29, normalized by the intensity of the turbulent kinetic energy TKE, where $\bar{u}$ is the average wind speed during the measurement period, is shown in Figure 30. The turbulent speed fluctuations are calculated using $u' \equiv (u - \bar{u})$. The intensity of the turbulence is defined as $s = TKE/\bar{u}$.

$$\text{TKE} \equiv \sqrt{\overline{\text{u}'^2}}$$

An examination of the wind power spectrum in Figure 30 shows that about 90 percent of the turbulent kinetic energy occurs at frequencies less than about $f = 0.03$ Hz. Using the average wind speed $\bar{u} = 2.43$ m/s observed during these measurements, the corresponding length scales of the turbulent fluctuations in the wind are expected to be on the order of $L_t \sim \bar{u}/f = 78$ m and

larger. As the length of the USV16 is much smaller than L_t, a single point measurement of the wind speed and direction is taken to be sufficiently representative of the wind characteristics acting across the entire vehicle.

C_X, C_Y, C_Z are the wind coefficients for the surge, sway and yaw axes. The non-dimensionalized wind coefficients can be computed as a function of γ_{rw}. The wind coefficients for horizontal plane motions can be approximated by:

$$C_X(\gamma_{rw}) = -c_x cos(\gamma_{rw}),$$

$$C_Y(\gamma_{rw}) = c_y sin(\gamma_{rw}),$$

$$C_Z(\gamma_{rw}) = c_z sin(2\gamma_{rw}),$$

In practice, typical ranges for these coefficients are $0.5 \leq c_x \leq 0.90$, $0.7 \leq c_y \leq 0.95$, and $0.05 \leq c_z \leq 0.20$. These coefficients were therefore initially set to $c_x = 0.70$, $c_y = 0.80$, $c_z = 0.10$, and then manually tuned based on the vehicle performance, leading to final values of $c_x = 0.50$, $c_y = 0.50$, $c_z = 0.33$.

Figure 28: Frontal (left) and lateral (right) projected areas.

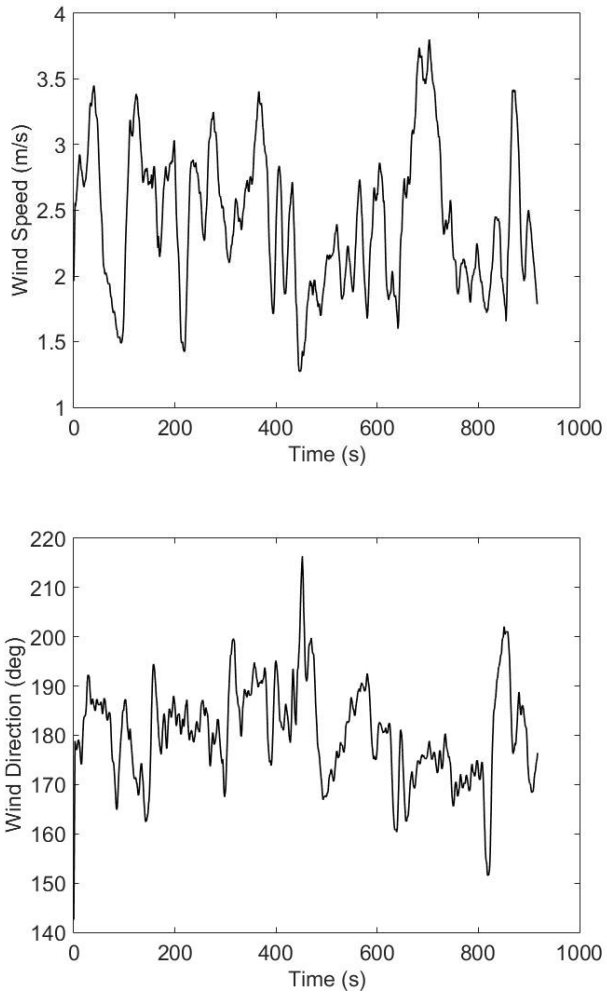

Figure 29: Apparent wind speed (top) and direction (bottom), collected from a stationary vehicle.

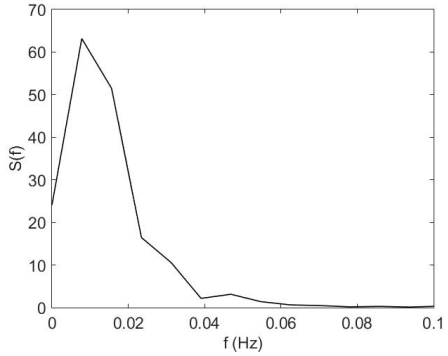

Figure 30: Normalized power spectral density of the turbulent speed fluctuations in the wind data recorded in Figure 29.

Based on the dynamic model of the USV16 and wind model explained above, a wind feedforward controller was designed to mitigate the wind disturbance. In similar studies, it has been noted that the wind feedforward controller should be used with caution because it has the potential to make the system unstable or reduce the performance of the main feedback controller. A block diagram of the control system, which includes the wind feedforward controller, can be seen in Figure 32.

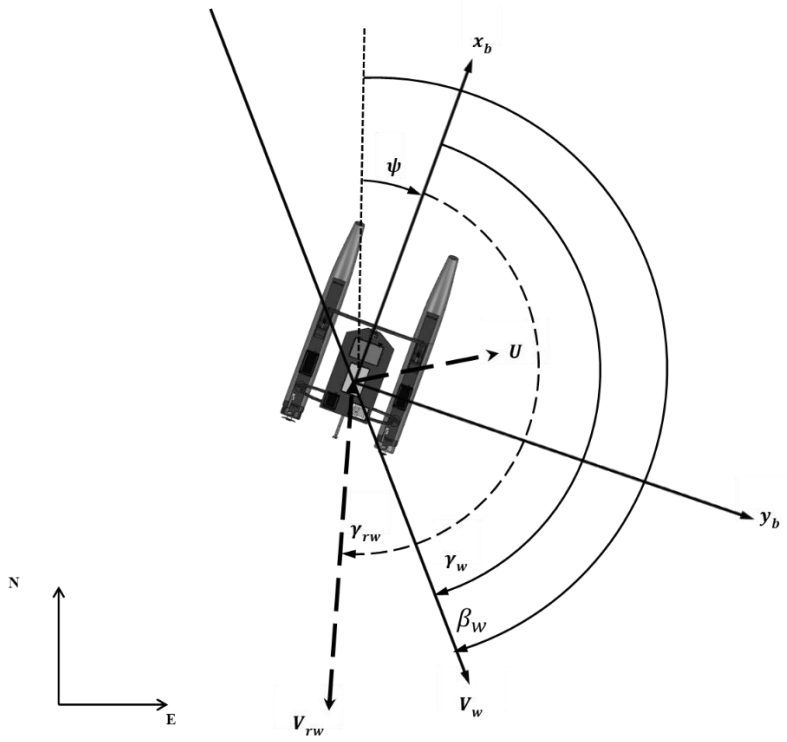

Figure 31: Representation of vehicle heading (ψ), velocity (U), true wind speed (V_w), true wind direction (β_w), true wind angle of attack (γ_w), apparent wind speed (V_{rw}), and apparent wind angle of attack (γ_{rw}).

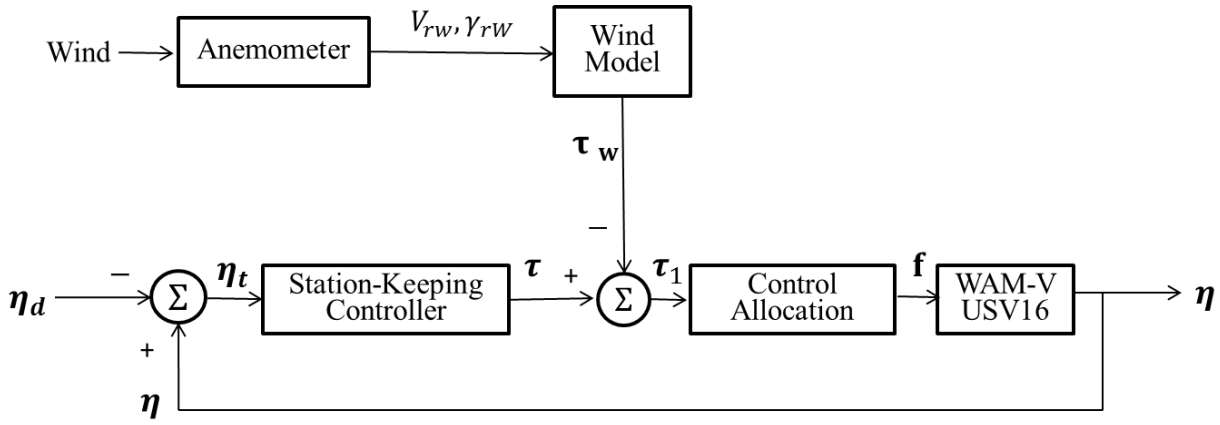

Figure 32: Block diagram of WAM-V USV16 control system with wind feedforward.

In addition to the state feedback, the control system utilizes two additional inputs: the apparent wind speed V_{rw} and direction γ_{rw}. The wind data output by the anemometer are low pass filtered, using a moving average filter with a span of 20 samples, before being input into the feedforward controller. V_{rw} and γ_{rw} are used to calculate the wind disturbance $\boldsymbol{\tau_w}$, which is then subtracted from the output of the feedback controller, leading to:

$$\boldsymbol{\tau_1} = \boldsymbol{\tau} - \boldsymbol{\tau_w}.$$

Here $\boldsymbol{\tau}$ is the output of the station-keeping controller, based solely on the vehicle state, and $\boldsymbol{\tau_1}$ is a more accurate estimate of the output required that takes into account the effect of wind on the system $\boldsymbol{\tau_w}$. $\boldsymbol{\tau_1}$ is calculated utilizing both the anemometer output and the system state, while $\boldsymbol{\tau}$ is based solely on the system state.

The control block for the wind feedforward control model is provided in Figure 33.

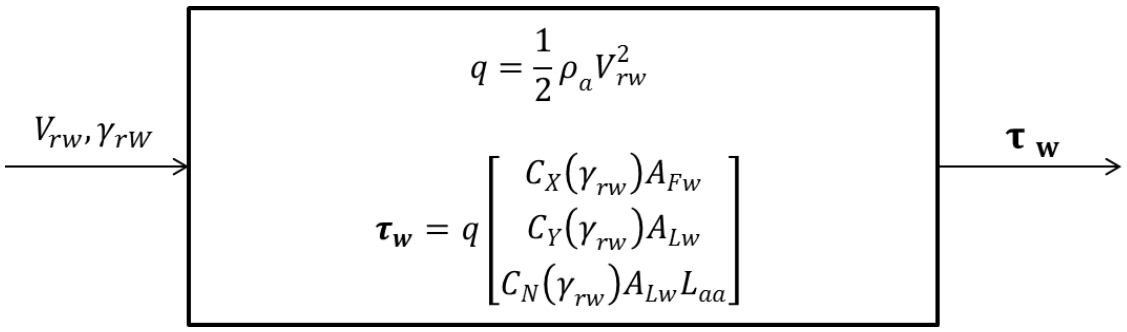

Figure 33: Wind feedforward model.

The theory developed above was implemented in software on the USV16. As the development of the low-level controller and control allocation system was conducted under funding from another source and only the control parameters were retuned for this effort, the associated software is not included in this project deliverable. See [47] for additional details.

5.1.2 Underwater Imaging System

A pneumatically-driven retractable boom was designed for the deployment of the sonar system. The sonar system was integrated into the USV's guidance navigation and control system through the design and implementation of a 'sonar topside unit', which controls both the retractable boom and the sonar. The sonar topside unit allows the sonar system to be controlled from a remote ground station and broadcasts live images from the sonar back to the ground station via long-range WiFi. On-water integration tests of the sonar system and USV were performed in October and November, 2015 with the sonar system mounted statically at the stern of a moored research vessel, under remote control on the USV16 and under automatic control on the USV16.

5.1.2.1 *Sonar System*

Several types of imaging systems were considered. It was felt that optical-based instrumentation would not be capable of providing good quality images in the highly turbid waters frequently

encountered near bridges in Florida waters. Several types of acoustic imaging systems were also studied. Echosounders were thought not to be appropriate for live bridge inspection, as they require substantial post-processing of data to construct images. Swath (side scan sonar) systems rely on a vehicle's forward motion to construct images. If an inspector were to need a detailed view of an area of concern, using such a system for bridge inspection would likely require multiple passes of a structure and complex trajectory planning of the vehicle path. Three dimensional imaging systems, such as the Measuretronics Blueview BV5000 System, have only recently been deployed from boats (and may require some additional development) and were found to be more expensive (~$130K with academic discount). In contrast, real-time multi-beam imaging sonar systems provide a continuous stream of sonar data, in a format that looks very similar to a video composed of optical images. Such systems are a fairly mature technology and have been used for construction offshore and in coastal waters, ship hull inspection and are small enough to be deployed on unmanned vehicles.

Several multibeam real-time imaging sonar systems were considered, including the Coda Octopus, the Gemini 720i and the Teledyne Reson Seabat 7128. Based on powering, size, cost, and institutional experience with similar sonar systems, the sonar system selected is an Aris 1800 real-time imaging sonar with an AR2 pan/tilt rotating mount (Figure 34). The Aris 1800 can be used to obtain real-time streaming images of underwater structures in turbid water. When configured with a long-range WiFi system, this functionality can permit streaming images of underwater structures to be broadcast to a ground station in real-time, which could enable bridge inspection teams to monitor inspections in-progress and perhaps redirect a USV to visualize areas of structural concern on the fly. The sonar system can be configured to image at different resolutions, distances and image acquisition rates.

Figure 34: The Aris 1800 imaging sonar.

5.1.2.1.1 Static Testing of the Aris Sonar System

Before deployment on the USV16, the sonar system was functionally tested from a static mount on the back of a departmental research vessel, which was moored to a dock in the FAU SeaTech marina (Figure 35). During the first several attempts to use the Aris, it worked precisely as expected, although it was noted that one of the cables was extremely difficult to connect to the sonar head. After approximately one week connectivity problems between the data acquisition laptop and Aris were experienced. We consulted the manufacturer (SoundMetrics), who suggested that there might be a power conditioning issue with the line power available on the research vessel. The system was then installed in a small indoor pool in the lab, the same problems were also experienced there. After a few days of trying to isolate the problem in phone consultation with the manufacturer, the system failed to turn on and was shipped back to the manufacturer for troubleshooting. Upon arrival at the manufacturer, it

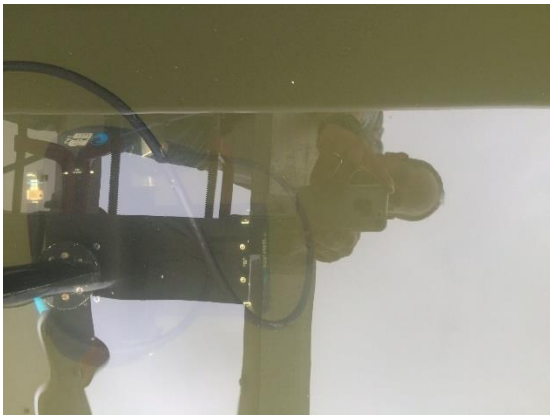

Figure 35: Static testing of the Aris System on the back of the FAU R/V Oceaneer.

was determined that a fuse had blown. The manufacturer shipped the unit back to us in working order. After the topside unit was fabricated, we again started to experience similar issues with the Aris. Again, we consulted with the manufacturer, who logged onto the system remotely and ran several diagnostic tests with and without our topside unit connected. The manufacturer suggested that it could be the construction of the FAU topside unit that was causing the issue. After several more days of testing the system at FAU, it was felt that the connector between the AR2 Rotator and the sonar head was not seating properly. The complete Aris sonar system, as well as the FAU-fabricated topside unit and data acquisition laptop, were shipped to the manufacturer for inspection. The manufacturer confirmed that the FAU topside unit was working properly and that it was providing the correct power to the Aris. The manufacturer also reported that the manufacturer-provided cable connecting the AR2 and sonar head appeared to have not been "burnt-in" properly and so was not seating correctly on the sonar head, which is why the connectors were so hard to use (and also likely why the fuse had blown during previous tests). The manufacturer replaced the problematic cable and shipped the units back to FAU. We have not experienced any additional problems with use of the Aris since that time.

5.1.3 Sonar System Retractable Boom Design

When mounted from the AR2 rotator, the frontal area of the Aris real-time imaging sonar system can be conservatively estimated (erring on the side of larger area, which would result in higher drag) to be about 0.1 m^2. In a 5-knot current, the system would have a drag of about 160 pounds acting on it. It was desired to mount the Aris unit so that it was about 2 feet below the waterline. This submergence depth helps to reduce surface reflections from the sonar signals sent out from the Aris, but at the same time, keeps the total draft of the system low, which helps to minimize the

possibility that it could become snagged on submerged obstacles not visible from the surface. Given the height of the payload tray on the USV16, mounting the Aris from the vehicle was expected to require a lever arm of about 4 feet, so that the torque required to support the Aris was anticipated to be as much as about 650 foot-pounds.

Other considerations that were taken into account in the design of the retractable mounting boom were its cost, reliability in sea water, ease of use and weight. The weight distribution of the system when the USV16 is underway is important. The Aris and AR2 rotator mount weigh a total of about 30 pounds. On a lightweight USV, suspending the combined weight of the Aris system and boom (about another 50 pounds) could adversely affect the running trim of the vehicle, which could in turn cause problems with excessive drag or cause the propeller immersion to be too low. Lastly, given the high cost of the Aris unit, it was desired to have the Aris stowed in a protected position when not in use to minimize the possibility of impact with bridge structures or floating obstacles.

Several designs were considered, including a DC-motor driven pivoting boom, a hydraulically actuated scissor-lift and two versions of a hydraulically-driven boom (see Figure 36). During the design process, CAD models of the system were developed and manually animated to explore the motion of the mechanism during transitions from fully extended (Aris system deployed) to fully stowed and back again. The approach permitted us to explore how to best orient the actuators and motors used to position the Aris and to qualitatively identify configurations that might be structurally weak or that could produce excessive drag while underway.

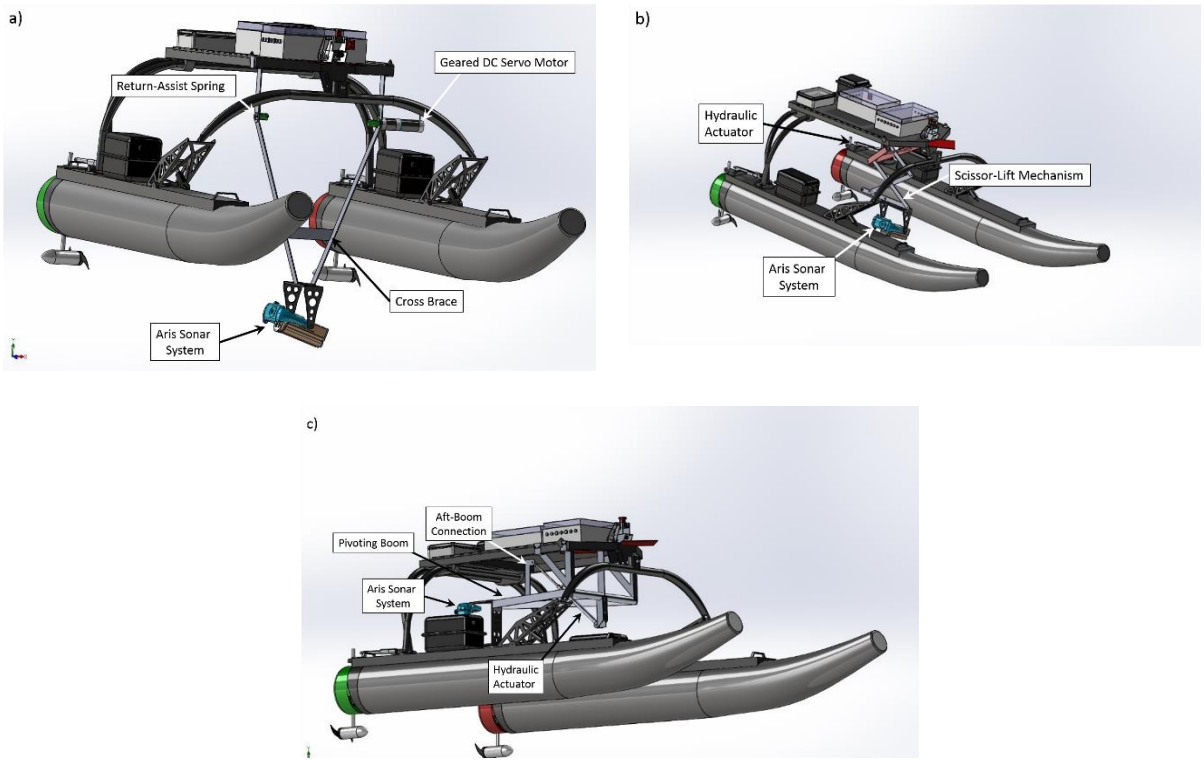

Figure 36: Early designs for the sonar deployment mechanism: (a) DC-motor driven pivoting boom; (b) scissor-lift mechanism; (c) hydraulically actuated pivoting boom with aft-side actuator mount.

It was felt that the cost, weight and power required for the DC-motor based pivoting boom was prohibitive; additionally the need for rotary return springs and gearboxes make the design relatively complicated. One of the main drawbacks of the scissor-lift design is its mechanical complexity. Given the large number of rotating joints, it was felt that use of the mechanism in seawater, where corrosion is difficult to prevent, could be risky in the long run. Additionally, unless designed with many cross-supports, such structures can be prone to deflection from relatively low forces perpendicular to the plane of the scissoring direction. The other early design considered is a hydraulically actuated pivoting boom. Overall, the system was found to be better than the other two approaches. However, as the end of the hydraulic actuator would be submerged

when the sonar is deployed, there was apprehension about the possibility of seawater entering the actuator through the seal on the extended end. An additional concern was that the actuator mounting configuration reduced the above water clearance of the USV and could be prone to snagging on floating obstacles. As explained below, the final design is a variation of the latter approach that uses a hydraulically actuated pivoting arm, with the actuator orientation configured to maximize above-water clearance and eliminate the possibility of water intrusion from the lower side of the seal.

5.1.3.1 *Final Sonar System Retractable Boom Design:*

The final configuration has a triangular support to provide good support against transverse forces and good over-water clearance (Figure 37). As can be seen, the system is completely contained within the length of the payload tray when stowed, which helps to protect the Aris system from potential impacts during a collision with a structure or other vessel on the water. Also, when the sonar is stowed, the weight of the Aris and AR2 rotator mount are longitudinally counter-balanced by the forward weight of the hydraulic actuator, pump and pivot, so that the vehicle runs at a good trim angle during operation. The weight distribution of the deployment mechanism is also symmetrically distributed about the centerline plane of the USV16 so that there is no undesirable list on the water. A 22 inch API Marine hydraulic hatch lift actuator (with a 1 inch diameter piston), driven by an API Marine PT406NM-3 power TT pump, provides the large moment required to keep the Aris deployed in a current while at speed.

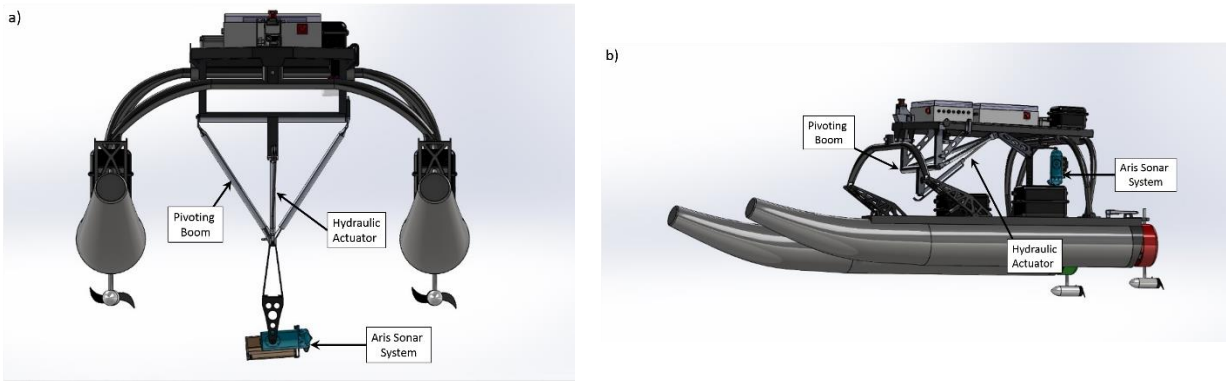

Figure 37: Final design of the sonar deployment system: (a) fully extended; and (b) stowed.

The sonar system is used in a tilt/rotate configuration allowing for precise viewing angles. It was found that the inspection of undermining and scour along channel bottoms can best be achieved with the sonar rotated zero degrees in roll and tilted downwards about sixty degrees (Figure 38a). Conversely, clear inspection images of vertical pilings can be obtained with the sonar rotated 180 degrees in roll and tilted about 30 degrees down from the free surface (Figure 38b). It was found that mounting the Aris AR2 rotating mount in the tilt/roll configuration permitted us to image both channel bottoms, by orienting the Aris with the bottom of the sensor facing downwards, and vertical walls of structures, by rotating the Aris 180^{o} so that the bottom of the sensor faces upwards. Note that the AR2 rotator unit is mounted such that at 0^{o} roll and 0^{o} tilt the sonar head point directly outwards from the starboard side of the USV16 (parallel with the sway axis of the vehicle). In this way the USV can be in compliance with COLREGs navigation rules by being located on the right side of a channel when imaging bridges and other structures.

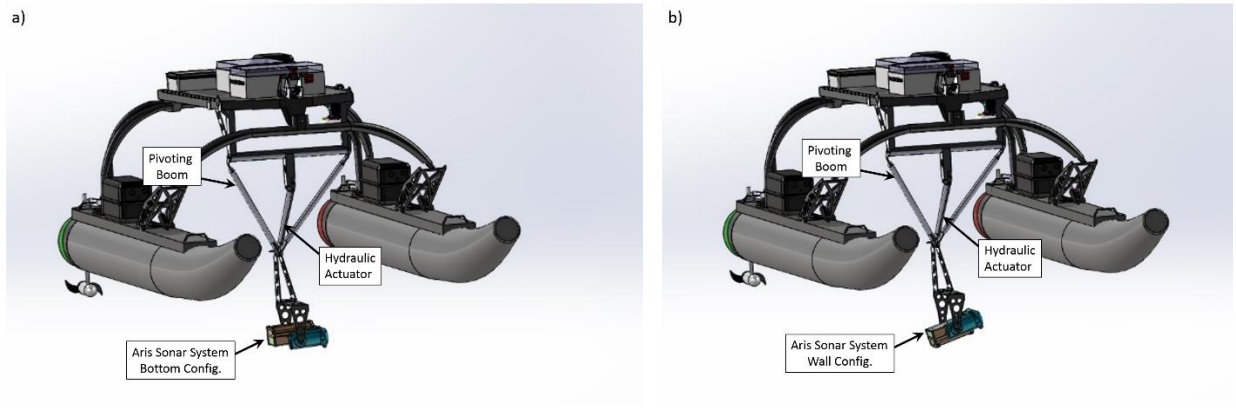

Figure 38: Configuration of Aris 1800 for (a) imaging channel bottoms, and (b) imaging vertical submerged structures.

The boom can be remotely controlled via a Futaba radio controller when the vehicle is in remote control (RC) mode, remotely via a desktop application from the ground station when the vehicle is in automatic control mode, or autonomously by the vehicle's main control box when the vehicle is in automatic control mode. During system assembly, a spacer was inserted into the piston of the hydraulic actuator to limit its range of motion to within the distance required for use on the USV16. In addition, the boom utilizes limit switches to ensure that its positioning controller cannot damage the system by attempting to move the sonar beyond its designed travel range in both the fully-deployed and fully-retracted positions. In autonomic control mode, the vehicle will travel to a designated waypoint, station keep alongside the point of interest, record and transmit images back to the ground station, and then repeat this procedure for the next point of interest. Pictures of the final design, as built, can be seen in Figure 39.

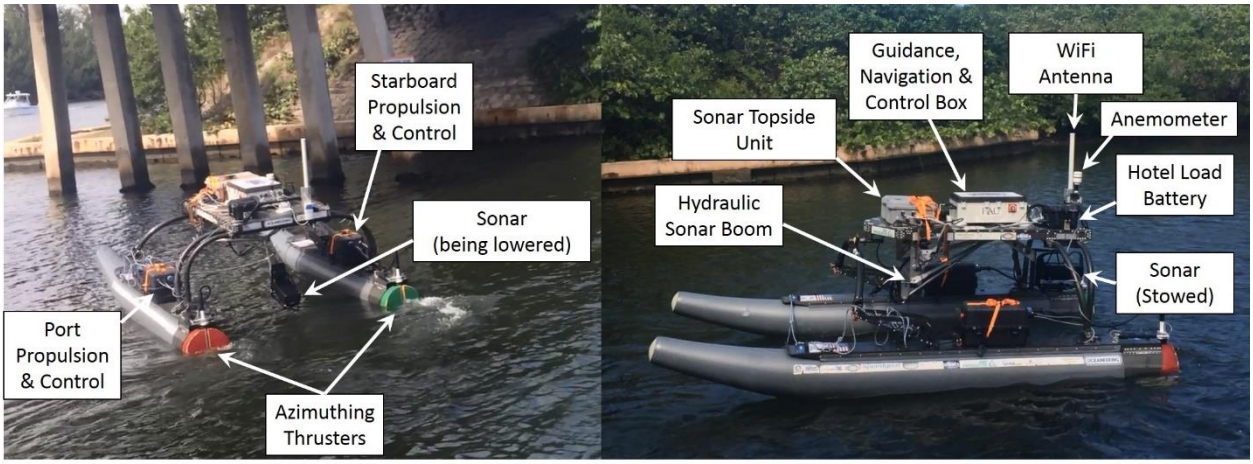

Figure 39: Images of the sonar system, retractable boom and sonar topside unit implemented on the USV. The pictures were taken while performing validation and functional tests on a concrete and steel bridge near FAU SeaTech Campus.

5.1.4 Aris Sonar Topside Unit

The sonar topside unit was designed and fabricated at FAU and is housed within a water-resistant Pelican case (Figure 40). Modifications to the Aris sonar system were avoided by using the standard manufacturer-provided cable. To enable this, a MKS(W)-3XL12-CCP Teledyne Impulse connector was special ordered from Teledyne and installed on the outside of the topside unit. The topside unit itself consists of a Lenovo Y50-70 laptop for collecting and processing sonar images, a RoboteQ LDC1430 motor controller for deploying and retracting the sonar boom, a VICOR V28B48C150BL DC-DC power supply unit (PSU) for the SoundMetrics sonar, and a USB Hub / CAT5 Ethernet adapter for networking with the USV16's guidance, navigation and control system, as well as, communication with a ground station through WiFi. The RoboteQ controller interfaces with the hard wired limit switches described above to prevent the hydraulic system from over-extending or over-retracting. To facilitate potential expansion or reconfiguration of the sonar deployment mechanism, the controller can be used in one of two configurations, depending on the hydraulic pump motor chosen. Hydraulic pump motors are available in two-wire or three-wire

models. When using a two-wire model (configuration currently implemented on vehicle) only the RoboteQ controller is utilized. However, a three-wire motor can be used with the available solid-state relays.

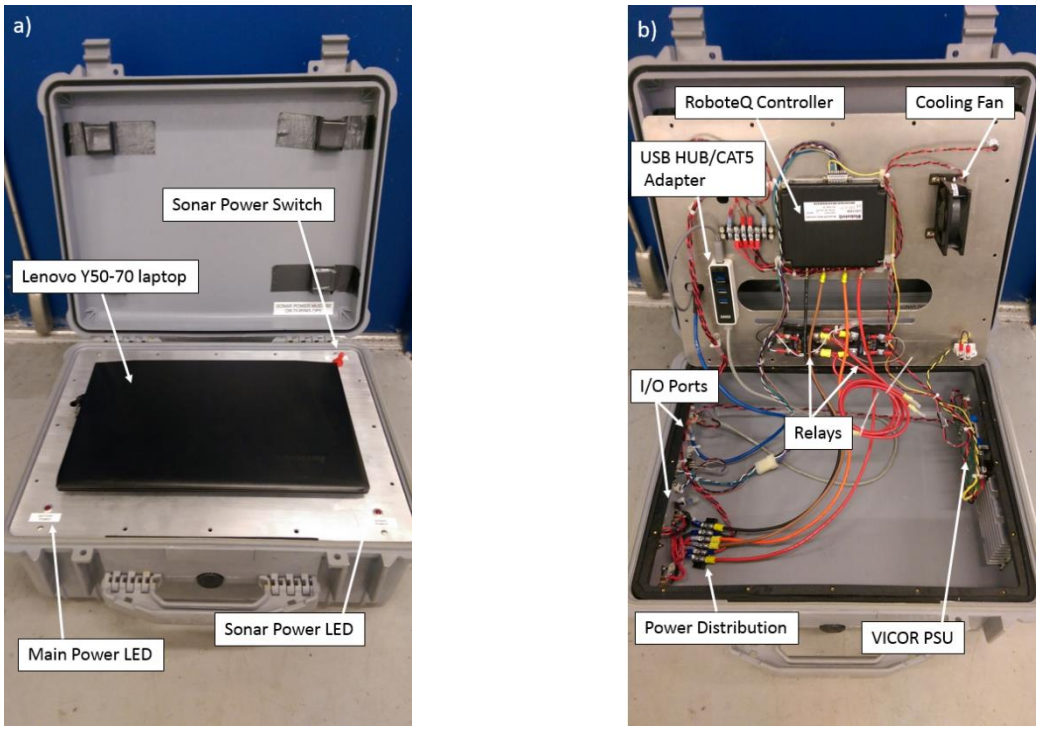

Figure 40: The in-house designed Aris sonar topside unit: (a) A laptop which is networked with the USV16's low level control system is used to control positioning and image capture from the Aris sonar system. (b) View of the inside of the Aris topside unit, which houses a motor controller for raising and lowering the hydraulically actuated sonar boom, a USB hub for networking the Aris laptop and input-output I/O ports for interfacing with the Aris sonar system and USV16's low level controller.

To accommodate the sonar, the USV16's resident powering system was augmented with an additional battery and some new power conditioning instrumentation. A VICOR PSU, DC-to-DC boost converter is used to step up the onboard 12 volt hotel load battery to 48 volts, as required for the sonar. This specific unit was selected, as it has been tested and approved by SoundMetrics for use with the Aris1800. There are two red LED indicators on the top plate. The 'Main Power LED'

indicates power into the topside unit and the ‘Sonar Power LED’ is tied to a toggle switch for sonar power only.

A Ubiquiti WiFi system is used to provide high data rate communications between the Aris computer and a remote ground station, where an inspection team can see the imagery collected by the sonar. An airMAX omnidirectional antenna is configured for 360 degree point-to-point coverage at a range of up to one mile. The antennas require line of sight and no more than 4 feet of height difference at a distance of 520 feet.

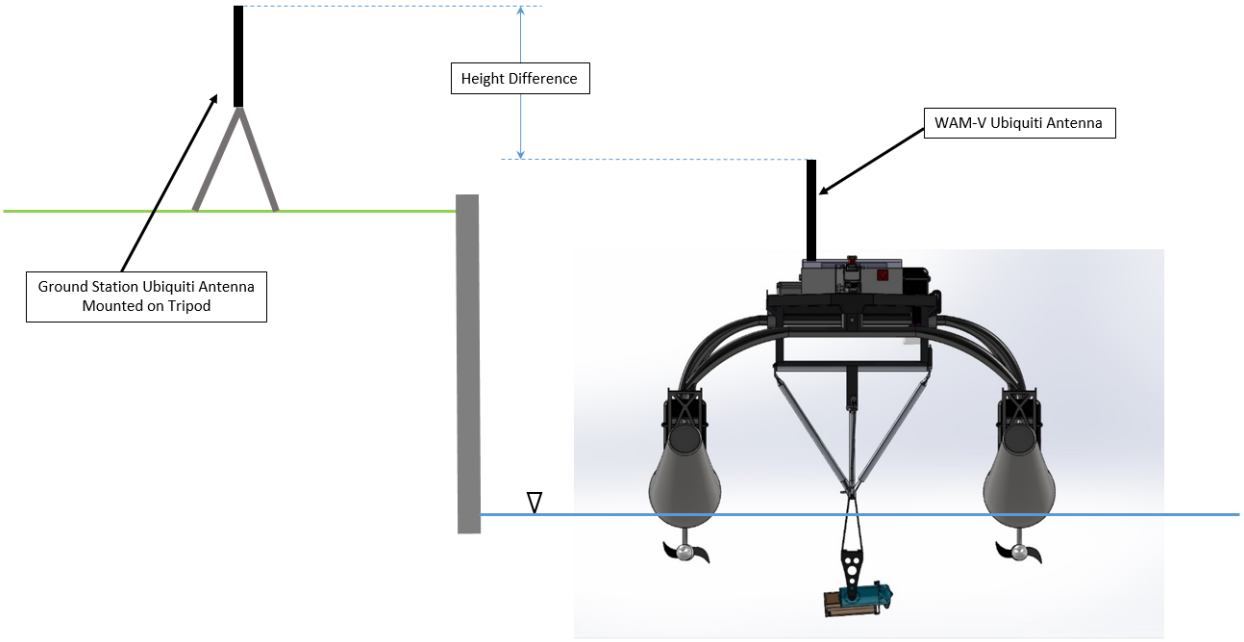

Figure 41: Long range WiFi setup to monitor sonar image collection from a remote ground station.

The signal strength of the WiFi system was tested for a horizontal antenna spacing of 520 feet and various heights, as shown in Table 4. The maximum height of 67.5 inches reduced the signal strength to roughly 58% and, at this level, video transmission resulted in high packet loss and was unsuitable for inspection.

Table 4: Experimentally measured WiFi signal strength versus antenna height at a horizontal spacing of 520 feet.

Height Difference (inches)	Signal Strength (%)
34.5	95
46.5	85
58.5	72
67.5	58

5.1.5 Topside Digital Camera

An existing GoPro Hero3 digital video camera was mounted on top of the starboard hull of the USV16 (Figure 42). As the real-time imaging sonar system acquires images of underwater bridge structures from the starboard side of the USV16, the position permits the simultaneous above- and underwater-recording of bridge structure images. The video streams from the camera and sonar system can be synchronized in post processing by correlating the time stamps from the sonar system and videocamera. Individual pictures that capture features of interest can be extracted from the videos (**Figure 43**).

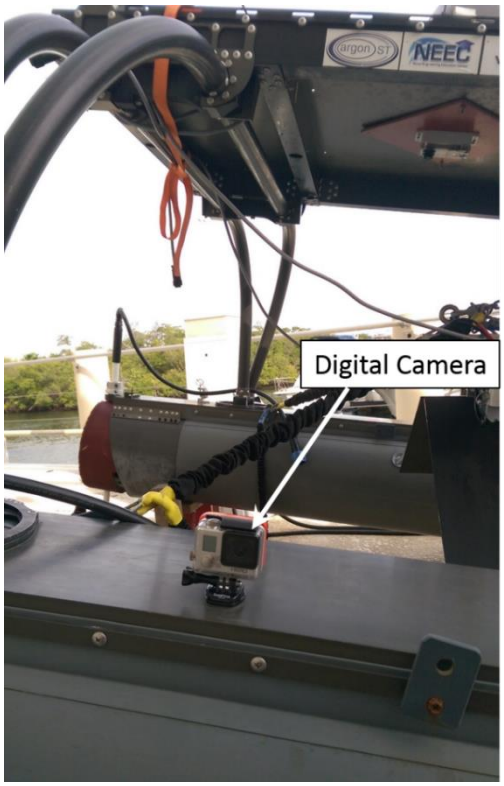

Figure 42: The digital video camera mounted on the USV16.

Figure 43: Example splash zone images of bridge structures acquired using the hull-mounted digital video camera.

5.2 Software and Human Interface

Software was written to interface the new sonar deployment mechanism with the existing navigation and control system on the USV16. A driver was developed, utilizing the Lightweight Communications and Marshalling operating system, to send control signals from the USV16 high-level state machine to the topside control unit, and in turn, to the Roboteq motor controller used to

control the hydraulic pump that drives the hydraulic actuator. In addition, a graphical user interface (GUI) was developed to control the Aris from a remote ground station (Figure 44). The GUI permits RF communication with the USV16 and power monitoring of the batteries.

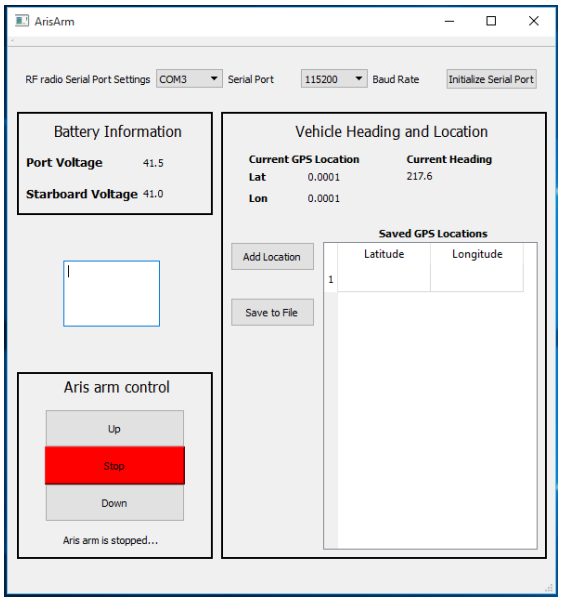

Figure 44: Desktop application used for diagnostics and waypoint collection.

The desktop application serves as a diagnostic tool to relay information about the vehicle's state. It also allows for easy collection of waypoints the first time the vehicle is deployed at an area of interest. During first time setup at an inspection area, the vehicle can be remotely navigated to a point of interest and set in station-keeping mode. The GPS point can then be collected with the *Add Location* button and the sonar can be deployed and retracted with the *Up, Down* and *Stop* buttons. Once all the desired points are collected, they can be saved to a file and uploaded to the vehicle's navigation system for later autonomous deployment.

As shown in Figure 45and Figure 46, the existing radio frequency (RF) communications system was extended to include a ground station receiver (Xtend-PKG-900 USB RF modem). The

RF modem and WiFi transceiver at the ground station permit continuous communication with the USV and enable live streaming images from the real-time imaging sonar to be displayed.

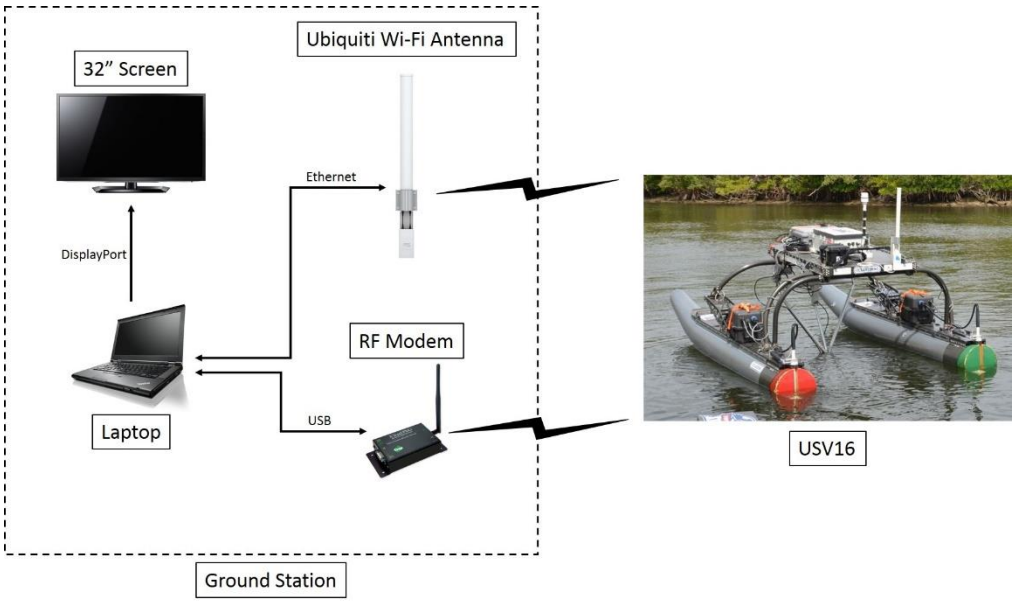

Figure 45: Schematic of the ground station. Together with the hand-held RC unit (see Figure 50 below), the laptop and large display monitor form the physical part of the human machine interface.

Figure 46: Ground station in use at a field test site.

6 Field Tests

6.1 On Water-Integration and Control System Tests

6.1.1 Performance Testing of USV Station Keeping and Path Following Capabilities

A series of sea trials were performed in the FAU SeaTech Marina in Dania Beach, FL to test the performance of the station-keeping controller and the control allocation scheme described above. In order for the vehicle to operate effectively, it cannot be used in sea states greater than sea state 1, wind speeds greater than 15 knots, wave heights greater than 0.2 meters and environments with heavy currents. Wind and current were therefore the two major causes of environmental disturbance. The effect of waves on the vehicle was neglected. While the wind disturbance on the vehicle could be estimated, and accounted for, the USV16 currently lacks of an appropriate sensor to measure water currents.

Two different locations were chosen to perform the experiments. A small map illustrating the desired state of the vehicle at each location is shown in Figure 47. The locations were selected to expose the vehicle to minimum (Location 1) and maximum (Location 2) local environmental disturbances. The desired heading of the vehicle was also chosen to reproduce the most friendly (Location 1) and the harshest (Location 2) scenarios.

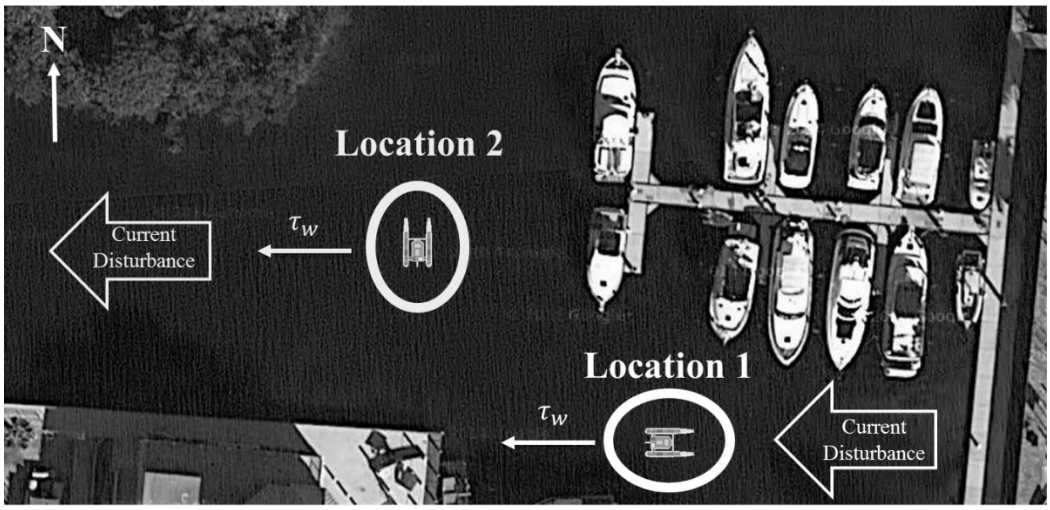

Figure 47: Test locations. Location 1 was more sheltered in comparison to Location 2. Location 2 exposed the vehicle to greater current disturbance due to the channel created between the northern and western inlets.

The USV16 is designed to navigate primarily in the surge direction; therefore this type of motion is considered the simplest to achieve. At Location 1, the vehicle's desired heading is in the opposite direction of the disturbance, therefore the controller will output a high force in the surge direction, T_x. This maneuver can be easily achieved and is consistent with a "friendly" scenario. As the azimuth angles available to the propulsion system are limited, the most difficult configuration to achieve will be one that requires a large sway force T_y, while simultaneously commanding a torque M_z. At Location 2 the vehicle's desired heading is 90º from the disturbance direction. Therefore, the controller will output a high force in the sway direction, T_y, to counteract the disturbance, creating the harshest scenario.

The apparent wind speed V_{rw} and apparent wind direction γ_{rw} was recorded directly from the vehicle during the experiments to quantify the sensed disturbance. Mean and standard deviation of V_{rw} and γ_{rw} at Location 1 and Location 2 over the time at which each controller was being tested is shown in Table 5 and Table 6 respectively. Note that all the mean values of V_{rw} have

similar magnitudes at both locations. However, the mean values of γ_{rw} average around 230° at Location 2 and 180° at Location 1, (meaning that the wind drag on the USV had a substantial transverse component at Location 2). For these reasons, and due to the tidal current direction, Location 2 presented a harsher environment for station-keeping.

Table 5: Mean and standard deviation of apparent wind speed and apparent wind, and wind turbulence direction at Location 1 for sliding mode station-keeping controller with and without wind feedforward control, the duration is 700 s.

Controller:	**Sliding Mode**	**Sliding Mode with feedforward**
Mean Apparent Wind Speed (m/s):	2.17	2.35
Standard Deviation of Apparent Wind Speed (m/s)	0.66	0.76
Mean Apparent Wind Direction (deg)	179.5	177.6
Standard Deviation of Apparent Wind Direction (deg):	13.8	14.2
Wind Turbulence Intensity $\boldsymbol{s} \equiv \boldsymbol{TKE}/\overline{\boldsymbol{u}}$ (%)	15.3	16.1

Table 6: Mean and standard deviation of apparent wind speed and apparent wind direction, and wind turbulence at Location 2 for sliding mode station-keeping controller with and without wind feedforward control, the duration is 700s.

Controller:	**Sliding Mode**	**Sliding Mode with feedforward**
Mean Apparent Wind Speed (m/s):	2.14	1.98
Standard Deviation of Apparent Wind Speed (m/s)	0.73	0.80
Mean Apparent Wind Direction (deg)	215.9	216.0
Standard Deviation of Apparent Wind Direction (deg):	28.89	40.44
Wind Turbulence Intensity $\boldsymbol{s} \equiv \boldsymbol{TKE}/\overline{\boldsymbol{u}}$ (%)	17.1	20.2

The performance of the controller was tested with and without the wind feedforward feature. All experiments were initialized by bringing the vehicle to its desired state manually using a remote controller outfitted on the GNC hardware. The system was then commanded to engage in autonomous mode and maintain its state for 700 seconds. This procedure allowed the controller to act on the vehicle at steady-state conditions with zero initial error. Previous sea trials showed that, if the station-keeping command was given with an initial error in heading and position, all controllers were able to drive the system steady-state rapidly. Heading and position were recorded throughout each run. To evaluate the performance of each controller, the errors in both heading and position were plotted. To evaluate the effectiveness of the wind feedforward feature, the state error was plotted for the station-keeping controller with and without the wind feedforward control.

Station-keeping Trials at Location 1: Vehicle Friendly Scenario

The results for the sliding mode station-keeping controller, with and without the wind feedforward control, operating at Location 1 are shown in Figure 48.

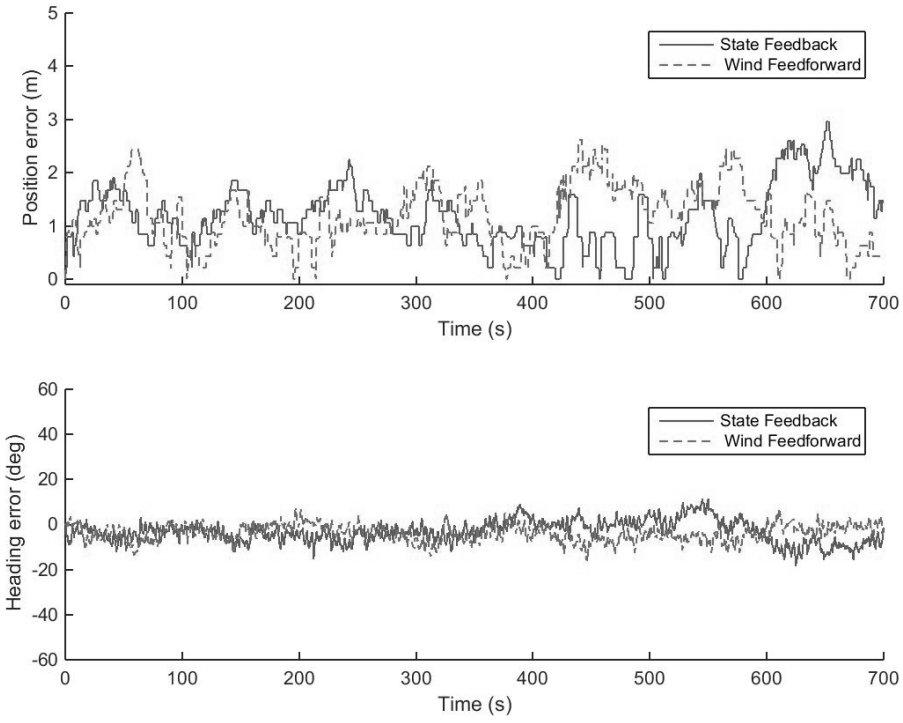

Figure 48: Position and heading errors for sliding mode station-keeping controller with/without wind feedforward control at Location 1. As the resolution of the GPS sensor is about 1 m, the position measurements exhibit step-like appearance.

Appropriate tuning of the sliding mode parameters was essential to maximize the performance of the sliding mode controller. More specifically, the boundary layer thickness, $\boldsymbol{E}$ had to be precisely defined, since excessively reducing its values caused constant saturation of the control output resulting in large errors, and excessively increasing it caused uncontrolled chattering that deviated the system from its desired state. The bound around the uncertainties, $\boldsymbol{R}$ in also had to be tuned accordingly, based on the controller performance. Extensive testing was carried out to manually refine these parameters, until the final values were identified. The improvement in performance was then evident, since the error was contained and slowly varied within the boundary layer thickness throughout the experiments. The performance of the sliding mode station-keeping

controller was not noticeably improved by applying wind feedforward control. The performance of the station-keeping controllers, is compared in Table 7.

Table 7: Mean and standard deviation of position and heading error at Location 1 for the sliding mode station-keeping controller with/without wind feedforward control.

Controller:	**Sliding Mode**	**Sliding Mode with feedforward**
Mean Position Error (m):	1.18	1.18
Standard Deviation of Position Error (m)	0.59	0.56
Mean Heading Error (deg)	4.69	4.28
Standard Deviation of Heading Error (deg):	3.37	3.07

Station-keeping Trials at Location 2: Vehicle Unfriendly Scenario

At Location 2 the vehicle is exposed to transverse current and wind disturbances, which the propulsion system can't counteract while maintaining the same USV heading ψ. This forces the vehicle to momentarily deviate from steady-state, leading to larger errors. Specifically, as position error in the y direction increases, the position error in the x direction and the heading error are maintained low. This scenario results in a controller output, $\boldsymbol{\tau}$, with very small surge force T_x and moment M_z, but a very large sway force T_y. The required propulsion system configuration, $\mathbf{f}$, then becomes very difficult to achieve due to the constraints in thrust and azimuthing angles. The results of the sliding mode station-keeping controller, with and without the wind feedforward control, operating at Location 2 are shown in Figure 49.

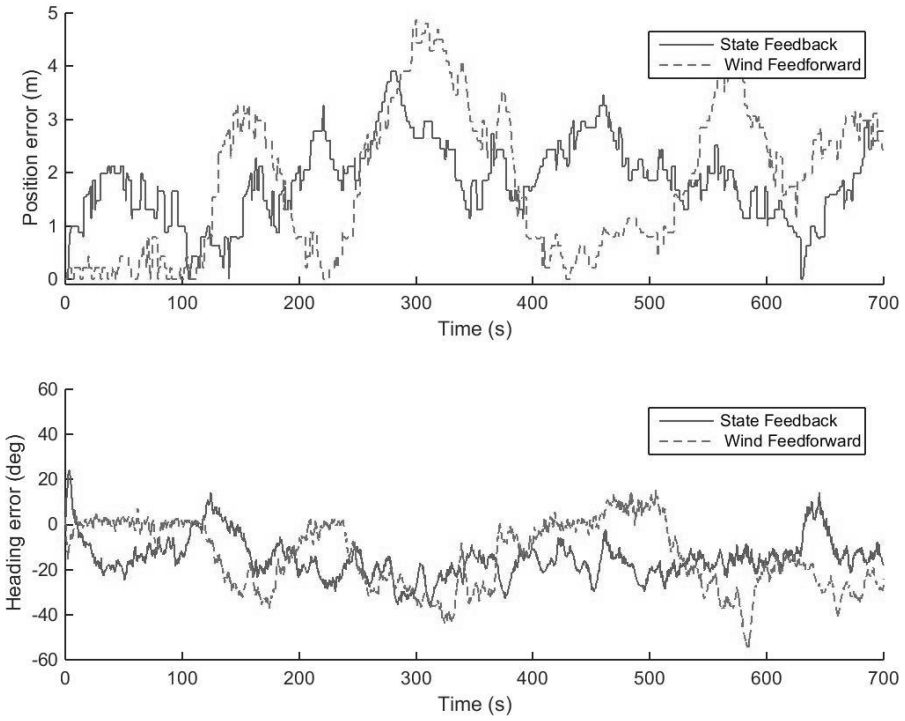

Figure 49: Position and heading errors for sliding mode station-keeping controller with/without wind feedforward control at Location 2.

At Location 2, the errors in both position and heading increase very slowly over time but are always brought back to near zero. However, while sliding mode control theory forces the system to reach and stay within the boundary layer, it does not guarantee a quick response to an increase in error, which causes the system to occasionally exit the boundary layer. As expected, when applying wind feedforward control, the positioning error is reduced slightly. The mean and standard deviation of position and heading error at Location 2 are presented for each station-keeping controller in Table 8.

Table 8: Mean and standard deviation of position and heading error at Location 2 for the sliding mode station-keeping controller with/without wind feedforward control.

Controller:	Sliding Mode	Sliding Mode with feedforward
Mean Position Error (m):	1.85	1.80
Standard Deviation of Position Error (m)	0.75	1.35
Mean Heading Error (deg)	15.96	16.03
Standard Deviation of Heading Error (deg):	7.08	12.85

6.1.2 Remotely Controlled Testing of the Sonar System

Use of the sonar deployment boom and sonar system was functionally tested using a handheld Futaba T14SG RC controller (Figure 50). The unit has several user-programmable switches that can be configured to actuate different types of systems. A three-position switch on the upper right hand side of the controller is configured so that (1) when toggled upwards the sonar system boom moves up, towards its stowed position under the payload tray, (2) in the neutral, middle position any motion of the boom stops, and (3) in the bottom position, the boom moves towards its fully deployed position with the hydraulic actuator fully extended.

The RC controller also controls the motion of the USV16, with the left and right levers controlling forward and reverse thrust on the port and starboard thrusters, respectively, and two small side levers (out of view in Figure 50) controlling the azimuth angles of each thruster. One of the two-position toggle switches on the upper left functions as a remote emergency stop to kill the propulsion system, and one of the two-position toggle switches on the upper right is used to switch between human RC control of the USV16 and on-board, autonomous, computer control.

Figure 50: Configuration of the hand-held RC Control unit.

Functional tests of the system included: 1) verifying that the hydraulically actuated sonar boom would extend and retract as expected; 2) qualitatively checking the speed of extension and retraction; 3) confirming that the travel limit switches mounted on the vehicle operate as expected to stop the boom before any mechanical damage occurs if an operator were to accidentally command the system to continue motion of the boom beyond the intended range; 4) validating that all of the toggle switches on the hand-held unit operate as intended.

Initial functional testing of the system in the marina at the FAU SeaTech Campus consisted of maneuvering the USV16 on the water with the sonar boom in the extended and stowed positions using a large aluminum angle bracket (of similar size to the Aris) in place of the sonar system. The USV16 was operated at the highest speeds achievable by the vehicle to ensure that the sonar deployment boom was mechanically sound; it was operated in forward, reverse and with the thrusters pivoted to produce a sideways (sway direction) motion. Vehicle direction and speed were rapidly varied to produce as much loading on the sonar boom as possible. The sonar boom

was found to be capable of withstanding these maneuvers with no deflection of the structure visible to the naked eye. The hydraulic actuator was able to hold the test angle bracket at any static user-set position against the hydrodynamically-generated forces when maneuvering.

As mentioned above, the speed of deployment and retraction of the sonar boom was also tested. It was tuned by adjusting a valve inside the lines of the hydraulic actuator so that it takes about 4 seconds to move from a completely retracted (stowed) to deployed (extended) position, or from a completely deployed position to a completely retracted position. This speed was deemed to be fast enough to retract the sonar unit in time to avoid a collision with an obstacle on the water, but gradual enough to prevent sudden jerking/jarring forces that could damage the sonar system during deployment or retrieval.

The ability to collect sonar images under remote control was also tested. The USV16 was piloted to a desired position and vehicle orientation and the sonar boom was deployed using the hand-held Futaba RC controller. Image acquisition was performed by remotely logging onto the Aris topside unit from a ground station via WiFi, configuring the sonar for the desired field of view, resolution, frame rate and orientation (with respect to the vehicle) and then sending a command to the Aris to initiate image capture. It was confirmed that the data collected by the Aris could be viewed in real time on a remote monitor at the ground station (a laptop computer initially and then later a large TV monitor connected to a laptop) and that the recorded images could be stored onboard the Aris topside unit. It was also confirmed that the recorded images could be viewed and post-processed later as video and that individual video frames could be extracted to document features of interest (Figure 51).

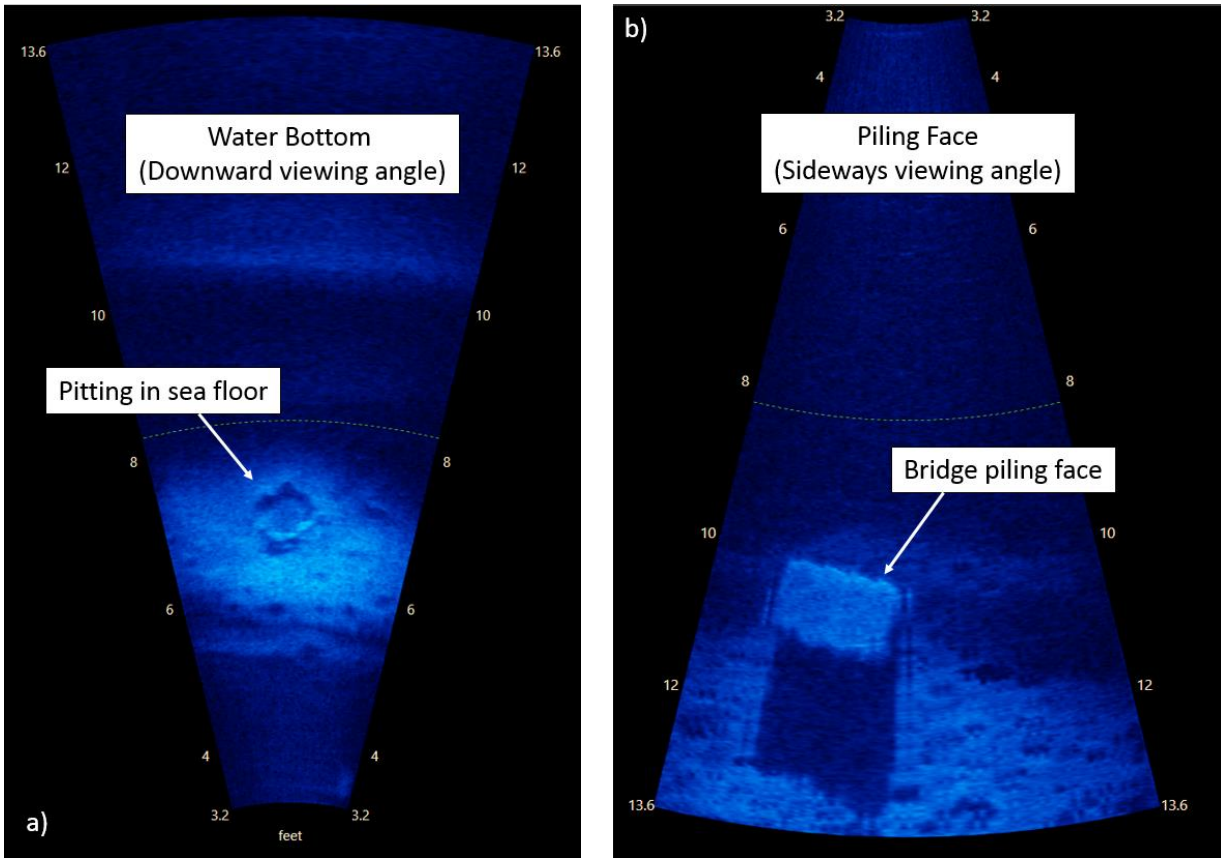

Figure 51: Representative images captured during remote controlled testing of the USV-based bridge inspection system in the FAU SeaTech Marina: (a) a depression on the channel bottom, similar to what would be seen in scour around the bottom of bridge pilings, obtained with the sonar oriented in its "Bottom Configuration"; (b) a small section of the face of a concrete bridge piling obtained in shallow water, obtained with the sonar oriented in its "Wall Configuration" (part of the AIA bridge leading into John U. Lloyd Park in Dania Beach, FL).

6.1.3 Integration of Vehicle's Existing Guidance & Control System with Sonar

The guidance, navigation and control system on the USV16 utilizes an XSens MTiG 700 GPS/IMU to measure vehicle position, speed and orientation. The sensor includes a WAAS-enabled GPS, capable of determining the vehicle's position and speed. The IMU measures the roll ϕ, pitch θ and yaw ψ angles of the vehicle, as well as, the angular rates, angular accelerations and linear accelerations in the surge x, sway y and heave z directions (Figure 52). u, v and w

correspond to the speeds measured by the sensor in the surge, sway and heave directions, respectively.

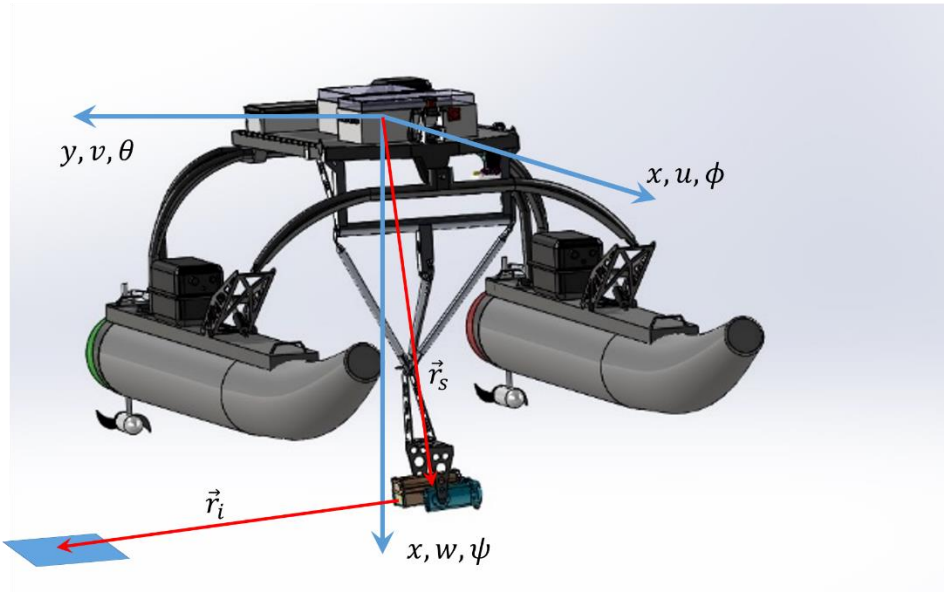

Figure 52: Vehicle coordinate system definitions.

The motion-compensated position of an underwater, acoustically-imaged area relative to a known, georeferenced, position on a bridge structure $\vec{R}_i$ can be obtained from measurements onboard the USV16. To determine this, the vector $\vec{r}_i$ is measured from the sonar unit to an imaged area – this vector is measured in the coordinate system of the sonar. The vector $\vec{r}_s$ between the sonar unit and XSens sensor can be measured before deployment and would be known in the vehicle-fixed coordinate system. The vector $\vec{R}_i$ in the Earth-fixed North-East-Down (NED) frame can then be calculated as $\vec{R}_i = \vec{r}_{vp} + \boldsymbol{R}_{bi}\vec{r}_s + \boldsymbol{R}_{bi}\boldsymbol{R}_{sb}\vec{r}_i$, where $\vec{r}_{vp}$ is the vector between the georeferenced position on the bridge and USV16 (taken to be at the XSens unit itself). Here, $\boldsymbol{R}_{bi}$ is a transformation matrix relating vectors in the vehicle's body-fixed coordinate system and the NED frame. Similarly, $\boldsymbol{R}_{sb}$ is a transformation matrix relating vectors in the Aris sonar head fixed

coordinate system to the vehicle's body-fixed coordinate system. These matrices can be calculated using the IMU-measured roll, pitch and yaw angles on the vehicle as:

$$\boldsymbol{R}_{bi} = \begin{bmatrix} \cos\psi\cos\theta & -\sin\psi\cos\phi + \cos\psi\sin\theta\sin\phi & \sin\psi\sin\phi + \cos\psi\cos\phi\sin\theta \\ \sin\psi\cos\theta & \cos\psi\cos\phi + \sin\phi\sin\theta\sin\psi & -\cos\psi\sin\phi + \sin\theta\sin\psi\cos\phi \\ -\sin\theta & \cos\theta\sin\phi & \cos\theta\cos\phi \end{bmatrix}.$$

If Euler angles are defined similarly for the sonar head, such that ϕ_s, θ_s, ψ_s are the roll, pitch and yaw angles of the sonar measured with respect to the vehicle coordinate axes, then $\boldsymbol{R}_{sb}$can be calculated in the exactly the same way as $\boldsymbol{R}_{bi}$ with ϕ replaced by ϕ_s, θ replaced by θ_s, and ψ replaced by ψ_s.

6.1.3.1 *Validation and Functional Testing of Automatically Controlled Sonar System*

Automatic control testing was performed with several considerations: (1) Waypoint navigation, (2) station keeping, (3) sonar boom deployment, and (4) image transmission. To test waypoint navigation, the vehicle was configured to perform several box-pattern operations in which the vehicle would first travel to a starting point and align the heading. The vehicle would then travel to the next point, turn ninety degrees, and continue on to the following point repeating four times. Station keeping was tested in much the same way, where the vehicle was configured to travel to a point and station keep. The vehicle would then travel to the next test point and perform station keeping again. The data collected from these tests was analyzed and processed for tuning the vehicle's systems which allows for accurate waypoint navigation and station keeping.

Sonar boom deployment was tested with a combination of waypoint navigation and station keeping. The vehicle was configured to travel to a starting point, deploy the sonar boom and station keep while transmitting images back to a ground station computer. The vehicle would then navigate to the next waypoint and station keep for image transmission (Figure 53). This test was

first performed with the vehicle retracting the sonar boom after each test point and extending when arriving at the following waypoint. It was discovered that the sonar system would reboot when the boom was retracted or extended. Testing revealed that the cause of this problem was that the hydraulic pump motor was drawing too much current when actuated. The problem was fixed by contacting the distributor and exchanging the pump motor for a model with a lower current draw. It was also found that for short distances between waypoints (around 100 meters or less), the vehicle and sonar perform well when the sonar boom remains deployed between waypoints. Operation of the vehicle was performed around several in-water structures in the vicinity of the FAU SeaTech Campus, including a wooden footbridge (Figure 53), a seawall, an aluminum and concrete fishing pier, and the A1A bridge into John U. Lloyd State Park.

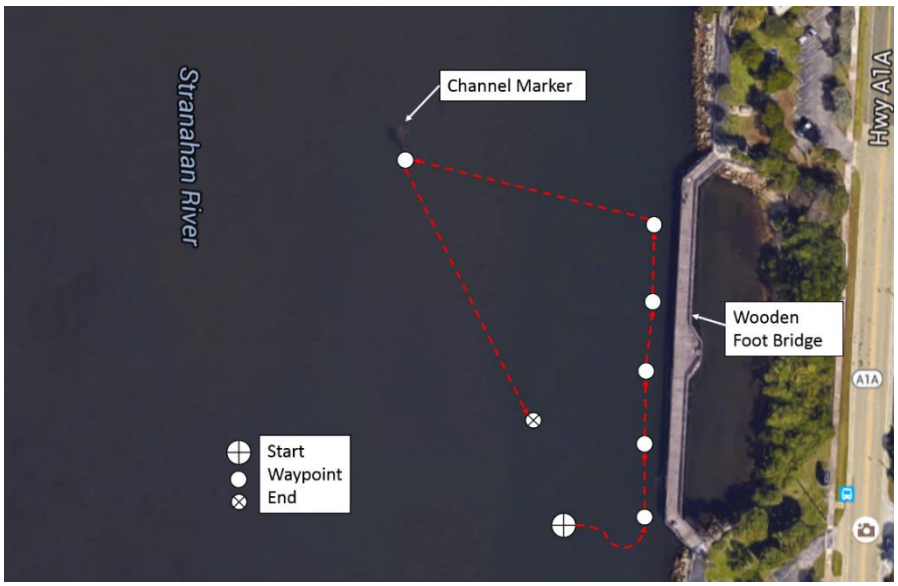

Figure 53: Example waypoint, station-keeping and image acquisition sequence during automatic control tests. Every other piling along the wooden foot bridge was imaged by programming the USV16 to stop at selected waypoints and perform image acquisition. To explore the ability of the system to operate in a cross current, the vehicle was also programmed to image a wooden dolphin used as a channel marker about 150 meters to the east of the foot bridge.

Waypoint selection can be performed in two ways. The waypoints can be entered as a series of GPS values and associated vehicle headings in a text file before the start of an inspection run, or the vehicle can be maneuvered under RC control and each waypoint and its associated heading can be manually added using the GUI shown in Figure 44. When imaging near a bridge or other structure a local GPS waypoint is selected as the origin of a local coordinate system. The software on the vehicle converts the waypoints from GPS latitude-longitude pairs to x- and y-coordinate values from the origin in meters. This approach was chosen, as it was felt to make the data collected easier to interpret by eye. Example waypoint tracking tests performed in the FAU SeaTech Marina can be seen in Figure 54-Figure 56.

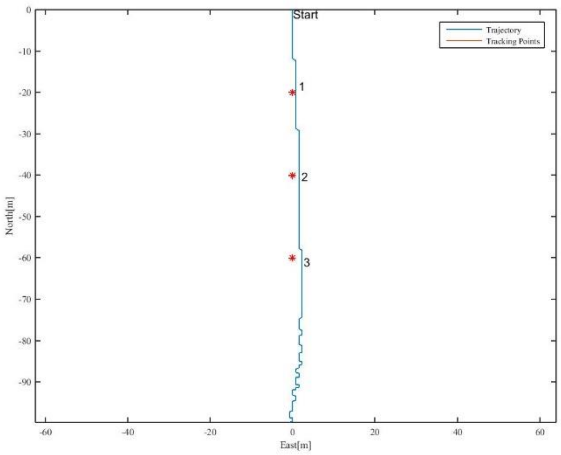

Figure 54: Desired waypoints and the resulting trajectory from waypoint tracking tests conducted in the FAU SeaTech Marina. The direction of the trajectory is roughly aligned with the prevailing current direction. The accuracy of the GPS sensor is < 1 meter, the step like changes are in the East-West measured position demonstrate that the trajectory was followed to within the resolution of the GPS sensor.

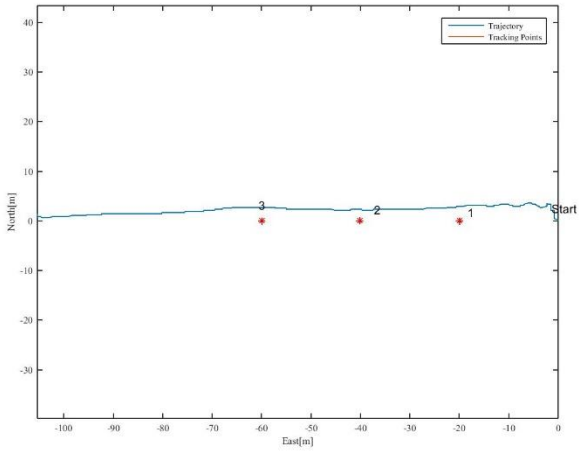

Figure 55: Desired waypoints and the resulting trajectory from waypoint tracking tests conducted in the FAU SeaTech Marina. The direction of the trajectory is oriented roughly 90º to the prevailing current direction.

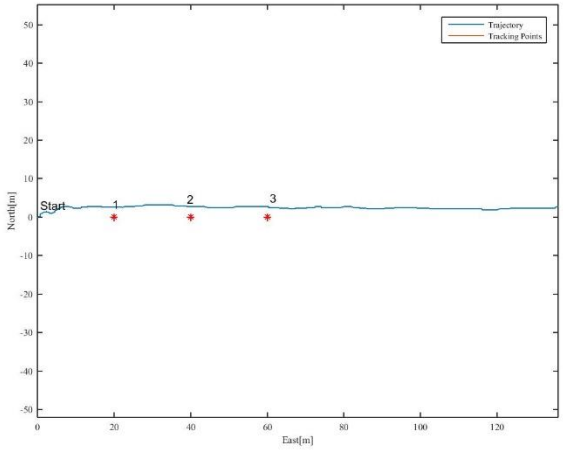

Figure 56: Desired waypoints and the resulting trajectory from waypoint tracking tests conducted in the FAU SeaTech Marina. The direction of the trajectory is oriented roughly 90o to the prevailing current direction.

6.1.4 Field Trials: Complete USV-Based Bridge Inspection System

Field trials of the USV-based bridge inspection system were conducted in Northern Florida from October 26-30, 2015. On October 25, the PI and two of his Ph.D. students transported the USV system to Carrabelle, FL in a rented box truck (Figure 57). With field operations support from personnel at the Gulf Unmanned Systems Center (GUSC), they conducted several field trials in the area.

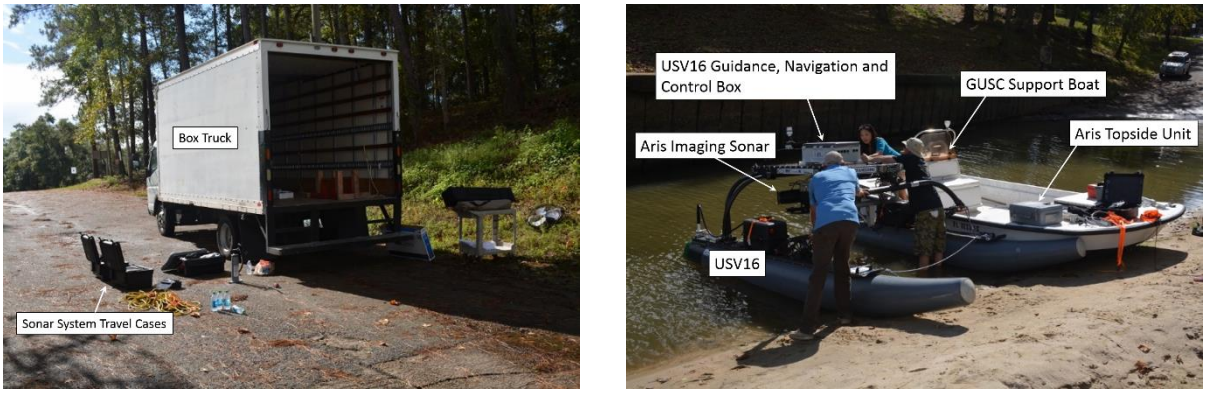

Figure 57: The box truck used to transport the USV based bridge inspection system from Dania Beach to Carrabelle and between test sites (left). The Range Operations Manager and a Contractor from GUSC assist one of the FAU Ph.D. students to assemble the USV system near the HWY 20 Bridge spanning the Apalachicola River near Blountstown, FL (right).

Owing to severe weather (very high winds gusting to about 40 mph and large waves) on October 26-27 and in the days preceding the experiments, the beginning of field testing was delayed until mid-day on October 28. On October 26 and 27 the team assembled and tested as many parts of the system as they could indoors at GUSC. Personnel from FAU and GUSC also discussed testing plans and drove to a couple of possible test sites to ascertain when weather conditions might be amenable to testing. On the advice of the Field Operations Manager from GUSC, it was decided to focus testing efforts on bridges closer to Carrabelle to maximize the remaining testing time (accounting for expected weather conditions and travel times). The system was tested at three field

sites (1) the northern section of HWY 98 (U.S. 319) bridge spanning the Carrabelle River and along Davis Island in Carrabelle, FL, (2) the HWY 20 bridge spanning the Apalachicola River near Blountstown, FL, and (3) the southern section of the HWY 300 (Franklin Blvd) bridge spanning Apalachicola Bay.

At the start of each field test, a visual survey of the area was conducted using a support boat from GUSC to ascertain potential features that might be best to image. The USV system was then deployed to image those areas, with personnel monitoring the acoustic imagery in real time and redirecting the positioning of the vehicle to collect good images. These experiments represented the first time that the entire USV-based bridge inspection system could be tested at length in a wide variety of field conditions and in different types of environments. Therefore, a significant amount of time was spent adjusting the orientation of the sonar system and its settings to explore how to obtain the best images possible (Figure 58).

Figure 58: One of the FAU Ph.D. students aboard the USV16 verifying the sonar orientation and imaging settings.

6.1.4.1 *U.S. 319 Bridge over the Carrabelle River*

Around mid-afternoon on Oct. 28, the PI and his two students, together with operational support personnel from GUSC, transported the USV16 and acoustic imaging system to the U.S. 319 Bridge spanning the Carrabelle River and Davis Island (Figure 59). Owing to the previous storms, the wind was still somewhat high and the river current was fairly strong. The vehicle was driven under

remote control from a boat ramp at the northeastern side of the bridge to a sheltered area between the western bank of the eastern section of Davis Island and the eastern side of the bridge.

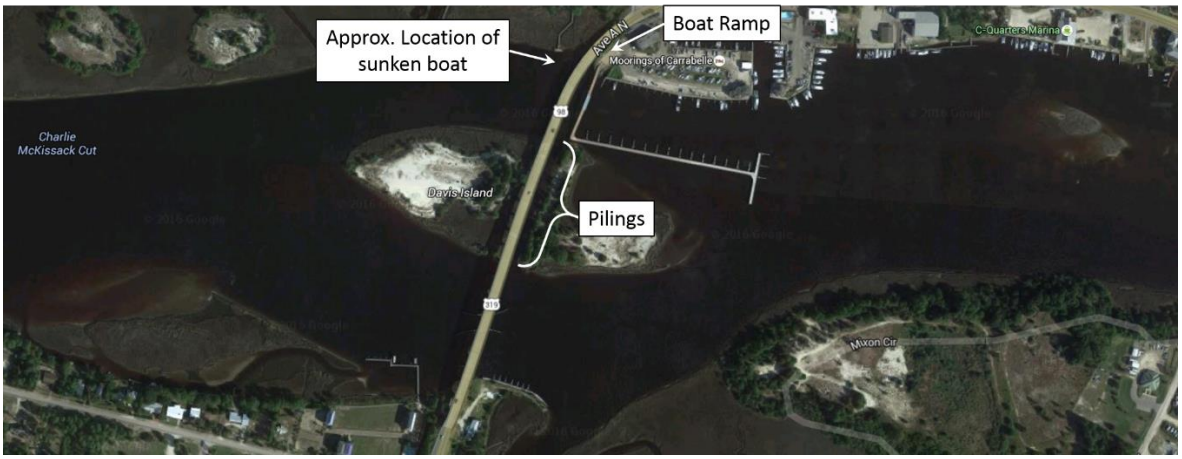

Figure 59: The October 27, 2015 test site at the US 319 bridge spanning the Carrabelle River in Carrabelle, FL.

Functional tests of the vehicle's ability to deploy the sonar system and to operate under automatic control were performed to ensure that the system had survived the 10 hour journey from Dania Beach, FL. The acoustic imaging system was also deployed and several bridge pilings (Figure 60), as well as, a sunken boat hull (Figure 61) were imaged. While these tests were mainly performed to verify that the system was working as expected and provided an opportunity for the GUSC and the FAU teams to familiarize each other with their respective operational approaches, several interesting features were noted in some of the sonar images. For example, it was possible to observe differences in the amount of marine growth and possible defects on bridge pilings.

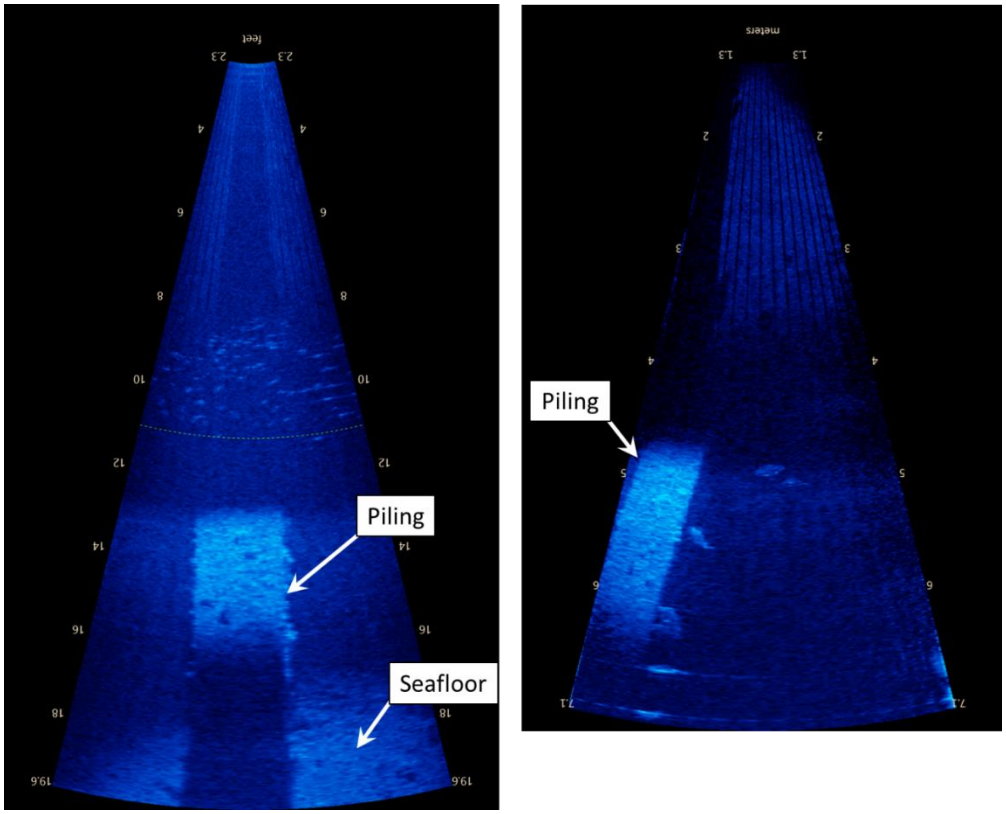

Figure 60: Left: Sonar image of piling and surrounding channel bottom with significant marine growth in about 20' water. Right: Sonar image of clean piling in about 20' water. Several fish swimming around the piling are evident in both images.

Sound waves are reflected differently by different materials. Many small vessels have echo sounders fiberglassed into their hulls to measure the depth they are operating in. As the fiberglass is somewhat acoustically transparent (depending on wavelength), it permits the sound waves from the echo sounder to propagate through the hull. The investigators were curious to see whether or not it would be possible to image a partially submerged fiberglass boat hull with the Aris real time imaging sonar. As can be seen in Figure 61, a submerged fiberglass hull can be quite clearly seen. As debris of this nature can be commonly found around bridges and port structures after strong storms, it is useful to know that such debris can be imaged using the real time imaging sonar on the USV based bridge inspection system.

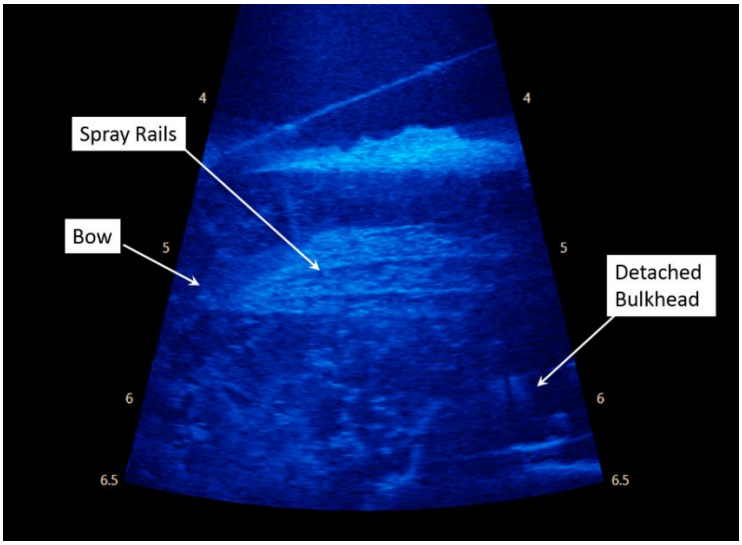

Figure 61: Sonar images of a sunken fiberglass boat hull.

6.1.4.2 *HWY 20 Bridge spanning the Apalachicola River near Blountstown, FL*

An attempt to collect data at the HWY 20 Bridge spanning the Apalachicola River near Blountstown, FL on October 29 was also made. Owing to the driving time from Carrabelle (about 1 hour) and to bad weather earlier in the day, there was only sufficient time for testing in the afternoon (Figure 57). Unfortunately, a problem with the motor controller on the USV16 prevented the collection of data, as we were unable to fix the issue until early evening.

6.1.4.3 *Southern section of the HWY 300 (Franklin Blvd) Bridge spanning Apalachicola Bay*

On October 30, the final day of testing near Carrabelle, the weather was sufficiently calm that we were able to collect a significant amount of data along the southern half of the HWY 300 (Franklin Blvd) bridge between Eastpoint and St. George Island, spanning Apalachicola Bay (Figure 62, Figure 63). The site was selected based on the recommendation of the Range Operations Manager at GUSC, who noted that it was a relatively sheltered area and possessed a number of potentially

interesting features to image. Other sites were also considered, but owing to strong winds, the waves in some areas of the Bay were very large (greater than about 4 feet).

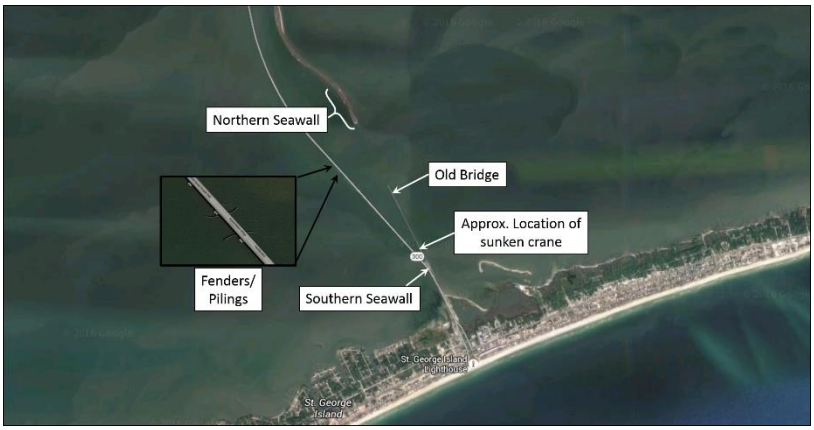

Figure 62: The HWY 300 (Franklin Blvd) Bridge spanning Apalachicola Bay.

Figure 63: Left Image: From left to right, the PI, his two Ph.D. students, and two range technicians from GUSC. Right Image: The USV based bridge inspection system assembled for deployment at the Hwy 300 bridge test site.

The site permitted us to collect data covering a nice variety of conditions and in different water depths that proved to be useful. The Franklin Blvd Bridge is parallel to a retired bridge that is currently used as a fishing pier. The situation allowed us to image both a newer structure and a nearby older structure erected in virtually the same environmental conditions. Even though the water was very cloudy to the naked eye, we were able to image construction debris in fairly fine detail. For example it is possible to see a steel cable lying along the channel bottom in the left image of Figure 64. This image shows both the underwater sonar image and the corresponding surface image. The images were automatically captured by the system in-situ and later synchronized in post processing to illustrate its capability of simultaneously imaging structures in the splash zone above water and underwater. (2) A crane had fallen into the water near a section of the bridge in about 25 feet of water. We were able to image the cab and door of the crane with the acoustic imaging system (right side of Figure 64).

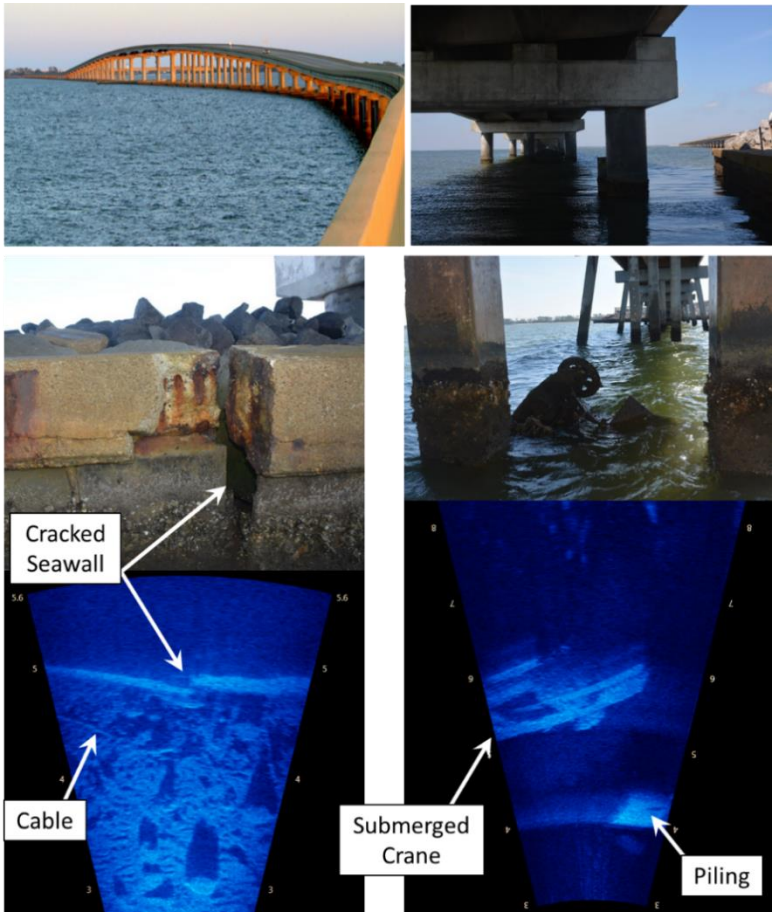

Figure 64: Top Left: St. George Island Causeway, FL. Top Right: Under causeway (old bridge on right). Bottom Left: Crack in seawall under causeway – bottom debris and steel cable visible on seafloor (in about 3 feet of water). Bottom Right: Sunken crane leaning against pier supports of old bridge in about 20 feet of water.

(3) The Northern seawall permitted us to image a variety underwater debris. The seawall essentially consists of piles of rocks and concrete blocks and is surrounded by a substantial amount of debris composed of disused pipes, cables and broken wooden structures. An example of this can be seen in Figure 65.

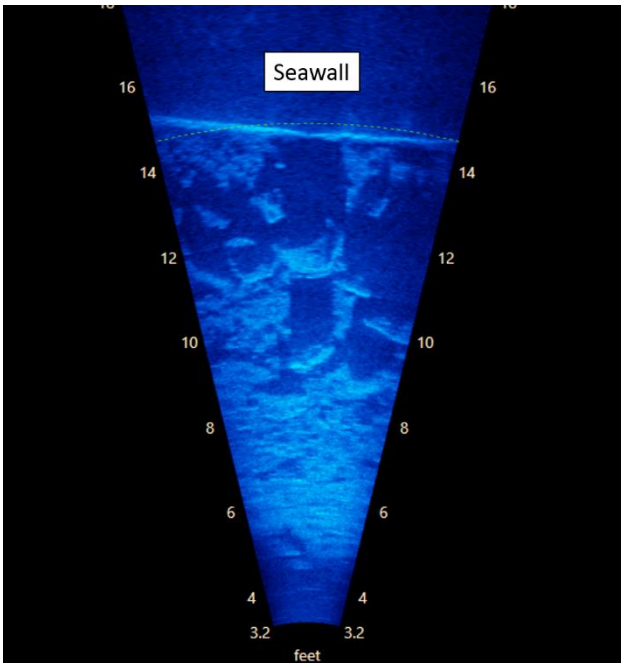

Figure 65: Sonar image of the debris field in front of the Northern Seawall shown in Figure 62.

(4) A set of pilings and fenders was also imaged at this site (Figure 66). At the waterline, the bridge support structures seemed to be large rectangular blocks. However, sonar imagery showed that a few feet below the surface each of the large concrete blocks is supported by several cylindrical pilings. The specific pilings shown in this image were on the side of a shipping channel near the highest point of the bridge. The channel is bordered by a fender to protect the bridge structure from accidental ship strikes (see inset of Figure 62). The square-shaped pilings supporting the fender can be seen in the top of Figure 66. As the intracoastal waterway shipping channel is bordered at both its North and South by a set of seawalls, it is possible that the faster parts of the flow moving

through the channel occur here. In any case, potential scour is evident on the channel bottom between the bridge pilings and fender pilings in Figure 66. It is possible that the eddying motion of the current moving past the pilings bordering the channel is causing some bottom erosion.

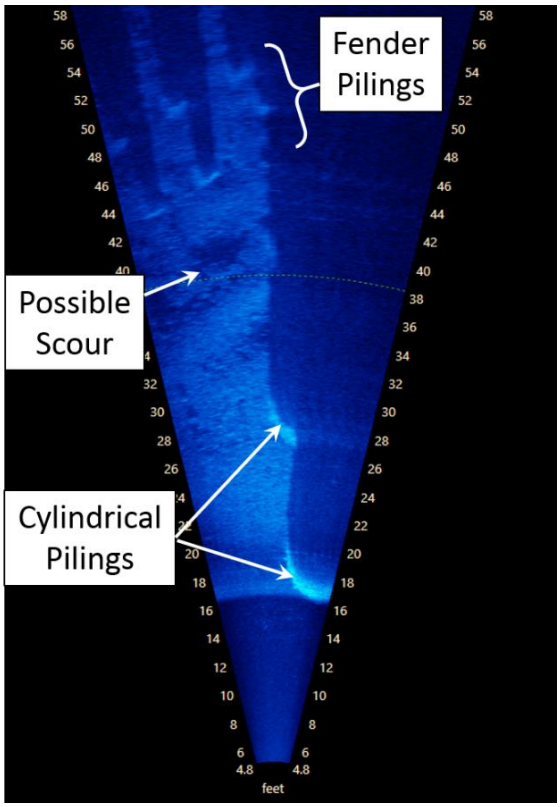

Figure 66: Pilings and fenders.

6.1.4.4 *Concrete and steel bridges in Intracoastal Waterway near FAU SeaTech Campus*

Field trials of the USV-based bridge inspection system were also conducted near the FAU SeaTech Campus in Dania Beach, FL. The pilings under the bridge spanning N. Ocean Dr. Bridge across Whiskey Creek in Dania Beach, FL were imaged (Figure 67).

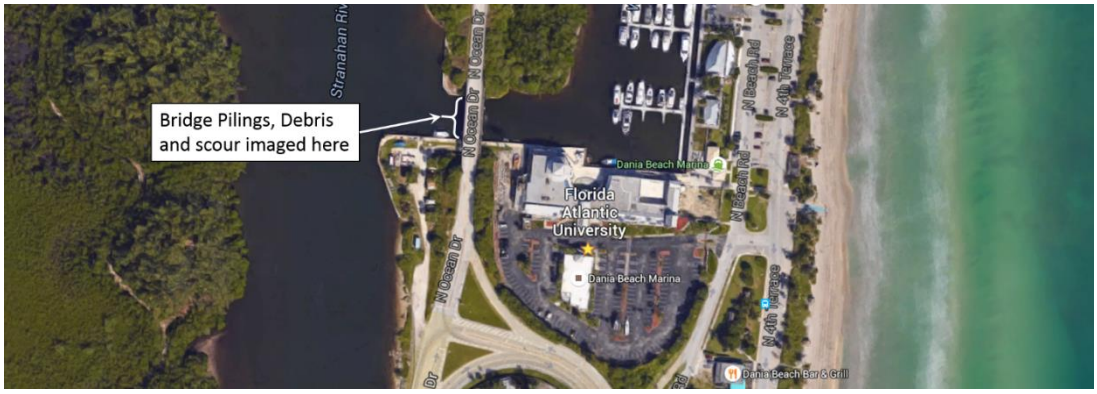

Figure 67: The N. Ocean Dr. Bridge spanning the Whiskey Creek inlet in Dania Beach, FL.

Example results can be seen in Figure 68. Again, one of the important features a bridge inspector would be interested in visualizing is the presence of scour and undermining around the base of bridge pilings. The darker, rough area between pilings in Figure 68 is thought to be scour caused by the high tidal currents caused in the channel where the image was taken.

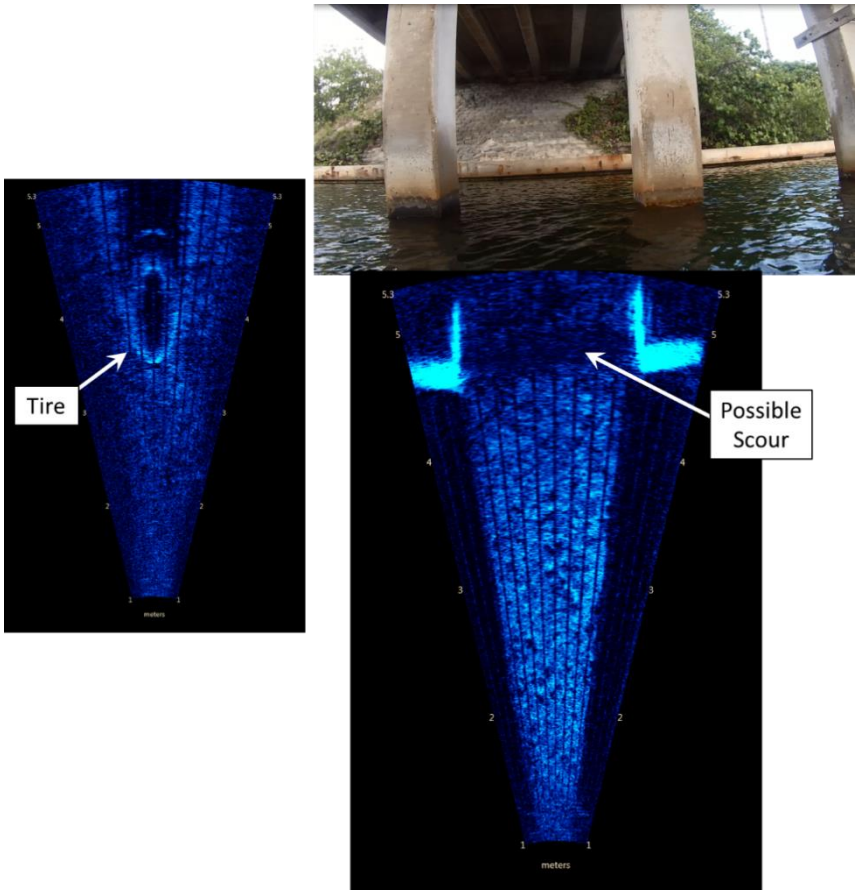

Figure 68: N. Ocean Dr. Bridge across Whiskey Creek in Dania Beach, FL. Top Right: Photo of bridge supports at waterline. Bottom Right: Corresponding sonar image of seafloor between supports – evidence of early scour visible as depression in seafloor between pilings. Left: Example of debris (tire) at base of bridge.

6.1.4.5 *Port Jacksonville, FL*

Live USV-based bridge inspection system demonstrations were given at the Florida Automated Vehicles Symposium in Port Jacksonville, FL on December 2, 2015. The PI and three of his students (Figure 69) transported the system from Dania Beach, FL to Jacksonville, FL in a rented box truck and rental car. From 8:30 AM – 12 PM and then again from approximately 1 PM – 3 PM, the 20 minute demonstration was repeated hourly.

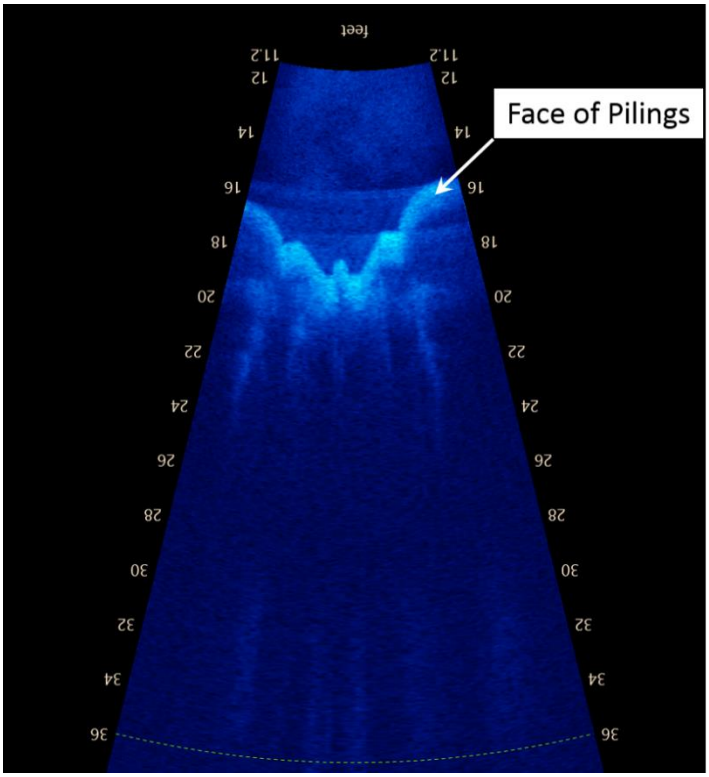

Figure 69: An above water image of the pier and a corresponding underwater image of the pier pilings obtained during the USV-based bridge inspection system at the FAVS. The sonar system was configured to image the faces of the pilings. The pilings can be seen to be a collection of both circular and square concrete pilings, which are arranged in a zig-zag pattern when viewed in a direction perpendicular to the seawall above the pilings.

6.1.4.6 *Concrete and steel bridges in Intracoastal Waterway near FAU SeaTech Campus*

In order to facilitate practical implementation of the system, one can imagine that a bridge inspection team would like to have a system that could perform continuous scans of underwater structures, with minimal interruption for repositioning or reconfiguration of the system. The trajectories likely to facilitate this should require minimal re-crossing of bridge sections already imaged and be easy for a bridge inspection team to set up. They should also be of the shortest distance possible, to extend the operational time available by preserving batter power, which can be especially important for scanning bridges in areas with high winds and current and with long spans. If only WAAS-enabled or differential GPS systems are available (as used on the existing system) rather than RTK-GPS systems, it would be helpful for the system to perform periodic excursions out from under the bridge and into the open where GPS satellite acquisition and updating of the vehicle's position is easier. Of course, maps and information about specific features of interest collected during previous inspections would help in the planning of appropriate inspection trajectories. An area of future research along these lines would be the development of approaches for automatic trajectory planning before an inspection and real-time, automatic, trajectory re-planning during an inspection using the data collected in-situ.

Based on the results of earlier tests (Sections 6.1.4.1-6.1.4.5), it was decided to explore an approach for constructing a continuous trajectory that would permit the underwater structure of a bridge structure to be automatically imaged in a single run. The trajectory shown in Figure 70 was manually planned prior to the tests and performed by the vehicle automatically in a single run. This pattern was chosen so that both sides of the pilings under the bridge and the streambed around them could be imaged in one go. As the real-time imaging sonar is positioned to image pilings on the starboard side of the vehicle, so that the USV will be moving in the same direction as nearby

traffic when along the side of a channel, the trajectory was chosen so that one continuous path could be traversed by the vehicle to image both sides of the pilings under the bridge, on both sides of the channel, without interruption. The trajectory tracking was accomplished using the sliding mode controller described in Section 5.1.1.4.

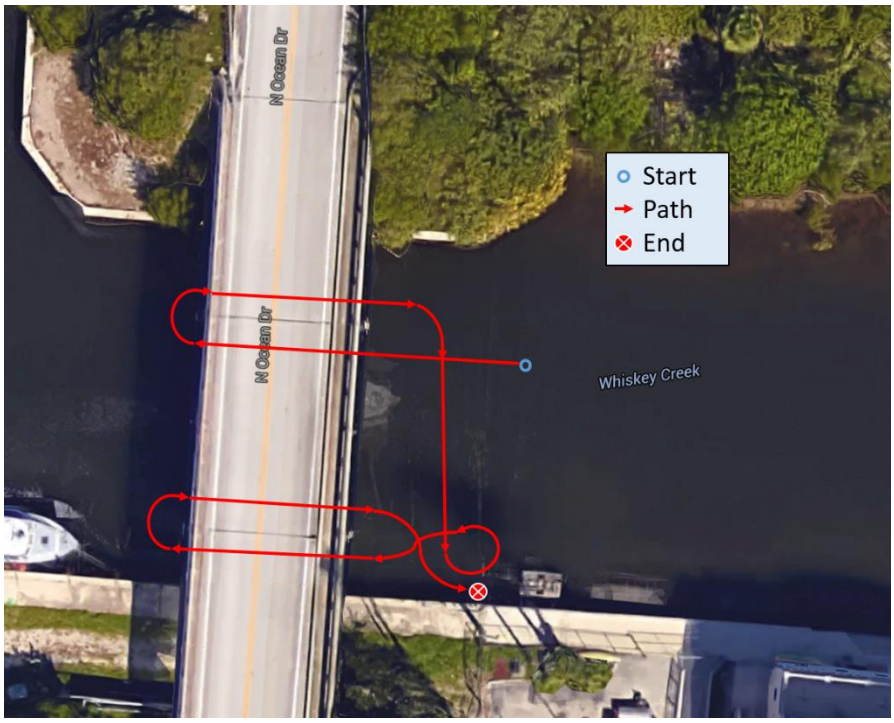

Figure 70: Example trajectory of the USV-based bridge inspection system during follow-on tests at a concrete and steel bridge near the FAU SeaTech Campus in Dania Beach, FL.

This type of continuous waypoint tracking along rows of pilings was found to be fairly effective as it did not require any system reconfiguration or repositioning of the vehicle during the inspection. Example above-water photos and corresponding underwater images of the pilings, which were simultaneously captured during the experiments, are shown in Figure 71-Figure 73. Note that cracks are also visible in the seawall in the background and that the condition of streambed around pilings has been visualized. It can be seen from the sonar images that the stream bed near the east and west side of each piling contains small depressions, which have north-south

dimensions of a size a little smaller than the width of each column. The positions and sizes of these depressions are consistent with current-induced scour, which one would expect to occur in a channel with high currents. The flow under the bridge is tidal and can be quite strong during ebb- and flood-tides (estimated at about 4 knots from qualitative visual observation). The eddies generated by the flow moving past the pilings at these times would tend to erode the channel bottom by removing small pockets of sediment in these areas.

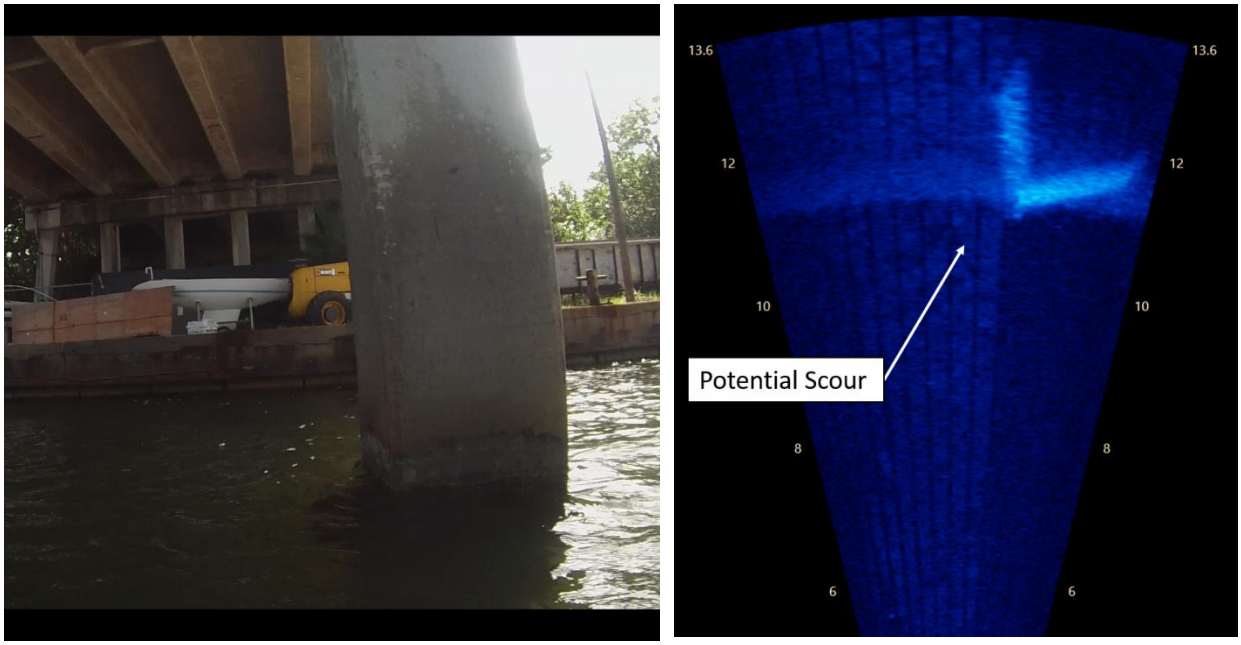

Figure 71: Above water and underwater images of the west-most piling imaged along the southern row of pilings. The conditions of the piling above water and the streambed underwater are visible in the images. At the waterline discoloration and repair work are visible.

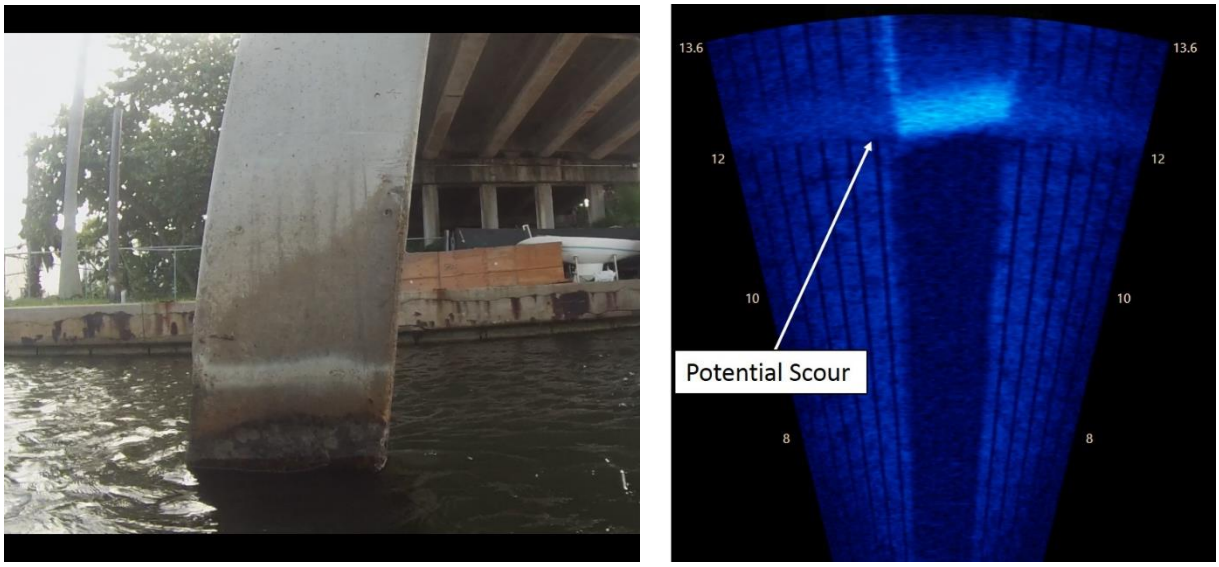

Figure 72: Above water and underwater images of the east-most piling imaged along the southern row of pilings. The conditions of the piling above water and the streambed underwater are visible in the images. At the waterline discoloration and repair work are visible. A long horizontal crack, about a foot above the waterline is visible in the above water image, as are small chipped sections of the corners.

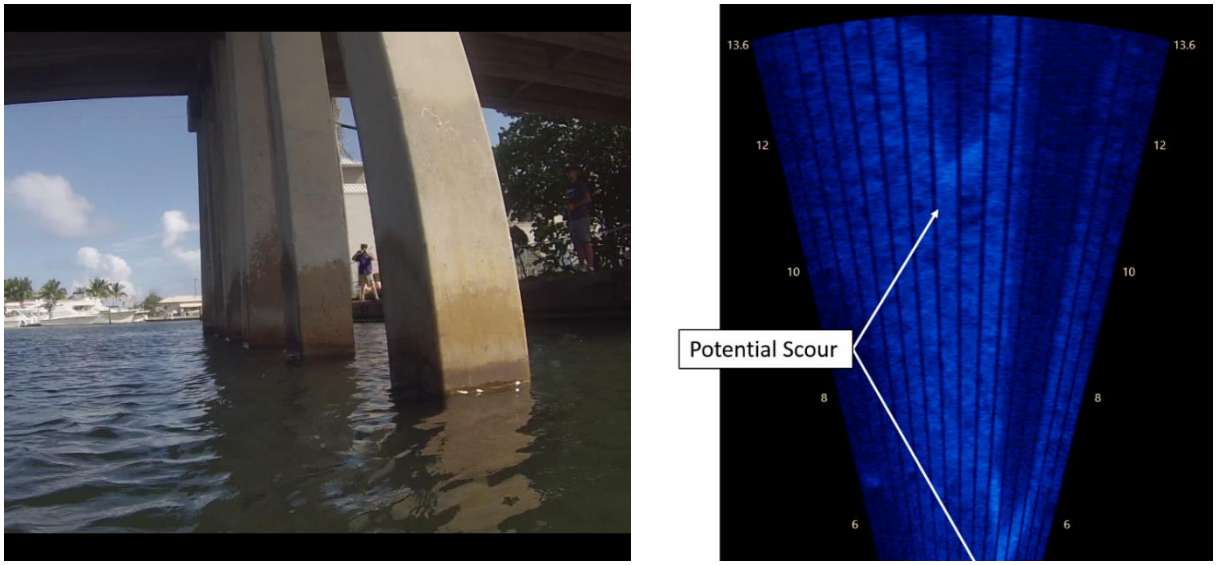

Figure 73: Above water and underwater images of the southern row of pilings showing multiple pilings imaged at the same time. In these images, the distance from the pilings is a bit further than in the previous images. One can see that the sonar images are taken at somewhat of an oblique angle and the condition of the pilings is not as clear as it is in the previous images. However, some of the streambed features are more easily visible from this vantage point.

7 Recommendations for Integrating USV into FDOT Standard Operating Procedures and for Future Research

7.1 USV-Based Underwater Bridge Inspection Operations

7.1.1 General

The underwater sonar inspection team should consist of a lead inspector, one to two dive inspectors, a safety boat operator and any additional personnel, as required. The inspection USV will work in tandem with the traditional inspection team by performing an autonomous inspection and alerting the inspectors at the ground station to any areas of interest that may require a more detailed level II or level III inspection by the dive inspectors. The USV will transmit and record both underwater sonar video and above water video to the inspectors at the ground station for review. A concept of operations for how USV-based bridge inspection could be conducted from start to finish is proposed in Section 4.1.1.

7.1.2 Preparation

Onsite preparation of the USV shall be performed prior to launching the USV. Operators shall perform a hands on check of all cable connection to ensure proper fit and tightness. After starting all control systems, verify proper operation of all RC aspects including thrusters, azimuthing actuators and sonar boom. Upon launching the USV, and navigating to a water depth of at least 30 inches, the sonar boom should be deployed, sonar power activated and proper sonar telemetry verified. Also, the above water video telemetry should be verified at this time.

7.1.3 Ground Station

The ground station should be erected in a shaded area either under the cover of the bridge or under a pop-up tent to avoid prolonged exposure to the sun. The ground station should consist of a table for the equipment, a portable or truck-mounted generator and an appropriate amount of chairs. The ground station should have a laptop computer for monitoring the USVs positional and sonar telemetry and is connected to a networking switch and ground station antenna. The ground station antenna tripod should be placed on a flat and level area and adjusted to match the on water height of the USV antenna. The computer will be wirelessly connected to the USVs electronic control unit (ECU) via telnet and be able to run the automation programs on the USV and connected to the onboard sonar computer via remote desktop protocol and display a live stream recordable sonar video.

7.1.4 Inspection Site Waypoint Collection

The first time an inspection team arrives at a site, waypoints must be collected for the automated inspection path to be generated. The USV will be manually navigated via radio control (RC) to each inspection point with the appropriate heading. At each inspection point, the inspector will use the computer to collect the waypoint and designate it as such in the path planning program. If the desired path will require the USV to change heading while maintaining position, the RC operator will need to affect this maneuver and, once at the desired heading, the inspector will input that point designated as a heading point in the path planning program. Once all the waypoints are collected and a path is generated and tested to satisfaction, this process is done and the path can be used for future inspections at this site.

7.1.5 Inspection

Once the USV is launched, the inspector can initiate the automated inspection program at which point the USV will autonomously follow the pre-programed inspection path. At each inspection point the inspector will visually observe the transmitted underwater sonar video and above water video and record the findings. If evidence of piling damage or scour is observed, it must be noted in the report for additional level II or level III inspections and inspection diver should be dispatched. During the inspection process, if the inspector sees an area of interest on one of the video feeds, he or she can instruct the USV to station keep while further inspecting the video telemetry. Likewise, if an area of interest is observed from shore or boat, the inspector can instruct the USV to navigate to that point outside of the path program for inspection. In the event the automated inspection was paused, for these or any other reason, the inspector can reinitiate the automated inspection and the USV will navigate back to the last automation point and resume the inspection routine.

7.1.6 Reporting

In addition to standard reporting procedures [57], the underwater sonar inspection report should contain the recorded underwater sonar video, recorded above water video, any screenshots taken and detailed notes of any observations requiring further level II or level III inspections. Depending on the water conditions due to daily tidal changes, seasonal changes or other changes over time, detailed observations related to the inspection path must be noted as the path may need to be updated or even multiple paths created for different times of day or year.

7.2 Future Research

As mentioned in Chapter 2, USV guidance, navigation and control is still very much an active area of research. There are several areas of robotics research, common to use on any type of unmanned vehicle (including aerial, ground and marine vehicles), that could make USVs more user friendly for bridge inspection teams and permit operations to be conducted under a wider variety of conditions and in more complex environments. There is also future work that could be done to facilitate the recording and interpretation of underwater acoustic inspection images.

7.2.1 Improved Teleoperation through Better Human Robot Interaction

Sparse advisory control refers to the ability to have a robotic system, such as a USV, mainly perform its work autonomously (independently of a human operator), with occasional inputs from a person in either the form of updated mission directives to be performed autonomously or complete teleoperation (manual remote control). A goal of sparse advisory control is to create a seamless transition between autonomous operation and teleoperation along a continuously sliding scale. The implementation of sparse advisory control requires the successful integration of three main components: (1) the software architecture of the autonomous agents; (2) a means of implementing 'sliding autonomy'; and (3) a human-robot interface that provides sufficient situational awareness, while still permitting a user to rapidly switch between tasks. The software architecture must facilitate the computational speed required for the calculations involved in integrated decision making, task assignment and trajectory planning, especially in systems where regular communication interruptions can occur. Since human operators are not guaranteed to be monitoring the USV at a given time, deciding when a USV should seek assistance from a human

team member on an assigned task is an important question. Associated with this approach are a number of important research issues:

- What is the minimum number of human operators in the team needed?
- How can sufficient situational awareness be provided to human operators so that they can focus on their main tasks, but still be able to guide the progress of the USV?
- Under what conditions should a human operator teleoperate a USV?

Prior research along these lines has involved the exploration of 'common agent architectures' includes: logic-based agents; reactive agents [58]; behavioral agents [59-61]; belief-desire-intention (BDI) agents [62-64] and layered architectures. For unmanned vehicles, it has been found that the more tractable architectures are those based on the use of layers of abstraction, where decision making, sensing and actuation are separated so that the number of internal states of a system can be kept to a minimum [65-68]. The architecture of individual agents within robot teams tend to have three or four layers [69-71] (Figure 74).

Mixed-initiative interactions between robots and human operators can be used in their collaborations [69]. The interactions consist of either the human or autonomous system deciding upon who is in control of aspects of a given task. The goal of the decision-making process is to optimize metrics, such as the expected time to complete the task or overall mission goal and the robustness of the process. Execution of a task may switch between human or robot control based on past performance, such as number of failed attempts or duration.

An important component for the implementation of multi-agent sliding autonomy is the design of the human interface. How quickly a human operator can re-attain situational awareness when transitioning between tasks is crucial for the overall performance of a human-robot team. Important questions are how much information should be presented to the human user, how should it be presented and how much data should be buffered or saved. UAV studies of human performance have suggested that humans are inherently bad at planning when presented with many complex possibilities and with an increased workload. They also suggest that more guidance on task scheduling should be provided as part of a user interface [72]. The dominant factors in human-robot interaction appear to be the neglect time, the interaction time, and the scheduling algorithm selected [73-74]. Monitoring human tasks during the neglect time appears to be a good gauge of whether a human operator is saturated and can be used for dynamic team sizing. Thus, it may be

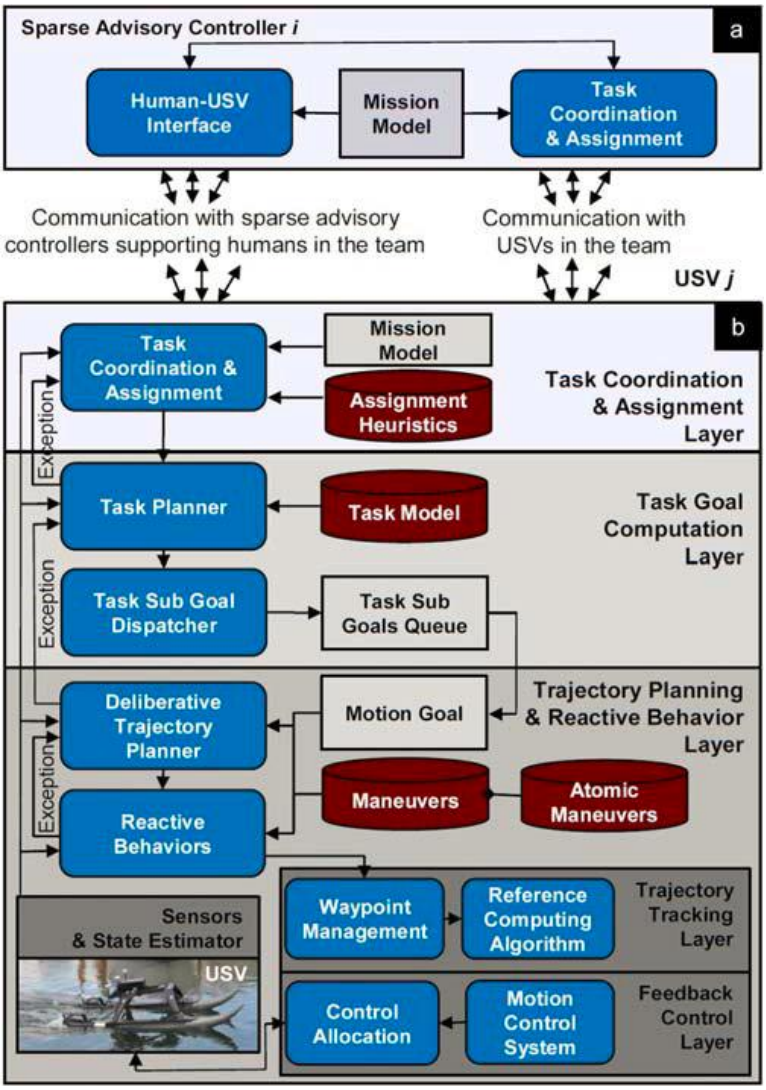

Figure 74: (a) Architecture for distributed sparse advisory control.

(b) Multilayer software architecture of USV (image developed jointly with Prof. S . K. Gupta, University of Maryland).

possible to develop adaptive scheduling algorithms that monitor a human user's performance over time and adjust the scheduling algorithm and team to improve the team's overall performance.

7.2.2 3D Obstacle Avoidance and Trajectory Planning

It is not possible for a software programmer to anticipate the infinite number of possible situations a USV might encounter in the field. In order for USVs to operate in complex environments, such as near bridges and in ports, a combination of advanced deliberative and reactive task and trajectory planning is necessary. This may be achieved through a realized set of "automatically-generated" behaviors, which enhance the planner so that it considers different classes of situations in pre-programmed ways, while taking the inherent limitations of the vehicle's dynamic response into account [56,75-76].

Efficient and safe navigation in highly cluttered, dynamic environments requires prediction of the future movement of dynamic obstacles that can interact with each other in complex ways. A planner needs to reason about the risk associated with each expected avoidance maneuver. It also needs to reason about the availability of contingency maneuvers to counteract scenarios such as the unpredicted behaviors of other vessels. These features cannot be incorporated into purely reactive planners [77-79]. Traditional, lattice-based, deliberative planners [80-82] can find a global optimal trajectory by employing multi-step look-ahead search. However, they are computationally slow when dealing with situations that involve fast moving obstacles. Autonomous USV operations need: (1) fast deliberative planners that can compute near-optimal trajectories by accounting for collision risks posed by dynamic obstacles in complex environments, and (2) reactive behaviors that can quickly generate collision avoidance maneuvers consistent with the planned trajectories to handle unexpected situations.

Recent work in this area includes the development of a model-predictive trajectory planning algorithm for USVs operating in civilian traffic [83]. The planner reasons about the availability of contingency maneuvers needed in case any of the civilian vessels breaches the COLREGs [84-85].

7.2.3 Station-Keeping

The environments around bridges can be strongly affected by wind, tides and wave conditions. The resulting currents and swells can vary substantially, both in time, and in space as a USV maneuvers around a bridge structure. Thus, USV-based bridge inspection will require robust station-keeping capabilities. Among the most important tasks expected to require this are object localization, feature imaging and possibly the launch and recovery of smaller subsystems [48]. Underwater object localization via acoustics can require maintaining a fixed position and orientation for up to one minute. The performance of acoustic sensors could be heavily affected if the vehicle drifts during this time. A similar case is that of the optical localization using a camera. Here, image processing algorithms may require a few seconds; however, the performance is heavily affected if the vehicle drifts, as small motions may result in dramatic changes in lighting conditions or image perspective.

Station-keeping requires collaboration between the controller and the propulsion system, both designed to allow the vehicle to perform this challenging maneuver (**Figure 75**). Small external perturbations, such as wind, waves and current, can have tremendous effects on low weight USVs. These can negatively affect the USV's ability to hold its state, resulting in large errors or oscillations. A robust controller capable of accounting for unmodeled dynamics, which lead to significant deviations between simulated and experimental results, is therefore essential. As pointed out in [48], the nonlinear control of unmanned surface vehicles is currently an active area

of research, with most efforts directed towards feedback linearization and backstepping methods [22,86-89], as well as sliding mode control [22], [90].

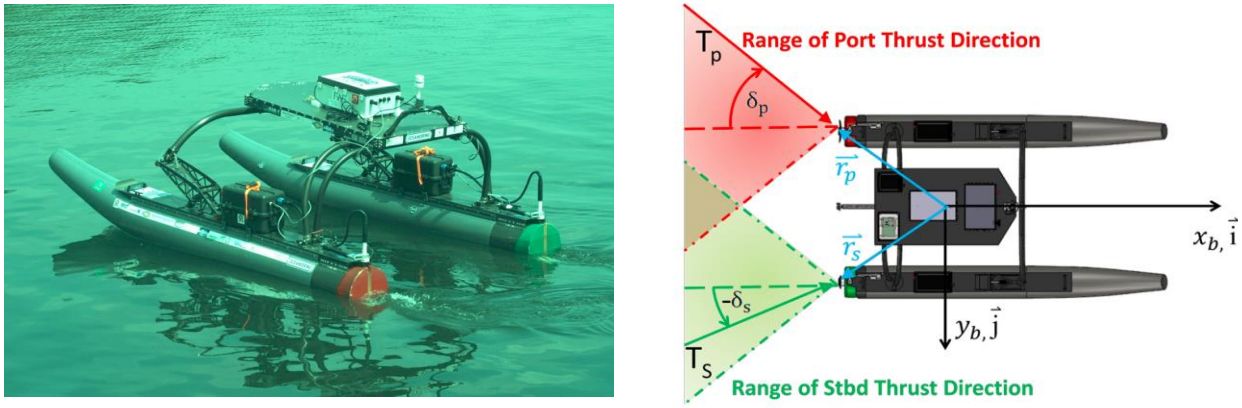

Figure 75: A USV configured with thrust vectoring for station-keeping [48].

One basic issue with much of USV control law development is that it is often limited to numerical simulation or small-scale experiments, rather than full-scale sea trials [91]. In fact, even in more technologically mature fields, such as AUV control, stabilization in the presence of environmental disturbances has only been partially addressed [92]. Several solutions have been proposed for the station-keeping of surface vehicles. In [93], experiments were performed on a small underactuated USV with high windage, where a feedforward wind model was modified to accommodate a PD-based heading autopilot. Switching between point and orientation stabilization and discontinuous control was employed to stabilize a marine vehicle to a point in the presence of a current using dipolar vector fields as guidance in [94] and [95]. Similarly, a hybrid approach was taken in [96] where multi-output PID controllers with and without acceleration feedback were used to stabilize a vehicle in high sea states by the use of an observer to estimate the peak wave frequency. The controller switched to controllers better suited to handle large disturbances as the peak wave frequency estimate decreased and, correspondingly, the sea state increased. Aguiar and Pascoal

[92] devised a nonlinear adaptive controller capable of station-keeping an AUV with uncertain hydrodynamic parameters in the presence of an unknown current. Backstepping also was suggested in [97] as means to station-keep a fully-actuated vehicle, although environmental disturbances were not explicitly stated in the problem formulation.

In [48], experiments of station-keeping controllers in environments of uncertain wind, current and wave disturbances show that the USV tested is best controlled by a nonlinear, backstepping, Multi-Input Multi- output (MIMO) PD controller, when coupled with a Lagrangian multiplier method for the control of thrust allocation. The USV was found to be capable of reaching and maintain a specific configuration of heading and position for a periods of ten or more minutes.

7.2.4 Wind Feedforward Control

As mentioned in Section 4.1.2 strong winds can exist around the base of bridges. In general, it has been found that wind can act as a strong disturbance on the station keeping operations of marine vehicles [98]. As USVs tend to be light weight and have a large windage areas, they are generally even more sensitive to wind disturbances than much larger vessels. Robust feedback controllers can be used to attenuate slowly changing wind disturbances, but have difficulty compensating for the rapid variation of wind speed and direction [99]. While there are a great number of studies concerning the automatic feedback control of USVs, feedforward control, such as wind feedforward control, still has not been widely explored. The main challenges encountered when designing wind feedforward controllers include:

1. Accurately measuring representative wind speed and direction. It has been found that wind gusts and turbulence can cause large measurement errors [98]. Anemometers should be mounted to ensure that measurements are minimally affected by wind interaction with the

vehicle's structure. One complication, is that the wind speed and direction can vary across different parts of a vessel. Thus, especially for larger vehicles, it may not be appropriate to analyze wind effects on the whole vessel with a single point measurement. For small USVs, a single anemometer can be used as it can be assumed that the wind acting on the vessel is approximately uniform.

2. Few wind models for estimating the wind forces and moments acting on small marine vessels have been developed. Most existing wind models were developed for large vessels, such as oil tankers, and commercial ships [98,100-102].

In [47] control and sensing strategies were developed to mitigate wind effects on a 4.9-meter long, 180-kg USV. A wind feed-forward controller was designed using an anemometer to measure the apparent wind speed/direction and a wind model to estimate the wind-induced forces and moments on the USV in real-time. Freely drifting tests were performed to evaluate the impact of the wind on an unpowered USV. The wind was strong enough to blow the vehicle more than 20 meters off station in 5 minutes when the mean wind speed was about 2m/s and the vehicle was allowed to freely drift with no control. Experiments also showed that the response time of the USV to wind gusts is about 5 seconds. The wind feedforward feature was added to different station-keeping feedback controllers, namely a PD controller, a robust backstepping controller, and a sliding mode controller. Station keeping tests of those controllers without/with wind feedforward controller were conducted. The experimental results show that a small USV can gain significant benefits from the inclusion of wind feedforward feature in both position and heading by an average of 75%, and 46%, respectively. It is likely that similar control strategies can be developed to handle the effects of strong currents due to tides, provided that suitable sensors can be identified.

7.2.5 Positioning

A concern of USV-based bridge inspection is that operating in the vicinity of a large bridge structure can affect precise positioning as GPS line of sight to overhead satellites may be blocked by parts of the structure. Use of sensor Kalman-filter based sensor fusion techniques can be used to improve positioning through combining dead-reckoning and GPS measurements to produce an improved estimate of a vehicle's location and heading. An additional solution would be to use Real Time Kinematic (RTK) GPS positioning technology, which can precisely measure a vehicle's position with respect to one or more fixed base stations.

System Localization and Mapping (SLAM) is an automated map-building technique, which was originally developed in robotics research to estimate the position of a robot within its environment [103,104]. SLAM allows one to probabilistically combine estimations of the motion of the vehicle with sensor observations of the environment to register previously seen areas with current observations in order to derive a self-consistent, maximum likelihood estimate of the mapped area. For example, SLAM has been implemented on a USV to combine LiDAR measurements, imagery from a spherical digital video camera, an inertial measurement unit (IMU) and a Doppler Velocimetry Logger (DVL) for vision based navigation and mapping under bridges [34]. Using GPS measurement updates, when available, to ground-truth position estimates it was found that SLAM-based navigation was better able to track vehicle position than traditional dead-reckoning and that a significant improvement in mapping of the bridge structures could be obtained (see **Figure 76** and **Figure 77**). SLAM based navigation and map building are a form of 'cooperative sensing' technique, where data collected from different types of sensors and sometimes from different platforms (vehicles) are combined to produce an improved estimate of the state (position,

orientation and speed) of a vehicle. An area of study that appears to be very promising would be to combine optical data taken using LiDAR and camera systems above the waterline with sonar imaging data of underwater structures and the channel bottom to build more accurate maps of a bridge's structure, which should also help to assess its condition through the identification of multiple features.

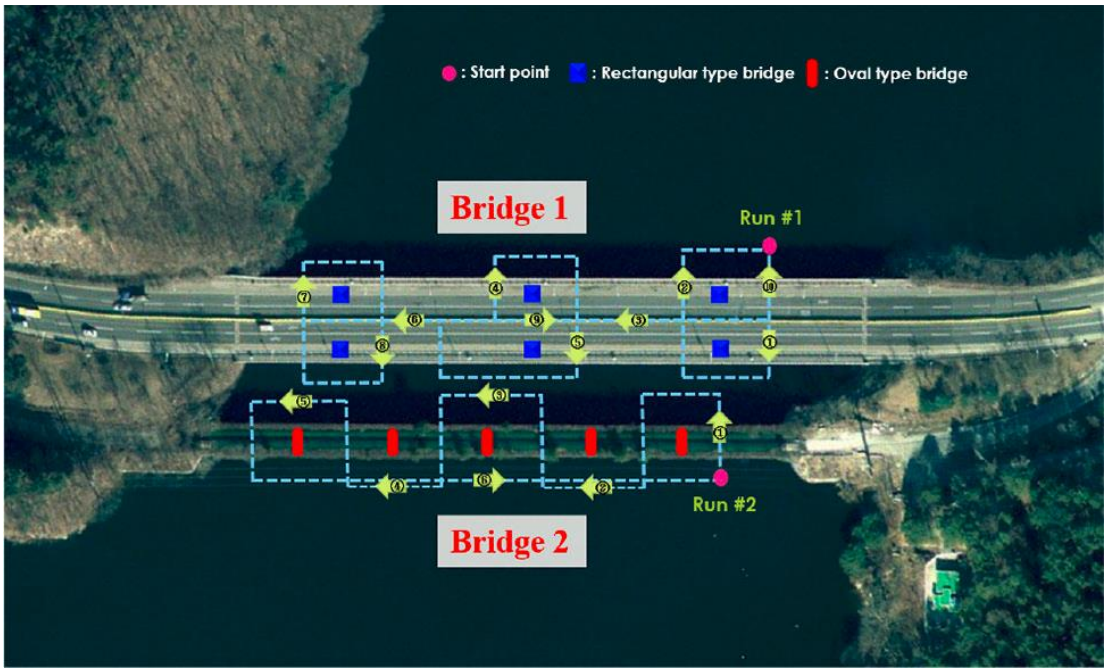

Figure 76: Survey path of USV for bridge mapping [34].

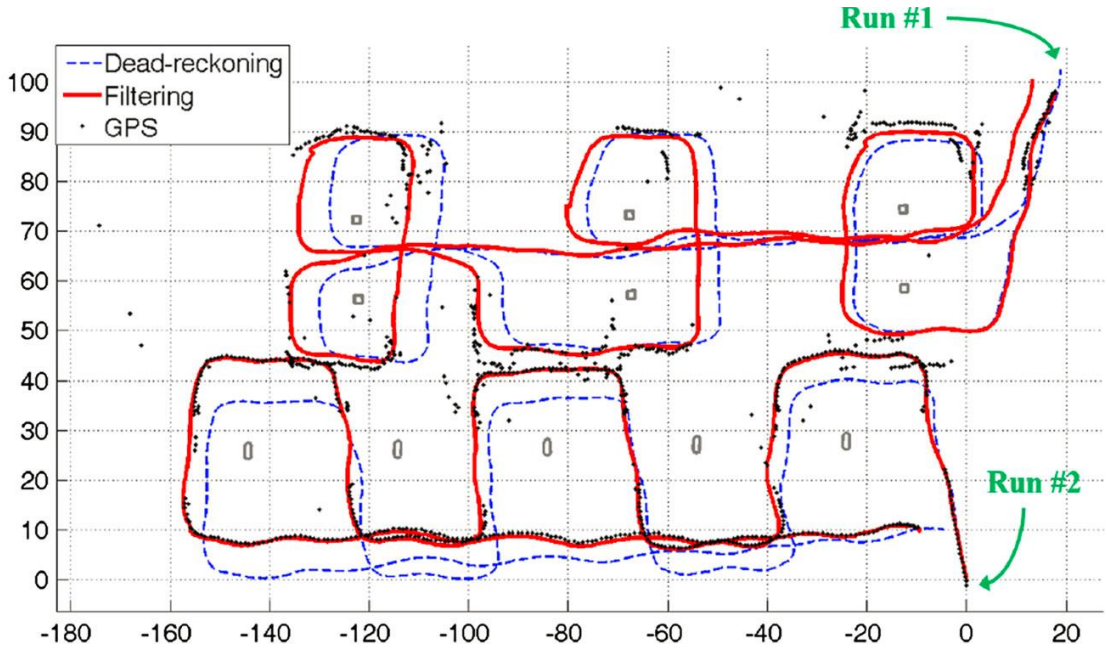

Figure 77: Comparison of estimated trajectory using SLAM (filtering), traditional dead reckoning and GPS [34].

7.2.6 Cooperative Sensing

7.2.6.1 *Multi-session Mapping of Bridge Structures*

Extracting maps from marine survey data is a time-consuming process that often requires large amounts of manual de-noising and adjustments using computerized tools. As mentioned above (Section 7.2.5), this process can be improved by using SLAM, which simultaneously builds a map from noisy sensor measurements and estimates the vehicle's trajectory within that map. Prior work has investigated robotic mapping of the seafloor operating in the underwater domain, using USVs [105] and AUVs [106-108]. Similarly, several papers have addressed robotic mapping in the ground [109,110] and aerial domains [111-113]. These approaches typically focus on a small temporal scale, where it is assumed the mapped environment remains largely static during the mapping session. A very interesting application for SLAM would to capture changes in bridge structures using maps obtained over repeated bridge inspections.

7.2.6.2 *Informative Path Planning for Multi-Session Mapping*

Multi-session mapping can be enhanced by leveraging research in informative path planning, which is the decision-making process that instructs the vehicle about where and how to intelligently gather more sensor measurements. This type of planning can assist in the mapping process by increasing efficiency (in relation to distance traveled, energy consumed, etc.), and by increasing quality of resulting map representation (in relation to accurate localization of important features, consistency of map, etc.). Prior work in the area of informative path planning related to mapping stems from research from the autonomous robotics community. Early work focused on autonomous exploration of unknown environments during a single mapping session [114,115]. More recent approaches sought to achieve accurate localization of robots as they traveled through environments to reach a specified goal [116,117]. However, these approaches do not specifically seek to maximize map quality. The most relevant work to informative path planning for environment mapping comes from the research areas of active SLAM [118,119], planning for information gathering [120], and uncertainty-aware planning for efficient area coverage [121,122]. However, there are still challenges within informative path planning that must be addressed to perform accurate multi-session mapping. Firstly, the planning process should adapt the path taken by the vehicle to the richness and density of terrain features. To efficiently perform multisession mapping of underwater bridge structures, the USV must maximize the information gathered about the environment while minimizing the energy spent in the process. For example, feature-less areas might be covered effectively using a low density of sensor measurements, while more complex and salient features might require denser sensor coverage to achieve finer resolution.

Secondly, the path planning algorithm should assist in change detection *online* by commanding control actions that result in increased confidence in the time-varying characteristics of suspected dynamic portions of the environment.

These automated additional actions could greatly increase the quality of the resulting map or increase confidence in map changes with minimal additional energy expended. Lastly, the path planning during each mapping event should guide the registration of maps across multiple sessions by ensuring that informative features from previous mapping sessions are re-observed and well-localized in new mapping sessions.

7.2.7 Imaging Sonar Systems

The use of real-time imaging sonar systems, such as the Aris 1800, is widespread in the oil & gas industry and in the U.S. Military, particularly for applications in underwater inspection (pipes, hulls and oil rig structures), underwater construction, object/mine detection and unmanned vehicle vision. In each of these applications imaging sonar systems have been shown to have the required accuracy, range and field of view. .However, conversations with FDOT inspectors at the Florida Automated Vehicles Summit and elsewhere suggests that the use of imaging sonar for bridge inspection operations by the FDOT and FHWA is very limited. A possible reason for this, is that until fairly recently, the cost of acoustic imaging systems has been quite high and access to such systems seems to have been restricted to specialized subcontractors or researchers. It is strongly recommended that the FDOT further explore the use of real time imaging systems, which could be deployed from either USVs, manned boats or by divers. Future work in this area could explore the use of automatic image processing and mosaicking software, coupled with motion compensation techniques to provide rapid, high quality images of underwater structures. In

combination with the mapping techniques described above in Subsection 7.2.6, it is anticipated that the use of imaging sonar could greatly improve the efficiency and effectiveness of bridge inspection teams. Further, it would be likely that a more widespread adoption by the FDOT, and other DOTs nationwide, could help to significantly reduce the cost of acoustic imaging systems.

8 Concluding Remarks

The use of unmanned surface vehicles (USVs) for bridge inspection has been explored. A detailed literature survey was conducted to study the requirements for USV-based bridge inspection, USV design for inspection, acoustic sensing techniques, control and dynamic positioning of USVs for bridge inspection; use of advanced robotics techniques, and how standard operating procedures can be modified to accommodate the use of USVs for bridge inspection. Based on the findings of the survey, it is suggested that investments in the application of advanced robotics techniques for Human-Robot-Interaction, station-keeping control and autonomous mapping/imaging would greatly assist the development of USV-based inspection systems. Further, it is strongly recommended that the FDOT explore the use of real-time acoustic imaging systems, for either manned or unmanned inspection.

A proof of concept system was developed and tested using an existing USV. The system was able to autonomously collect images of bridge structures, both underwater and at the waterline, by traversing a series of preprogrammed waypoints along a bridge and station-keeping at locations of interest. Given that the USV was initially designed for other applications, it should be noted that it functioned fairly well in this preliminary study, after only slight modifications. It is expected that a vehicle designed from the start to handle the operational, environmental, data collection and reporting requirements of unmanned bridge inspections would, of course, perform better.

References

[1] J. E. DeVault, "Robotic System for Underwater Inspection of Bridge Piers," *IEEE Instrumentation & Measurement Magazine,* vol. 3, no. 3, pp. 32-37, 2000.

[2] J. P. Broomfield, *Corrosion of steel in concrete: understanding, investigation and repair, Second Edition,* New York, NY USA: Taylor & Francis, 2007.

[3] B. M. Phares, G. A. Washer, D. D. Rolander, B. A. Graybeal and M. Moore, "Routine highway bridge inspection condition documentation accuracy and reliability," *Journal of Bridge Engineering,* vol. 9, no. 4, pp. 403-413, 2004.

[4] R. R. Murphy Et al., "Robot-assisted bridge inspection after Hurricane Ike," in *2009 IEEE Intl Workshop on Safety, Security & Rescue Robotics (SSRR),* Denver, CO USA, 2009.

[5] R. R. Murphy, E. Steimle, M. Hall, M. Lindemuth, D. Trejo, S. Hurlebaus, Z. Medina-Cetina and D. Slocum, "Robot-Assisted Bridge Inspection," *Journal of Intelligent & Robotic Systems,* vol. 64, pp. 77-95, 2011.

[6] R. R. Murphy Et al., "Cooperative use of unmanned sea surface and micro aerial vehicles at Hurricane Wilma," *J Field Robotics,* vol. 25, no. 3, pp. 164-180, 2008.

[7] J. E. Manley, "Unmanned surface vehicles, 15 years of development," in *MTS/IEEE OCEANS 2008,* Quebec City, QC Canada, 2008.

[8] P. F. Rynne and K. D. von Ellenrieder, "Unmanned Autonomous Sailing: Current Status and Future Role in Sustained Ocean Observations," *Marine Technology Society Journal*, vol. 43, no. 1, pp. 21-30, 2009.

[9] P. F. Rynne and K. D. von Ellenrieder, "Development and preliminary experimental validation of a wind & solar powered autonomous surface vehicle.," *IEEE J. Oceanic Engineering*, vol. 35, no. 4, pp. 971-983, 2010.

[10] T. Pastore and V. Djapic, "Improving autonomy and control of autonomous surface vehicles in port protection and mine countermeasure scenarios," *Journal of Field Robotics*, vol. 27, no. 6, pp. 903-914, 2010.

[11] C. Kitts, P. Mahacek, T. Adamek, K. Rasal, V. Howard, S. Li, A. Badaoui, W. Kirkwood, G. Wheat and S. Hulme, "Field operation of a robotic small waterplane area twin hull boat for shallow-water bathymetric characterization," *Journal of Field Robotics* , vol. 29, no. 6, pp. 924-938, 2012.

[12] N. Metni and T. Hamel, "A UAV for bridge inspection: Visual servoing control law with orientation limits," *Automation in Construction*, vol. 17, no. 1, pp. 3-10, 2007.

[13] N. Hallermann and G. Morgenthal, "Visual inspection strategies for large bridges using Unmanned Aerial Vehicles (UAV)," in *7th International Conference on Bridge Maintenance, Safety and Management*, Shanghai, China, 2014.

[14] J. Guerrero and Y. Bestaoui, "UAV path planning for structure inspection in windy environments," *Journal of Intelligent & Robotic Systems,* vol. 69, no. 1-4, pp. 297-311, 2013.

[15] A. Ellenberg, L. Branco, A. Krick, I. Bartoli and A. Kontsos, "Use of Unmanned Aerial Vehicle for Quantitative Infrastructure Evaluation," *Journal of Infrastructure Systems*, vol. 21, no. 3, p. 04014054, 2014.

[16] J. Oh, A. Lee, S. Oh, Y. Choi, B. Yi and H. Yang, "Design and control of bridge inspection robot system," in *International Conference on Mechatronics and Automation ICMA 2007*, Harbin, China, 2007.

[17] R. S. Lim, H. M. La, Z. Shan and W. Sheng, "Developing a crack inspection robot for bridge maintenance," in *IEEE International Conference on Robotics and Automation (ICRA)*, Shanghai, China, 2011.

[18] A. Mazumdar and H. Asada, "Mag-foot: A steel bridge inspection robot," in *IEEE/RSJ International Conference on Intelligent Robots and Systems, IROS 2009*, St. Louis, MO, USA, 2009.

[19] J. Oh, G. Jang, S. Oh, J. Lee, B. Yi, Y. Moon, J. Lee and Y. Choi, "Bridge inspection robot system with machine vision," *Automation in Construction,* vol. 18, no. 7, pp. 929-941, 2009.

[20] J. Shang, B. Bridge, T. Sattar, S. Mondal and A. Brenner, "Development of a climbing robot for inspection of long weld lines," *Industrial Robot: An International Journal*, vol. 35, no. 3, pp. 217-223, 2008.

[21] R. R. Murphy, E. Steimle, M. Hall, M. Lindemuth, D. Trejo, S. Hurlebaus, Z. Medina-Cetina and D. Slocum, "Robot-assisted bridge inspection after Hurricane Ike," in *2009 IEEE International Workshop on Safety, Security & Rescue Robotics (SSRR)*, Denver, CO USA, 2009.

[22] H. Ashrafiuon, K. R. Muske, L. C. McNinch and R. Soltan, "Sliding-mode tracking control of surface vessels," *IEEE Transactions on Industrial Electronics*, vol. 55, no. 11, pp. 4004-4012, 2008.

[23] R. R. Murphy, E. Steimle, C. Griffin, C. Cullins, M. Hall and K. Pratt, "Cooperative use of unmanned sea surface and micro aerial vehicles at Hurricane Wilma," *Journal of Field Robotics*, vol. 25, no. 3, pp. 164-180, 2008.

[24] G. H. Elkaim, "System identification-based control of an unmanned autonomous wind-propelled catamaran," *Control Engineering Practice* , vol. 17, no. 1, pp. 158-169, 2009.

[25] B. S. Bingham, E. F. Prechtl and R. A. Wilson, "Design requirements for autonomous multivehicle surface-underwater operations," *Marine Technology Society Journal*, vol. 43, no. 2, pp. 61-72, 2009.

[26] V. Howard, J. Mefford, L. Arnold, B. Bingham and R. Camilli, "The unmanned port security vessel: an autonomous platform for monitoring ports and harbors," in *MTS/IEEE Oceans '11*, Kona, HI USA, 2011.

[27] J. Manley and G. Hine, "Persistent unmanned surface vehicles for subsea support," in *Offshore Technology Conference*, Houston, TX USA, 2011.

[28] W. Fink, M. Tuller, A. Jacobs, R. Kulkarni, M. Tarbell, R. Furfaro and V. R. Baker, "Robotic lake lander test bed for autonomous surface and subsurface exploration of titan lakes," in *2012 IEEE Aerospace Conference*, Big Sky, MT USA, 2012.

[29] E. T. Steimle and M. L. Hall, "Unmanned surface vehicles as environmental monitoring and assessment tools," in *MTS/IEEE Oceans '06*, Boston, MA USA, 2006.

[30] T. M. Browne, T. J. Collins, M. J. Garlich, J. E. O'Leary, D. G. Stromberg and K. C. Heringhaus, "Underwater Bridge Inspection FHWA-NHI-10-027," U.S. Department of Transportation Federal Highway Administration, Washington, D.C. USA, 2010.

[31] T. W. Ryan, J. E. Mann, Z. M. Chill and B. T. Ott, "Bridge Inspector's Reference Manual: BIRM, Report No. FHWA NHI 12-049," U.S. Department of Transportation, Federal Highway Administration, Arlington, Virginia, 2012.

[32] American Society for Nondestructive Testing, "Introduction to Nondestructive Testing," American Society for Nondestructive Testing, [Online]. Available:

https://www.asnt.org/MinorSiteSections/AboutASNT/Intro-to-NDT.aspx. [Accessed 22 July 2015].

[33] E. E. Allmendinger, Submersible vehicle systems design, Jersey City, NJ USA: Society of Naval Architects & Marine Engineers, 1990.

[34] J. Han, J. Park, T. Kim and J. Kim, "Precision navigation and mapping under bridges with an unmanned surface vehicle," *Autonomous Robots,* vol. 38, no. 4, pp. 349-362, 2015.

[35] V. Bertram, "Unmanned surface vehicles–a survey," *Skibsteknisk Selskab,* pp. 1-14, 2008.

[36] A. Motwani, "A survey of uninhabited surface vehicles.," Technical Report MIDAS.SMSE.2012.TR.001. School of Marine Science and Engineering, Plymouth University, Plymouth, UK, 2012.

[37] J. G. Marquardt, J. Alvarez and K. D. von Ellenrieder, "Characterization and System Identification of an Unmanned Amphibious Tracked Vehicle," *IEEE Journal of Oceanic Engineering,* vol. 39, no. 4, pp. 641-661, 2014.

[38] M. H. Tall, P. F. Rynne, J. M. Lorio and K. D. von Ellenrieder, "Visual-Based Navigation of an Autonomous Surface Vehicle," *Marine Technology Society Journal,* vol. 44, no. 2, pp. 37-45, 2010.

[39] D. Savitsky, *On the subject of high-speed monohulls,* Athens, Greece: Society of Naval Architects and Marine Engineers, 2003.

[40] D. Andrews, "Multi-hulled Vessels," in *Ship Design and Construction, Vol. II*, Jersey City, NJ USA, Society of Naval Architects and Marine Engineers, 2004, pp. 46-1 - 46-45.

[41] M. D. Dhanak, P. Ananthakrishnan and K. D. von Ellenrieder, "Seakeeping characteristics of a Wave-Adaptive Modular Unmanned Surface Vehicle," in *ASME Offshore Mechanics and Arctic Engineering Conference*, Nantes, France, 2013.

[42] J. Fratello and M. Ahmadian, "Multi-body Dynamic Simulation and Analysis of Wave-adaptive Modular Vessels," in *11th International Conference on Fast Sea Transportation FAST 2011*, Honolulu, HI USA, 2011.

[43] A. Peterson, M. Ahmadian, M. Craft and A. Shen, "Simulation and scale-testing to improve the next generation of wave-adaptive modular vessels," in *Proceedings of the 2013 Grand Challenges on Modeling and Simulation Conference*, Toronto, ON Canada, 2013.

[44] W. Klinger, I. R. Bertaska and K. D. von Ellenrieder, "Control of an Unmanned Surface Vehicle with Uncertain Displacement and Drag," *IEEE Journal of Oceanic Engineering*, (Submitted, under review).

[45] K. D. von Ellenrieder, "Free running tests of a waterjet propelled unmanned surface vehicle," *Journal of Marine Engineering & Technology*, vol. 12, no. 1, pp. 1-9, 2013.

[46] O. M. Faltinsen, Hydrodynamics of High-Speed Marine Vehicles, New York, NY: Cambridge University Press, 2005.

[47] H. Qu, E. I. Sarda, I. R. Bertaska and K. D. von Ellenrieder, "Wind Feed-forward Control of a USV," in *MTS/IEEE Oceans '15*, Genova, GE Italy, 2015.

[48] E. I. Sarda, I. R. Bertaska, H. Qu and K. D. von Ellenrieder, "Development of a USV Station-Keeping Controller," in *MTS/IEEE Oceans '15*, Genova, GE Italy, 2015.

[49] N. Khare and P. Singh, "Modeling and optimization of a hybrid power system for an unmanned surface vehicle," *Journal of Power Sources,* vol. 198, pp. 368-377, 2012.

[50] M.-J. Kim and H. Peng, "Power management and design optimization of fuel cell/battery hybrid vehicles," *Journal of Power Sources,* vol. 165, no. 2, pp. 819-832, 2007.

[51] S.-I. Sohn, J.-H. Oh, Y.-S. Lee, D.-H. Park and I.-K. Oh, "Design of a Fuel-Cell-Powered Catamaran-Type Unmanned Surface Vehicle," *IEEE Journal of Oceanic Engineering,* vol. 40, no. 2, pp. 388-396, 2015.

[52] D. M. Kocak and F. M. Caimi, "The Current Art of Underwater Imaging – With a Glimpse of the Past and Vision of the Future," *Marine Technology Society Journal,* vol. 39, no. 3, pp. 5-26, 2005.

[53] D. G. Stromberg and T. Browne, "Guidelines for underwater inspection and imaging of railroad bridges," in *American Railway Engineering and Maintenance-of-Way Association Annual Conference*, Indianapolis, IN USA, 2013.

[54] F. M. Caimi and F. R. Dalgleish, "Subsea laser scanning and imaging systems," in *Subsea Optics and Imaging*, Cambridge, UK, 2013, pp. 327-352.

[55] D. M. Kocak, F. R. Dalgleish, F. M. Caimi and Y. Y. Schechner, "A focus on recent developments and trends in underwater imaging," *Marine Technology Society Journal*, vol. 42, no. 1, pp. 52-67, 2008.

[56] I. R. Bertaska, B. C. Shah, A. J. Sinisterra, P. Svec, K. D. von Ellenrieder, M. R. Dhanak and S. K. Gupta, "Experimental Evaluation of Approach Behavior for Autonomous Surface Vehicles," *Journal of Ocean Engineering*, Accepted, in Press.

[57] Florida Department of Transportation, Maintenance Office, *Topic No.: 850-010-030-i Bridge and Other Structures Inspection And Reporting*, Tallahassee, Florida: Florida Department of Transportation, 2014.

[58] R. A. Brooks, "Elephants don't play chess," *Robotics and autonomous systems* , vol. 6, no. 1, pp. 3-15, 1990.

[59] J. Rosenblatt, S. Williams and H. Durrant-Whyte, "A behavior-based architecture for autonomous underwater exploration," *Information Sciences*, vol. 145, no. 1, pp. 69-87, 2002.

[60] J. J. Bryson, "Intelligence by design: principles of modularity and coordination for engineering complex adaptive agents. Ph.D. Thesis," Massachusetts Institute of Technology, Cambridge, MA USA, 2001.

[61] C. Flanagan, D. Toal and M. Leyden, "Subsumption and fuzzy-logic, experiments in behavior-based control of mobile robots," *International Journal of Smart Engineering System Design*, vol. 5, no. 3, pp. 161-175, 2003.

[62] S. M. Veres, "Principles, architectures and trends in autonomous control," in *Autonomous Agents in Control*, London, UK, Institution of Electrical Engineers, 2005, pp. 1-9.

[63] M. Wooldridge, An introduction to multiagent systems, Chichester, UK: John Wiley & Sons, 2009.

[64] P. Urlings, C. Sioutis, J. Tweedale, N. Ichalkaranje and L. Jain, "A future framework for interfacing BDI agents in a real-time teaming environment," *Journal of Network and Computer Applications* , vol. 29, no. 2, pp. 105-123, 2006.

[65] E. Gat, "On the role of stored internal state in the control of autonomous mobile robots," *AI Magazine*, vol. 14, no. 1, p. 64, 1993.

[66] E. Gat, "On three-layer architectures," *Artificial intelligence and mobile robots*, vol. 195, p. 210, 1998.

[67] P. Ridao, J. Batlle, J. Amat and G. N. Roberts, "Recent trends in control architectures for autonomous underwater vehicles," *International Journal of Systems Science*, vol. 30, no. 9, pp. 1033-1056, 1999.

[68] B. S. Bingham, J. M. Walls and R. M. Eustice, "Development of a flexible command and control software architecture for marine robotic applications," *Marine Technology Society Journal*, vol. 45, no. 3, pp. 25-36, 2011.

[69] B. Sellner, F. W. Heger, L. M. Hiatt, R. Simmons and S. Singh, "Coordinated multiagent teams and sliding autonomy for large-scale assembly," *Proceedings of the IEEE*, vol. 94, no. 7, pp. 1425-1444, 2006.

[70] J. Borges de Sousa, K. H. Johansson, J. Silva and A. Speranzon, "A verified hierarchical control architecture for co-ordinated multi-vehicle operations," *International Journal of Adaptive Control and Signal Processing*, vol. 21, no. 2-3, pp. 159-188, 2007.

[71] P. DeLima, D. Zarzhitsky and D. Pack, "Decentralized cooperative control of autonomous surface vehicles," in *Dynamics of Information Systems*, New York, NY USA, Springer, 2010, pp. 257-273.

[72] M. L. Cummings and P. M. Mitchell, "Management of multiple dynamic human supervisory control tasks for UAVs," in *Human Computer Interaction International Human Systems Integration Conference*, Las Vegas, 2005.

[73] S. Mau and J. Dolan, "Scheduling for humans in multirobot supervisory control," in *IEEE/RSJ International Conference on Intelligent Robots and Systems, IROS 2007*, San Diego, CA USA, 2007.

[74] D. R. Olsen and M. A. Goodrich, "Metrics for evaluating human-robot interactions," in *Proceedings of PERMIS*, Gaithersburg, MD USA, 2003.

[75] I. R. Bertaska, B. C. Shah, J. M. Alvarez, A. J. Sinisterra, K. D. von Ellenrieder, M. R. Dhanak, B. C. Shah, P. Svec and S. K. Gupta, "“Experimental Evaluation of Approach Behavior for Autonomous Surface Vehicles," in *ASME Dynamic Systems and Control Conference*, Stanford, CA USA, 2013.

[76] I. R. Bertaska, A. Sinisterra, B. C. Shah, P. Švec, K. D. von Ellenrieder, M. D. Dhanak and S. K. Gupta, "Field Testing of Dynamics-Aware COLREGs-Compliant Behaviors for USVs," in *Robotics Science and Systems 2014 Workshop on Autonomous Control, Adaptation, and Learning for Underwater Vehicles*, Berkeley, CA USA, 2014.

[77] P. Svec, B. C. Shah, I. Bertaska, W. B. Klinger, A. J. Sinisterra, K. D. von Ellenrieder, M. D. Dhanak and S. K. Gupta, "Dynamics-Aware Target Following for an Autonomous Surface Vehicle Operating under COLREGS in Civilian Traffic," in *IEEE/RSJ International Conference on Intelligent Robots and Systems*, Tokyo, Japan, 2013.

[78] T. Fraichard and H. Asama, "Inevitable collision states—a step towards safer robots?," *Advanced Robotics*, vol. 18, no. 10, pp. 1001-1024, 2004.

[79] D. Fox, W. Burgard and S. Thrun, "The dynamic window approach to collision avoidance," *IEEE Robotics & Automation Magazine*, vol. 4, no. 1, pp. 23-33, 1997.

[80] M. Greytak and F. Hover, "Motion planning with an analytic risk cost for holonomic vehicles," in *IEEE Conference on Decision and Control*, Shanghai, China, 2009.

[81] P. Svec, M. Schwartz, A. Thakur and S. K. Gupta, "Trajectory planning with look-ahead for unmanned sea surface vehicles to handle environmental disturbances," in *IEEE/RSJ International Conference on Intelligent Robots and Systems, IROS 2011* , San Francisco, CA USA, 2011.

[82] M. Pivtoraiko, R. A. Knepper and A. Kelly, "Differentially constrained mobile robot motion planning in state lattices," *Journal of Field Robotics,* vol. 26, no. 3, pp. 308-333, 2009.

[83] B. C. Shah, P. Svec, I. R. Bertaska, Wilhelm, A. J. Sinisterra, K. D. von Ellenrieder, M. R. Dhanak and S. K. Gupta, "Trajectory planning with adaptive control primitives for autonomous surface vehicles operating in congested civilian traffic," in *IEEE/RSJ International Conference on Intelligent Robots and Systems IROS '14*, Chicago, IL USA, 2014.

[84] M. R. Benjamin, J. Curcio, J. J. Leonard and P. M. Newman, "Navigation of unmanned marine vehicles in accordance with the rules of the road," in *Proceedings 2006 IEEE International Conference on Robotics and Automation ICRA 2006*, Orlando, FL USA, 2006.

[85] U. C. G. Commandant, "International Regulations for Prevention of Collisions at Sea (72 COLREGS)," US Coast Guard , 1972.

[86] Y. Liao, Y. Pang and L. Wan, "Combined speed and yaw control of underactuated unmanned surface vehicles," in *2nd IEEE International Asia Conference on Informatics in Control, Automation and Robotics*, Wuhan, China, 2010.

[87] T. I. &. S. J. P. Fossen, "Tutorial on nonlinear backstepping: applications to ship control," *Modeling, Identification and Control,* vol. 20, no. 2, p. 83, 1999.

[88] C. R. Sonnenburg and C. A. Woolsey, "Modeling, identification, and control of an unmanned surface vehicle," *Journal of Field Robotics,* vol. 30, no. 3, pp. 371-398, 2013.

[89] A. P. Aguiar and J. P. Hespanha, "Position tracking of underactuated vehicles," in *Proceedings of the American Control Conference*, Denver, CO USA, 2003.

[90] J. M. Alvarez, I. R. Bertaska and K. D. von Ellenrieder, "Nonlinear control of an unmanned amphibious vehicle," in *ASME Dynamic Systems and Control Conference*, Stanford, CA USA, 2013.

[91] H. Ashrafiuon, K. R. Muske and L. C. McNinch, "Review of nonlinear tracking and setpoint control approaches for autonomous underactuated marine vehicles," in *American Control Conference*, Baltimore, MD USA, 2010.

[92] A. P. Aguiar and A. M. Pascoal, "Dynamic positioning and way-point tracking of underactuated AUVs in the presence of ocean currents," *International Journal of Control,* vol. 2007, no. 7, pp. 1092-1108, 2007.

[93] A. Pereira, J. Das and G. S. Sukhatme, "An experimental study of station keeping on an underactuated ASV," in *IEEE/RSJ International Conference on Intelligent Robots and Systems, IROS 2008*, Nice, France, 2008.

[94] D. Panagou and K. J. Kyriakopoulos, "Dynamic positioning for an underactuated marine vehicle using hybrid control," *International Journal of Control*, vol. 87, no. 2, pp. 264-280, 2014.

[95] D. Panagou and K. J. Kyriakopoulos, "Switching control approach for the robust practical stabilization of a unicycle-like marine vehicle under non-vanishing perturbations," in *IEEE International Conference on Robotics and Automation, ICRA 2011*, Shanghai, China, 2011.

[96] T. D. Nguyen, A. J. Sørensen and S. T. Quek, "Design of hybrid controller for dynamic positioning from calm to extreme sea conditions," *Automatica*, vol. 43, no. 5, pp. 768-785, 2007.

[97] T. Fossen and T. Johansen, "A survey of control allocation methods for ships and underwater vehicles," in *14th Mediterranean Conference on Control and Automation*, Ancona, Italy, 2006.

[98] R. Stephens, "Wind Feed Forward–Blowing Away the Myths," in *Marine Technology Society Dynamic Positioning Conference*, Houston, TX USA, 2011.

[99] D. Schlipf, L. Y. Pao and P. W. Cheng, "Comparison of feedforward and model predictive control of wind turbines using LIDAR," in *IEEE 51st Annual Conference on Decision and Control* , Maui, HI USA, 2012.

[100] R. Gould, "The estimation of wind loads on ship superstructures, Report No. RINA-MTM-8," Royal Institution of Naval Architects, 1982.

[101] R. M. Isherwood, "Wind resistance of merchant ships," *Transactions Royal Society of Naval Architects - Supplementary Papers,* no. 327-338, p. 114, 1972.

[102] W. Li, J. Du, Y. Sun, H. Chen, Y. Zhang and J. Song, "Modeling and Simulation of Marine Environmental Disturbances for Dynamic Positioned Ship," in *Chinese Control Conference*, Hefei, China, 2012.

[103] H. Durrant-Whyte and T. Bailey, "Simultaneous localization and mapping: Part I," *IEEE Robotics & Automation Magazine*, vol. 13, no. 2, pp. 99-110, 2006.

[104] T. Bailey and H. Durrant-Whyte, "Simultaneous localization and mapping (SLAM): Part II," *IEEE Robotics & Automation Magazine,* vol. 13, no. 3, pp. 108-117, 2006.

[105] G. Hitz, F. Pomerleau, F. Colas and R. Siegwart, "State Estimation for Shore Monitoring Using an Autonomous Surface Vessel," in *International Symposium on Experimental Robotics* , 2014.

[106] S. Barkby, S. B. Williams, O. Pizarro and M. V. Jakuba, "A featureless approach to efficient bathymetric SLAM using distributed particle mapping," *Journal of Field Robotics,* vol. 28, no. 1, pp. 19-39, 2011.

[107] S. Barkby, S. Williams, O. Pizarro and M. Jakuba, "Bathymetric particle filter SLAM using trajectory maps," *International Journal of Robotics Research,* 2012.

[108] C. Roman and H. Singh, "A Self-Consistent Bathymetric Mapping Algorithm," *Journal of Field Robotics,* vol. 24, no. 1-2, pp. 23-50, 2007.

[109] S. Thrun, "Robotic mapping: A survey. CMU-CS-02-111," School of Computer Science, Carnegie Mellon University, Pittsburg, PA USA, 2002.

[110] P. B. W. Agarwal and C. Stachniss, "Survey of Geodetic Mapping Methods: Geodetic Approaches to Mapping and the Relationship to Graph-Based SLAM," *IEEE Robotics & Automation Magazine,* vol. 21, no. 3, pp. 63-80, 2014.

[111] Y. Lin, J. Hyyppä and A. Jaakkola, "Mini-UAV-borne LIDAR for fine-scale mapping," *IEEE Geoscience and Remote Sensing Letters,* vol. 8, no. 3, pp. 426-430, 2011.

[112] N. Michael, S. Shen, K. Mohta, Y. Mulgaonkar, V. Kumar, K. Nagatani, Y. a. K. S. Okada, K. Otake, K. Yoshida, K. Ohno, E. Takeuchi and S. Tadokoro, "Collaborative mapping of an earthquake-damaged building via ground and aerial robots," *Journal of Field Robotics,* vol. 29, no. 5, pp. 832-841, 2012.

[113] L. Heng, D. Honegger, G. H. Lee, L. Meier, P. Tanskanen, F. Fraundorfer and M. Pollefeys, "Autonomous visual mapping and exploration with a micro aerial vehicle," *Journal of Field Robotics,* vol. 31, no. 4, pp. 654-675, 2014.

[114] H. H. González-Banos and J. C. Latombe, "Navigation strategies for exploring indoor environments," *International Journal of Robotics Research,* vol. 21, no. 10-11, pp. 829-848, 2002.

[115] C. Stachniss, G. Grisetti and W. Burgard, "Information Gain-based Exploration Using Rao-Blackwellized Particle Filters," in *Robotics: Science and Systems Conference,* Cambridge, MA USA, 2005.

[116] J. Van Den Berg, S. Patil and R. Alterovitz, "Motion planning under uncertainty using iterative local optimization in belief space," *International Journal of Robotics Research,* vol. 31, no. 11, pp. 1263-1278, 2012.

[117] R. Valencia, M. Morta, J. Andrade-Cetto and J. M. Porta, "Planning reliable paths with Pose SLAM," *IEEE Transactions on Robotics,* vol. 29, no. 4, pp. 1050-1059, 2013.

[118] S. M. Chaves, A. Kim and R. M. Eustice, "Opportunistic sampling-based planning for active visual SLAM," in *IEEE/RSJ International Conference on Intelligent Robots and Systems, IROS 2014,* Chicago, IL USA, 2014.

[119] A. Kim and R. M. Eustice, "Active visual SLAM for robotic area coverage: Theory and experiment," *International Journal of Robotics Research,* vol. 34, no. 4-5, pp. 457-475, 2015.

[120] G. A. Hollinger and G. S. Sukhatme, "Sampling-based robotic information gathering algorithms," *International Journal of Robotics Research,* vol. 33, no. 9, pp. 1271-1287, 2014.

[121] E. Galceran and M. Carreras, "A survey on coverage path planning for robotics," *Robotics and Autonomous Systems,* vol. 61, no. 12, pp. 1258-1276, 2013.

[122] E. Galceran, R. Campos, N. Palomeras, M. Carreras and P. Ridao, "Coverage path planning with realtime replanning for inspection of 3d underwater structures," in *IEEE International Conference on Robotics and Automation, ICRA 2014*, Hong Kong, China, 2014.

[123] R. R. Murphy Et al., "Robot-Assisted Bridge Inspection," *J Intell & Rob Sys,* vol. 64, pp. 77-95, 2011.